AEDC TR-95-5

Subscale Study of Engine Bellmouth Inlet Vortices in Test Cell R1D

James A. Reed and Robert S. Hiers, Jr.
Sverdrup Technology Inc., AEDC Group

May 1995

Final Report for Period October 1992 — September 1994

ARNOLD ENGINEERING DEVELOPMENT CENTER
ARNOLD AIR FORCE BASE, TENNESSEE
AIR FORCE MATERIEL COMMAND
UNITED STATES AIR FORCE

NOTICES

When U. S. Government drawings, specifications, or other data are used for any purpose other than a definitely related Government procurement operation, the Government thereby incurs no responsibility nor any obligation whatsoever, and the fact that the Government may have formulated, furnished, or in any way supplied the said drawings, specifications, or other data, is not to be regarded by implication or otherwise, or in any manner licensing the holder or any other person or corporation, or conveying any rights or permission to manufacture, use, or sell any patented invention that may in any way be related threto.

Qualified users may obtain copies of this report from the Defense Technical Information Center.

References to named commercial products in this report are not to be considered in any sense as an endorsement of the product by the United States Air Force or the Government.

This report has been reviewed by the Office of Public Affairs (PA) and is releasable to the National Technical Information Service (NTIS). At NTIS, it will be available to the general public, including foreign nations.

APPROVAL STATEMENT

This report has been reviewed and approved.

DAN MAGEE, Capt, CF
Directorate of Technology
Deputy of Operations

Approved for publication:

FOR THE COMMANDER

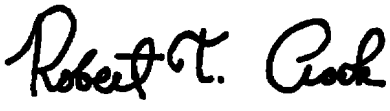

ROBERT T. CROOK
Deputy Director of Technology
Deputy of Operations

REPORT DOCUMENTATION PAGE

Form Approved
OMB No. 0704-0188

1. AGENCY USE ONLY (Leave blank)	2. REPORT DATE	3. REPORT TYPE AND DATES COVERED
	May 1995	Final Report October 1992 - September 1994

4. TITLE AND SUBTITLE

Subscale Study of Engine Bellmouth Inlet Vortices in Test Cell RID

5. FUNDING NUMBERS

0096
1929

6. AUTHOR(S)

Reed, James A., and Hiers, Robert S., Jr.
Sverdrup Technology, Inc., AEDC Group

7 PERFORMING ORGANIZATION NAME(S) AND ADDRESS(ES)

Arnold Engineering Development Center/DOT
Air Force Materiel Command
Arnold Air Force Base, TN 37389-9011

8. PERFORMING ORGANIZATION (REPORT NUMBER)

AEDC-TR-95-5

9 SPONSORING/MONITORING AGENCY NAMES(S) AND ADDRESS(ES)

Arnold Engineering Development Center/DOT
Air Force Materiel Command
Arnold Air Force Base, TN 37389-9011

10. SPONSORING/MONITORING AGENCY REPORT NUMBER

11 SUPPLEMENTARY NOTES

Available in Defense Technical Information Center (DTIC).

12A DISTRIBUTION/AVAILABILITY STATEMENT

Approved for public release; distribution is unlimited.

12B. DISTRIBUTION CODE

13 ABSTRACT (Maximum 200 words)

A technology program was conducted in Test Cell RID concerning bellmouth flow quality. Flow visualization was used to determine the presence of inlet vortices. It was shown that these vortices can be eliminated using a 45-deg conical extension attached to the bellmouth inlet. Design guidelines were developed to assist in determining acceptable cone angles and axial and radial gaps between the conical extension and the bellmouth inlet.

14 SUBJECT TERMS

bellmouth flow quality inlet vortices

15. NUMBER OF PAGES

124

16. PRICE CODE

17. SECURITY CLASSIFICATION OF REPORT	18. SECURITY CLASSIFICATION OF THIS PAGE	19. SECURITY CLASSIFICATION OF ABSTRACT	20 LIMITATION OF ABSTRACT
UNCLASSIFIED	UNCLASSIFIED	UNCLASSIFIED	SAME AS REPORT

PREFACE

The work reported herein was conducted by the Arnold Engineering Development Center (AEDC), Air Force Materiel Command (AFMC), at the request of the Directorate of Technology. The results of the test were obtained by Sverdrup Technology, Inc., AEDC Group, support contractor for propulsion test facilities at AEDC, AFMC, Arnold Air Force Base, TN under Job Numbers 0096 and 1929. The Air Force Project Managers were Capt. J.E.P. Lacasse (CF) and Capt. D. Magee (CF). The data analysis was completed on September 30, 1994, and the manuscript was submitted for publication on March 16, 1995.

CONTENTS

ILLUSTRATIONS

Figure | Page

Figure Page

TABLES

Table Page

1.0 INTRODUCTION

Direct-connect tests of turbine engines in the Arnold Engineering Development Center (AEDC) Engine Test Facility (ETF) altitude test cells employ a bellmouth to connect the engine inlet with the facility air-supply plenum. In most cases these contoured bellmouths penetrate into the plenum and terminate in the central region of the plenum away from both the plenum endwall and sidewall. Figure 1 illustrates a typical Propulsion Development Test Cell with the engine directly connected to a relatively large diameter bellmouth.

During an engine test in the Propulsion Development Test Cell T-2, a region of low pressure was discovered at the engine inlet plane. Initially, it was thought that the low-pressure reading might be an instrumentation problem. However, during several test entries, three different instrumentation setups simultaneously recorded the same low-pressure region. Thus, it was then believed that the phenomenon was aerodynamic in nature. Examination of the pressure data led to the postulation that the low-pressure region could possibly be caused by a vortex. This speculation was based primarily on the similarity of pressure readings from a four-hole cone probe; i.e., the pressures on both sides of the cone were reading low pressures as if in the eye of a tornado. Similar vortices, often referred to as inlet vortices, have been observed in the inlet of turbine engines on aircraft during taxi operations or on ground-level test stands. The effectiveness of a bellmouth extension, a conical fairing that provides an aerodynamic interface between the plenum and the bellmouth, in preventing the anomaly further supports this hypothesis.

A careful examination of historical bellmouth exit-plane total pressure data was conducted. This examination revealed that the exit-plane total pressure data, obtained with an "industry-standard, steady-state" 40 pitot probe rake conventionally used to verify facility/bellmouth flow quality, have suggested the existence of localized, *unsteady* total pressure losses in the core flow of some particular bellmouths. The historical data indicate that total pressure losses may occur instantaneously at almost any probe location, although the losses tend to concentrate temporally and spatially at preferred locations. This evidence of unsteady bellmouth total pressure losses acquired by probes designed with limited time response led to the postulation of the existence of unsteady vortices being formed in the facility plenum and being ingested into the bellmouth entrance. The total pressure losses are then considered manifestations of the large viscous losses associated with the very large velocity gradients in the core regions of viscous-rotational vortices.

Based on this assessment, experiments were conducted to determine the cause of the flow anomaly and to develop remedial methodologies. The objectives of the technology project were as follows:

1. Prove the postulation that the observed total pressure losses were the result of bellmouth vortices by providing direct visual evidence of vortices entering the bellmouth using a smoke injector and laser illumination technique for flow visualization. Further modeling of bellmouth flows will also benefit from independent knowledge of the existence of vortices.
2. Determine the effectiveness of bellmouth extensions as a function of cone angle, radial gap, and axial gap. The gaps are measured between the bellmouth inlet and

the extension exit. One purpose for this parametric sensitivity study is to determine if a single "universal" extension might eliminate the anomalous total pressure losses for more than one bellmouth that include unsealed gaps that would necessarily exist between the bellmouths and the "universal" extension.

3. Determine the limits of radial and axial gaps that can be employed without introducing other unacceptable flow quality degradations such as excessive boundary-layer thickening, flow distortion, or increased turbulence. Flow distortion might result from nonsymmetric reattachment of the extension flow to the bellmouth, for example, or as an unacceptable increase in turbulence.

The work reported herein was conducted under two different projects: Job Number 0096, Facility Technology Advancements, and 1929, Improved Turbine Test Technology. The effort under 0096 was accomplished during FY93 and was primarily concerned with determining the cause and a "fix" for the flow anomaly. The effort conducted under 1929 was accomplished in FY94 and involved a subscale test to try to develop a "universal" fix for the AEDC Propulsion Development Test Cells and to complete the FY93 data analysis.

2.0 APPARATUS

2.1 GENERAL

A 1/6th linearly scaled Plexiglas® model of the Test Cell T-2 plenum was installed in the Icing Research Test Cell R1D. The installation is shown schematically in Fig. 2, and an installation photograph is shown in Fig. 3. The R1D test cell was configured to utilize the Von Karman Facility (VKF) high-pressure air system as the air source. The instrumentation used during the test is shown in Figs. 4 and 5. The flow visualization and recording instruments, shown in Fig. 4, consist of a smoke injection probe, a still camera, a laser with a polarizing lens to create a light sheet, a video camera and recorder. A Helium-Neon laser (Red) was used during FY93 testing, and an Argon-Ion laser (Green) was used during FY94. The switch to the green laser was done to provide better contrast on the videotape. In addition, the laser installation was modified to allow more flexibility in viewing the plenum model.

During FY93, the bellmouth flow-field pressure measurements were made with a five-hole cone probe and two pitot pressure probes. A photograph of these probes is shown in Fig. 5. The cone probe had a 20-deg half angle and a 1/8-in. diameter and was located 2 in. downstream of the bellmouth exit plane. The two pitot tubes were in the same horizontal plane as the cone probe and offset 1-1/2 in. on either side. The probes were mounted on a remote-controlled traversing mechanism which allowed a vertical traverse similar to data collected in the Test Cell T-2 cold flow bellmouth test.

The probe took approximately 20-40 sec to complete a traverse, depending on the diameter of the bellmouth. The 7 sec per inch movement was slow enough to prevent any transient effects on the probe measurements. A pitot probe was also made that could traverse the plenum, as warranted, based on an examination of the cone probe data. This probe was a 1/8-in.-diam tube with a pitot orifice approximately 1 in. from the brazed end of the tube. All pressure and temperature data were recorded on a personal computer (PC) data acquisition system which used a sixteen

channel, in-place calibrated, electronically scanned pressure measuring system. The use of this system allowed the review of the pressure profiles obtained on-line and helped to guide the test plan.

During FY94, the bellmouth flow-field pressure measurements were made with the same five-hole cone probe and seven pitot pressure probes replacing the previous two. The additional pitot probes were the same design as the existing pitot probes. All of the cone probe data were taken without smoke generation. In addition, the pressure rake was parked outside of the bellmouth exit during smoke generator operation to protect a pressure orifice from becoming clogged with residue from the smoke generator. In addition, there were five dynamic pressure transducers used during the FY94 tests. Two of these transducers were installed on the traversing rake, two in the downstream plenum model wall that the bellmouth penetrates, and one mounted in the R1D facility 12-in. duct just upstream of the model.

The smoke generator is shown in Fig. 6 and consisted of two short pipe sections, a cigar, and 5-psi shop air. The smoke generator was attached to an injector tube (1/16-in.- diam stainless-steel tubing with a 0.040-in. wall) that could be inserted into the plenum model at several axial and circumferential locations.

Additional details of the test apparatus are given in the following sections.

2.2 SUBSCALE MODELS

The subscale T-2 plenum was designed to replicate the Test Cell T-2 plenum. Given the ducting sizes available in R1D, a 1/6th scale was chosen for the models. The plenum design included the manways (entrances into the plenum), the handholds used to assist entering the plenum, the foreign object damage (FOD) screen, and the flow-straightening honeycomb. Geometric scaling was used for all components of the subscale installation, including the FOD screen wire size and the honeycomb for the flow straightener. In the original test plan, the manways were to have two configurations--with a cavity exposed to the flow and with covers which were smooth with the plenum wall. The manway covers were installed when the plenum model was received and were never removed during testing since the vortices were present with the covers in place.

There were three baseline bellmouth configurations (Figs. 7 through 9) used during the study. These figures and the ones describing the cone extensions first present a photograph of the bellmouth or extension followed by a schematic. These bellmouths had diameter ratios of 0.25 (Configuration A), 0.375 (Configuration B), and 0.5 (Configuration C). The diameter ratio (DR = d/D) is defined to be the full-scale bellmouth exit diameter (engine inlet diameter), d, divided by the full-scale plenum diameter, D. To further illustrate the three configurations, the bellmouth inlet lip diameter to plenum diameter was 0.383, 0.74, and 0.986 for Bellmouths A, B, and C, respectively. Therefore, there is a significant gap outside Bellmouths A and B, but Bellmouth C reaches nearly to the plenum wall. Configurations A (Fig. 7) and C (Fig. 8) are models of bellmouths typically used in Test Cells T-2 and T-1, which have 6-ft-diam plenums. Configuration B (Fig. 9) is a model of a bellmouth typically used in Propulsion Development Test Cells C-1, J-1,

and J-2, which have 8-ft-diam plenums. All configurations used the same model plenum, therefore Configuration B was 1/8th scale based on plenum diameter but secondary features such as FOD screens and manways were unchanged. The inlet contours for Bellmouths B and C are made of two circular arc segments (Figs. 8b and 9b, respectively), while the inlet contour for Bellmouth A (Fig. 7b) is made of an elliptical segment. These contours were geometrically scaled for the subscale models.

During FY93, conical extensions for Bellmouths A and B were fabricated and tested. The Configuration A extension, Fig. 10, was a 45-deg conical extension that was machined integral with the Bellmouth A; i.e., a one-piece combination of bellmouth and extension versus the two pieces that were used for Configuration B. The Configuration B extension was also a 45-deg conical extension rolled as a separate piece and attached to Bellmouth B using a flanged joint. The internal surface where the two pieces met was sealed with RTV to create a relatively smooth transition surface. A 90-deg extension was also made and tested for Configuration B.

For FY94, a series of extensions for Bellmouths A and B were fabricated. These extensions, Fig. 11, were used to investigate the effects of axial and radial gaps and the impact tangency of the mating surfaces might have. These extensions were rolled using a brake machine and did not produce as smooth an internal surface as the extensions that were rolled without using the brake machine in FY93. Using the brake machine also produced upstream and downstream surfaces that were not as flat (perpendicular to the conical extension longitudinal centerline) as those produced in FY93. It will be shown that this fabrication technique impacted the test results. Conical extensions of 30, 45, a combined 30/45, and 60 deg were fabricated for Configuration A. Only 45-deg extensions were fabricated for Configuration B.

2.3 PRESSURE PROBE RAKES

Several probe rake configurations were used to traverse the subscale bellmouth exit plane and the plenum flows during the separate phases of this work. The bellmouth exit plane rakes were mounted on a screw-driven slide table and were driven vertically by a manually controlled DC motor at a nominally constant rate of about 0.16 in./sec. A schematic of a typical rake installation in the subscale test cell is shown in Fig. 12. The relative positions of the bellmouth rake, the bellmouth exit plane, the pressure sensing ZOC® module, and the slide table located in the test cabin are indicated. The relative positions of the transparent plenum model, which replaced a section of the air supply piping for the test cell, and the plenum pitot pressure rake are also illustrated in Fig. 12. The rake pressure sensing lines were routed directly to a Scanivalve® pressure sensing ZOC unit which was mounted on the rake traversing mechanism, as close as possible to the pitot probes to achieve fast time response.

The plenum flow rake which clamped directly on the exterior of the Plexiglas plenum at one of a number of circumferential and axial positions along the model plenum was used to radially traverse across the diameter of the plenum. The plenum pitot probe consisted of a 1/8-in.-diam tube sealed at one end with a single orifice drilled into the upstream facing surface on the cylindrical stagnation line, one-half in. from the sealed end. The plenum rake is also illustrated in Fig. 12, showing the 1/8-in. pitot probe tube penetrating the plenum wall through an unsealed, small clearance hole.

The routing of bellmouth exit rake pitot probe plenum static, bellmouth wall, test cell static, and atmospheric pressure, ZOC calibrate, reference and control pressure tubing is indicated on Fig. 12. The definition of coordinate systems describing model geometry is also shown.

Although only a single rake pitot probe is illustrated schematically, up to seven pitot probes spanning a horizontal plane were used to traverse vertically along the projection of chord lines of the bellmouth exit. Up to three pitot probes in a vertical line were also employed to survey the entire exit when the bellmouth was removed. Such overlapping probes were required for covering the 12-in. exit with an 8-in. mechanism stroke. All bellmouth exit surveys were made with pitot probe tips 2 in. downstream of the bellmouth exit plane. Photographs illustrating various aspects of the probe/rake installations are shown in Figs. 13 through Fig. 17.

The location of the chord lines traversed by each bellmouth rake probe and the plenum diameter traversed by the plenum rake for each phase of testing are illustrated on the diagram in Fig. 18. The vertical and horizontal locations of each probe tip when the rake is located on the horizontal centerline of the bellmouth exit are shown in Fig. 19. The orientations of the Kulite® acoustic pressure transducers are also shown in Fig. 19.

A slow response pitot probe, located at the apex of the flow angularity probe, had the smallest diameter orifice and tubing and was the more highly damped of the orifice-tube-transducer systems. Consequently, this probe is the primary source of the quasi-steady-state pressure profile used to evaluate the distortion parameters at the bellmouth exit since it is least sensitive to facility turbulence. The other higher response (larger orifice) pitot probes were used primarily for detecting sudden pressure changes that could represent the presence of a vortex.

Acoustic pressures are used for detecting resonance between the bellmouth exit flow and other regions of the flow where the sensors were located. The Kulite acoustic pressure sensors mounted on the bellmouth rake were also used to compute turbulence parameters (Section 4.4.3).

2.4 INSTRUMENTATION

A Scanivalve® Corporation model Hyscan 2000 personal computer (PC) based system with self-contained data sampling, processing, and system calibration capability was used to sense and record probe pressures. The pressure measurement system is shown schematically in Fig. 20.

The principal components comprising the Hyscan 2000 system include:

1. A model ZOC 14 electronically scanned pressure sensor module containing 16 solid-state 15-psid pressure sensors. Each probe pressure orifice was "hard-plumbed" to a separate sensor for continuous recording capability.
2. A model DAQ 2002 data acquisition system capable of sampling and transmitting calibrated data at rates up to 50,000 measurements per second.
3. A model CALMOD 2000 calibration module incorporating a Mensor Corporation Quartz Bourdon Tube traceable, secondary-pressure-standard Model 11603 (0-15 psid range).

To minimize time response of the pressure measuring system, the ZOC 14 pressure sensor module was mounted inside the cell on the traversing rake mechanism to maintain the smallest practical tubing lengths. The experimental response of a typical pressure tubing system to a step change in pressure is shown in Fig. 21. A first-order system time constant of about 0.01 sec has been inferred from these data. The pressure sensor module was insulated, and its mounting plate was conditioned with water flow to limit temperature excursions and subsequent thermal drift of the sensors during cell temperature changes. .

One channel of the ZOC 14 pressure sensor module was used to measure local atmospheric pressure with tubing that penetrated the test cell wall to the outside, as indicated in Fig. 3. This atmospheric pressure was continually compared with the local precision barometric pressure to detect thermal drift of the ZOC 14 transducer module and to ascertain the need to recalibrate the system on-line to maintain the uncertainty within established limits.

Acoustic pressure data sensed with Kulite transducers were recorded on the facility magnetic tape system for posttest analysis. Two Kulite Semiconductor, Inc. Model XDBL-093-5D 5-psid pressure transducers were mounted on the traversing rake, as illustrated in Fig. 12. Two Kulite model XT-190-25D 5-psid transducers were mounted in the downstream plenum model bulkhead, and a third was mounted upstream of the plenum model in the R1D facility 12-in. ducting to give an indication of facility acoustic pressure signature. Besides being recorded on magnetic tapes, these acoustic pressure signals were also routed to a spectrum analyzer for on-line monitoring.

In addition to the probe rake pressures, the test cell static, bellmouth wall, and plenum wall static and pitot pressures were also measured.

3.0 EXPERIMENTS

3.1 TEST PROCEDURE

The general procedure for managing test cell operations, configuration changes, and pressure and smoke flow visualization data acquisition are described in this section. These procedures provided the planned framework for conducting the tests, which were then adapted and modified as required by circumstances.

To avoid contamination of the pressure measuring systems, pressure data were routinely recorded prior to the introduction of smoke for the flow visualization studies. Following injection of smoke for the flow visualization tests, pressure sensing orifices and lines were examined for smoke condensate and cleaned as required prior to acquiring additional pressure data.

Pressure data were acquired during rake traverses and fixed position dwells in the following manner.

1. Following installation of the desired model configurations and prior to initiating facility flow, the probe rake was positioned in a pre-test "park" position out of the bellmouth exit plane flow field, as shown in Fig. 13.
2. The Scanivalve pressure data acquisition system was then calibrated and allowed to stabilize with all channels sensing atmospheric pressure. Channel-to-channel com-

parison and comparisons with the precision barometric pressure verified test readiness when the instrumentation was operating within the established uncertainty bounds.

3. Flow was then established, usually beginning at M = 0.1 at the bellmouth throat.
4. The probe rake was then traversed downward about 8 in. through the bellmouth free-jet to a position out of the flow while recording each pressure channel at the rate of 40 data points per second or about 240 data points per inch of rake travel.
5. Following termination of data acquisition, the rake was immediately traversed upward while recording repeat data. Acoustic pressure data were also recorded by the Kulite system during these traverses.
6. Following the traverses, the rake was halted in three positions corresponding to the horizontal centerline of the bellmouth, the upper bellmouth wall projection, and the lower bellmouth wall projection, respectivefully. These positions included regions of high pitot pressure fluctuation levels. Both fast response conventional pitot pressure, recorded with the Scanivalve pressure system, and acoustic pressure were acquired for 60 sec at each of these three fixed dwell positions. Acoustic pressure data were of primary interest at the fixed rake positions for evaluating turbulence parameters.
7. The sequence of five tests was repeated for bellmouth throat Mach numbers of 0.3 and 0.6.

Since this research cell was supplied with air from the nominal 4000-psia Von Karman Facility (VKF) high-pressure air storage system, Joule-Thompson cooling was encountered during throttling to plenum conditions. During long duration tests at high mass flows, the test cell supply air cooled to a minimum of about 20°F. For shorter duration and lower mass flow tests, the instantaneous Joule-Thompson cooling effect combined with the thermal mass of the entire test cell/supply piping complex resulted in ambient test cell temperatures between ambient and this 20°F minimum. The pressure sensor module water conditioning and insulation jacketing maintained a constant module temperature for short duration/low mass flow tests, but allowed the transducer module to drift to cooler temperatures at high mass flows and for longer duration tests.

The Scanivalve system was usually recalibrated two or three times, as required by observing the output of the atmospheric pressure sensing channel during the described sequence of testing, to minimize thermal drift for the purpose of maintaining the measurement uncertainty presented later in this section.

Larger biases in the uncertainty were allowed to develop between Scanivalve data channels during tests for which the Scanivalve data were not of primary interest, such as during the acoustic pressure tests at fixed rake position. The increased uncertainty associated with these test procedures is described in a later section. The same procedure was used with the Scanivalve data acquisition system for all other unique tests conducted, including pitot pressure traverses in the plenum.

A summary of the test conditions and type of data acquired during these subscale tests is presented in Table 1, including bellmouth test conditions and type of data acquired, as well as indicating the bellmouth, extension, and plenum geometry. A schematic showing the reference plane for the axial and radial gap measurements is shown in Fig. 22.

3.2 DATA REDUCTION

3.2.1 Plenum Stagnation Pressure

The ratio of bellmouth pitot pressure and plenum total pressure was used for evaluating flow quality since this parameter is usually a direct measure of local total pressure loss. Since this pressure ratio was essentially constant in a flow with small quasi-steady, time-varying supply pressure excursions, its use also eliminated the concern of confusing an instantaneous pressure reduction in the facility supply with a total pressure loss in the bellmouth.

As is often done in full-scale facilities, the plenum static wall pressure was measured instead of the desired plenum stagnation pressure during these subscale tests. For a small bellmouth diameter relative to plenum diameter and for lower bellmouth Mach numbers, the difference between plenum wall and stagnation pressure becomes small compared to measurement uncertainty and can be neglected. However, the difference between plenum wall and stagnation pressure becomes significant for larger bellmouth diameters and higher Mach numbers. A first-order estimate of the plenum stagnation pressure can be computed for these cases by estimating the plenum one-dimensional (1-D) Mach number from isentropic flow relations and the geometrical area ratio of the plenum and bellmouth. The total pressure computed in this manner may be used for the intermediate bellmouth diameters and Mach numbers of the subscale study with negligible error. However, when this simple geometrical model was applied for the larger bellmouth diameter and higher Mach number test conditions, the computed stagnation pressure was substantially less than the bellmouth core-flow pitot pressure (relative to pressure measurement uncertainty). Plenum pitot pressure surveys for a particular large bellmouth/high Mach number test case showed that the geometrical area ratio model (1-D flow assumption) underpredicted the average plenum Mach number, because of a reduction in the "effective" cross-sectional flow area in the plenum arising from flow separation downstream of the FOD screen retaining flange and from boundary-layer growth.

An effective plenum-to-bellmouth area ratio, computed from these plenum survey results, was applied to other large bellmouth/high Mach number test data as an approximation for estimating the *average* plenum stagnation pressure. Anticipated results were found; i.e., the computed average plenum stagnation pressure and the nearly constant bellmouth core-flow pitot pressure profile agreed within the measurement uncertainty for all except the largest bellmouth/highest Mach number tests.

For these tests, an apparent significant spatial variation of the pressure ratio parameter was found, above and below the expected valve of unity, in the bellmouth central core region. This spatial variation was a result of the spatially varying bellmouth pitot pressures being ratioed to an average (constant) computed plenum stagnation pressure. Although this spatial variation could

be misinterpreted as a spatial variation of total pressure loss in the bellmouth core flow, the explanation was believed to be a result of plenum pressure nonuniformities. In fact, spatial variations of pitot pressure were found during plenum surveys at these test conditions. The magnitudes of the pitot pressure variations across the plenum and bellmouth core were found to be similar, with differences explained by differences in axial plane. These spatial variations in plenum pitot pressure appear to arise from nonuniformities introduced by the vane/screen section since the character of the plenum total pressure variation (as well as the bellmouth total pressure variations) changes dramatically with different rotational orientations of the vane/screen section. Examples of plenum and bellmouth pitot pressure surveys illustrating these flow characteristics are presented in Section 4.0 entitled Discussion of Results.

Because of the limited plenum surveys obtained, no attempt was made to find the local plenum stagnation pressure on each streamline corresponding to a bellmouth pitot pressure measurement. It is merely pointed out that the bellmouth core variations of the pressure ratio parameter do not represent bellmouth total pressure loss in all cases for higher Mach number/largest bellmouth tests, but merely the variation of total pressure in the plenum. Consequently, these variations may be ignored for the purpose of evaluating "bellmouth" distortion and turbulence parameters based on "loss of total pressure" in these cases. However, these variations do represent lateral gradients in axial velocity and may be important for other measures of flow quality.

3.2.2 Flow Quality Parameters

A classical technique for assessing the quality of bellmouth flows for the purpose of direct-connect turbine engine testing was to compare experimentally determined measures of flow quality with independently established criteria. One such procedure employed a bellmouth pitot rake with typically 40 probes in an area-weighted spatial distribution, as recommended in Ref. 1. Such rakes normally measure both the steady-state and fluctuating components of pitot pressure (with specified frequency response usually based on turbomachinery rpm) at each probe location. Measures of flow quality computed from these pitot pressure results include distortion and turbulence.

Distortion is a measure of flow quality computed from the steady-state value of pitot pressure over a region specified, a priori, by the locations of the pitot probes and is defined as the difference between the maximum and minimum steady-state pressures in the region ratioed to the area-weighted average pressure in the region. Although classical inlet distortion cannot be computed for these subscale tests because data were not acquired at the standard 40 relative probe locations, a relevant inlet "distortion parameter" was defined for the subscale tests. The distortion parameter was defined for these subscale tests as identical to the classical inlet distortion parameter, except the definition is applied only to a single, representative chord line traversed by the rake (up to 1000 probe locations) instead of the conventional 40 specific area-weighted locations in the bellmouth cross-sectional area. The vertical extent of the bellmouth traverse over which the distortion parameter was to be evaluated, corresponding to the maximum radial location of a probe in the classical 40-probe array, was specified independently as follows:

1. For the subscale tests, the appropriate "core flow" region for which the computed distortion parameter was to be compared with criteria was the core flow outside of the

experimentally determined boundary-layer edge ($U_e/U_\infty = 0.995$) for the configurations with zero gaps. This definition should provide a distortion parameter that is directly applicable to comparing the effects of gaps at subscale and is useful for estimating the magnitude of the analogous classical inlet distortion expected at full scale.

2. For the purpose of turbine engine testing, turbulence is a measure of the maximum root-mean-square (RMS) of fluctuations about the steady-state pitot pressure at one of the 40 probe locations. Specifically, turbulence at each of the 40 probe locations is classically defined as the RMS of the fluctuations about the local mean value of pitot pressure ratioed to the weighted average of the 40-probe steady-state pitot pressures. For these subscale tests, a "turbulence parameter" analogous to the "distortion parameter" was defined for characterizing the flow quality associated with the fluctuating component of total pressure. As with the distortion parameter definition, the turbulence "parameter" was defined identically with classical definition of turbulence, except that the effective core was the same used for the distortion parameter.
3. For the purpose of computing the distortion and turbulence parameters, the average total pressure in the central core region of the bellmouth, excluding the reduction associated with the boundary-layer edge, was taken as the appropriate average over the entire effective core. This procedure was somewhat conservative since the only significant variation in total pressure across the core was the *reduction* associated with the approach of the boundary-layer edge.

The definitions of distortion and turbulence parameters are illustrated schematically in Section 4.4, along with summaries of the parameters computed from the subscale tests results.

4.0 DISCUSSION OF RESULTS

This section is comprised of observations and comments on the results of the experiments conducted. The following subsections include results on flow visualization, effects of the bellmouth total pressure losses, effect of the extension gaps on bellmouth flow fields, flow quality, measurement uncertainity, and turbulence effects on the rake pressure results.

4.1 LASER/SMOKE FLOW VISUALIZATION

Bellmouth vortices were suspected of being the mechanism that causes the large, unsteady total pressure losses in full-scale turbine engine test cells. The smoke flow visualization phase of this subscale work was designed for the purpose of demonstrating that vortices existed in the presence of total pressure losses similar to those observed at full scale. Additionally, to demonstrate a causal relationship, it needed to be shown that bellmouth vortices were not present if the pressure losses were eliminated by some corrective action such as the addition of bellmouth extension.

The characteristics of the local bellmouth inlet flow conspired with smoke density, plenum velocity, and smoke injection techniques to produce high quality visual images of unsteady vorti-

ces under laser illumination. The vortices were observed at the bellmouth inlet for several bellmouth/Mach number combinations. These results provided the definitive proof of the existence of vortices in bellmouths without an extension.

A particularly good example of a single image from the videotape record is shown in Fig. 23 for the smallest diameter bellmouth (Configuration A) and lowest bellmouth Mach number (M = 0.1). The location of this vortex relative to the subscale test cell is illustrated in Fig. 24. It is noted that the velocity in the plenum for these flow visualization results was the lowest encountered for these tests and as will be seen, the results of these smoke tests suggest that plenum velocity may have been an important parameter influencing vortex formation, intensity, and/or frequency and amplitude of the unsteady motion about some preferred location, and for visual detectability.

The vortex for this case was visually intense and persistent but moved substantially about the position indicated. For short periods of time, the vortex was not illuminated at this location, suggesting the discrete vortex moved erratically over large distance but remained at a preferred location long enough to be captured instantaneously on the video record. The visual evidence could rather imply, perhaps, the repeated formation and collapse of separate vortices.

The smoke injection technique, itself, was not believed to significantly contribute to the perceived vortex motion since similar results were obtained as the flow visualization technique was improved and modified. As the Mach number was increased for Configuration A bellmouth, the visual evidence of vortices was more and more diffuse and dispersive with only furtive glimpses of a discrete vortex core materializing under smoke illumination. For the larger diameter bellmouths, definitive vortex cores were never captured on videotape and were only rarely perceived as spurious rotations by observers. However, for these higher plenum velocity cases, the smoke at the bellmouth inlet exhibited a diffuse, unstructured form with high-frequency unsteadiness which possibly obscured visual clarity.

The apparent frequencies of the unsteadiness of the vortex motion at low plenum velocity to the unsteadiness of the diffuse, unstructured smoke patterns at high plenum velocity increased with plenum velocity. The plenum velocity increased by a factor of greater than 15 from the minimum Mach number for the smallest diameter bellmouth to the maximum Mach number for the largest diameter bellmouth.

As the plenum velocity increased, there was a lack of visual evidence of the existence of vortices in all bellmouths at all Mach numbers. This loss of visually perceived vorticity was consistent with an increasingly rapid unsteady fluctuation of the vortex posistion with increased plenum velocity. Hence, an individual vortex may not reside in one place long enough to produce a good image, and the smoke to produce the image was further diffused throughout a larger volume.

The visualization of a vortex with high plenum velocity was also difficult because the smoke filaments produced under these conditions in the plenum upstream of the bellmouth were generally diminished in intensity. This may have resulted from the smoke flow rate not increas-

ing with streamtube mass flow, as well as filament dispersion. The latter would increase at the higher tubulence that accompanied increased plenum velocity or from turbulence from the smoke probe.

The bellmouth total pressure loss results described in the next section also suggested that rapidly moving discrete vortices or some other source of distributed vorticity existed under conditions of higher plenum velocity for some bellmouths. Further results of the flow visualization test revealed that smooth streamline flow existed at the bellmouth when extensions presented a conical, acute approach angle of less than 60 deg. Under these conditions, the flow visualization data indicate that the addition of an extension was effective in suppressing the formation of bellmouth vortices.

4.2 EFFECTS OF EXTENSIONS ON BELLMOUTH TOTAL PRESSURE LOSSES

The unsteady, unsymmetrical, and localized nature of the total pressure losses that were typically found for the bellmouths without an extension (with the small bellmouth to plenum diameter ratio) is shown in Fig. 25. This figure illustrates four repeat traverses downstream of the exit plane in which the general magnitude of the maximum total pressure loss was approximately the same for each repeated traverse. However, the distribution of losses did not repeat and appeared to vary randomly which also suggested that a discrete vortex was moving over the core in a rapid, erratic manner. The discrete vortex was consistent with observations from the flow visualization results and was responsible for the total pressure losses.

The effect of adding conical extensions to the inlets of the bellmouths for each Mach number tested to eliminate the discrete vortices is shown in Fig. 26 for Bellmouth A (DR = 0.25) and Fig. 27 for Bellmouth B (DR = 0.375). Figure 26 shows that adding a conical, 45-deg half-angle extension to Bellmouth A (the smallest diameter) completely eliminated the total pressure losses in the core of this bellmouth for each Mach number. The character of the total pressure losses without the extensions was completely different for each of the three Mach numbers, similar to what was found for the repeat traverses of Fig. 23 for a single Mach number. Because of the erratic nature of the total pressure losses, no further generalizations were drawn from these data except to note that while the loss of total pressure as a fraction of the plenum total pressure varies between Mach numbers, the fractional loss of total pressures as a percent of *dynamic pressure* was essentially constant. Also, there appears to be somewhat less vortical activity for the lowest Mach number (Fig. 26).

The effect of adding a 45-deg conical extension to Bellmouth B (the intermediate diameter) was also found to completely eliminate any vortex activity in the bellmouth for each Mach number (Fig. 27). The characteristics of the vortex activity for Bellmouth B was similar to that found for Bellmouth A at Mach numbers of 0.1 and 0.3, where the vortical activity seemed to occur as isolated spikes. While at M = 0.6, the Bellmouth B apparent vorticity appeared almost as a continuum distribution across the entire freejet flow. This suggested that the vortex was moving rapidly over the entire bellmouth flow for these higher plenum velocities and did not remain at any position for a significant period of time, since the isolated "spikes" of total pressure loss separated by regions of nearly loss-free regions observed for the smallest diameter bellmouth (Fig.

26) were not found. A 90-deg extension was also fitted to Bellmouth B (Fig. 27). This 90-deg extension did not eliminate the apparent vortex-induced total pressure losses. In fact, the character of the losses was essentially unchanged with respect to the effect of Mach number, since isolated total pressure loss spikes were also found at M = 0.1 and 0.3, whereas at M = 0.6, a more continuous distribution of total pressure loss was found. The approximate magnitude of the total pressure losses was also unchanged with and without the 90-deg extension. Significantly, however, the distribution of the total pressure losses has materially changed; in fact, the regions of higher total pressure loss have almost swapped positions with the regions of lower pressure loss found for the bellmouth without extension. This was interpreted to mean that the addition of the 90-deg extension simply moved the preferred location of the vortical activity without changing its nature.

Pitot pressure surveys for the largest diameter bellmouth (Configuration C) tested are presented in Fig. 28 for the three test Mach numbers. Bellmouth-only results are shown since no extensions were fitted, because the diameter of the bellmouth inlet is nearly equal to the plenum diameter. For the two higher Mach numbers, a larger deviation from a flat profile of total pressure existed over the bellmouth exit, which included a significant change in total pressure over about 30 percent of the core diameter.

Total pressure decrements were not detectable as an individual isolated spike, implying that a loss mechanism, if it existed, was due to a very rapidly fluctuating vortex system, as suggested previously for Configuration B at the high plenum velocity condition. There was no resolvable total pressure decrement at M = 0.1, which might indicate that the total pressure decrements at Mach = 0.3 and 0.6 may be due to plenum total pressure gradients and not bellmouth total pressure losses. When vortical activity was detected in the two previous bellmouths using flow visualization, it appeared at all Mach numbers evaluated. The total pressure data were replotted in Fig. 28b ratioed to bellmouth dynamic pressure. This type presentation exaggerated pitot pressure gradients (as well as measurement randomness and response to cell turbulence) in the core, but permits detection of total pressure gradients at M = 0.1 on a common basis with the two higher Mach numbers. The presentation in Fig. 28b demonstrated that similar distributions of total pressure gradients occured for each Mach number (including now M = 0.1). Recall that although no discrete vortices were detected in the flow visualization results for this bellmouth, a very high-frequency, general unsteadiness was observed in certain regions of the bellmouth inlet, perhaps suggesting some type of rapidly fluctuating or distributed vortex activity.

The increased randomness of the total pressure in the regions of reduced total pressure between a rake vertical position of 0 and 2 in. in Fig. 28 suggested a high-frequency, rapidly moving vortex could be causing a stagnation pressure loss and was responsible for this decrement in pitot pressure. However, there was also evidence to suggest that the gradient in total pressure across the core may have been associated with a gradient in total pressure across the plenum. Recall that the total pressure ratio results presented are formed with a constant plenum total pressure computed from the plenum wall static pressure.

Since it was suspected that any transverse plenum pitot pressure gradient (if it exists) might be introduced by the FOD vane/screen section, a repeat pressure survey in the Bellmouth C was

obtained at M = 0.3, with the vane/screen section oriented in a different circumferential roll position to determine if the bellmouth total pressure gradient changed as the FOD screen orientation changed. The results are presented in Fig. 29, which shows that the gradient was indeed strongly affected by the FOD screen orientation suggesting that the bellmouth total pressure gradients, at least partially, are caused by the total pressure gradient in the subscale plenum. Thus, there is evidence to suggest that the total pressure gradient at larger bellmouth exit may be caused by either total pressure losses in the bellmouth associated with vortex activity, or by total pressure gradients in the plenum, or a contribution of both. However, on the basis of the data obtained during this study, the explanation for the spatial gradients in bellmouth total pressure distribution for the largest diameter bellmouth remains unresolved.

To gain further insight into the nature of the flow in the subscale plenum, the bellmouth was removed, and total pressure profiles were obtained with the bellmouth rake traversing across the freejet produced by the plenum exiting directly into the research cell test cabin. The profiles were obtained with and without the entire FOD screen system (vanes and screens) installed. The plenum Mach number for these profiles was 0.07 and is comparable to the Bellmouth B plenum Mach number with a bellmouth Mach number 0.6, as shown in Table 2. The results of these tests are illustrated in Fig. 30, indicating the FOD screen system indeed introduced a variation of total pressure across the plenum. The existence of such plenum pressure gradients was important and considered in the interpretation of bellmouth/extension performance in the following section.

4.3 EFFECT OF EXTENSION GAPS ON BELLMOUTH FLOW FIELDS

The general characteristics of the bellmouth exit pitot pressure surveys are examined in this section to develop insight into the detailed effect of the addition of extensions to the bellmouth. The individual effects of the radial and axial gaps between the bellmouth and extension are examined. The effect of variation in the conical half-angle of the extension is also evaluated. Because of imperfections (lack of perfect cylindrical symmetry) in the as-built geometry of the extension and perhaps in other components of the subscale plenum model, it was found that the circumferential roll orientation of the extension about the subscale plenum axis had a significant effect on bellmouth exit total pressure distributions for certain conditions. As shown in the last section, the details of the FOD geometry may also have an influence on perceived bellmouth/extension performance, as indicated by pitot pressure traverses.

These issues are examined in the present section to provide a basis for the quantitative assessment of bellmouth exit flow quality presented in the next section. Recall that the addition of extensions always eliminated bellmouth vortices, hence vortices per se are not an issue in the analysis of data in this section. The data for each of the two bellmouths, A and B, for which extensions were employed are addressed separately in the following sections.

4.3.1 Bellmouth A (DR = 0.25)

4.3.1.1 Axial Gap Varied, No Radial Gap

The effect of increasing axial gap for a fixed radial gap of zero is illustrated in Fig. 31 for each of the conical half-angles employed (30, 45, combined 30 and 45, and 60 deg). The core

region of nearly constant total pressure ratio is found to decrease in lateral extent as the axial gap is increased for each of the conical half-angles.

For the 30-deg conical half-angle (Fig. 31a), the "constant core" region diminishes uniformly and symmetrically as the axial gap is increased; whereas for the 45-deg conical half-angle (Fig. 31b), a significant nonsymmetry develops for the largest axial gap. The extension with a combined 30-deg and 45-deg conical half-angle (Fig. 31c) exhibits characteristics similar to the results for the 30- and 45-deg half-angle extension and displays a similar nonsymmetry. Finally, the core region diminishes the maximum amount with increasing gap for the extension with the 60-deg half-angle (Fig. 31d), although the profile remains symmetrical.

The development of significant nonsymmetry in the bellmouth flow for large axial gaps at zero radial gap may be associated with the preferential reattachment of the flow "jumping the gap" from the extension. The preference may be a function of the inherent instability and hysteresis normally associated with separating and reattaching flow in a perfectly symmetric geometry and any imperfections (i.e., axial asymmetric) in the actual geometry.

The discovery that extension roll orientation effects were significant lead to the addition of tests with roll angle systematically varied for a large axial gap, a zero radial gap, and the extension with a 45-deg conical half-angle. The results on varying extension roll are illustrated in Fig. 32. These results correspond with and ideally would be expected to reproduce the data of Fig. 31a for an axial gap of 1.67 in. with the roll orientation unknown.

Clearly, the bellmouth total pressure traverses for each of the four known roll positions of Fig. 32b and the unknown roll configuration of Fig. 31a vary significantly and do not appear to bear a simple relationship with the extension roll orientation. These results suggest that the nonsymmetrical attachment of the flow on the bellmouth inlet is probably controlled by geometric imperfections in the extension or the other components of the plenum model.

The above type of nonsymmetrical total pressure profile was generally observed for geometries with large axial gaps relative to the radial gap. For theses conditions, the freejet leaving the extension outlet probably contracts to a cross-sectional area less than the bellmouth inlet, permitting a region of preferential attachment of flow to the bellmouth. The preference in turn is controlled by the local details of the plenum/extension geometry.

4.3.1.2 Axial Gap and Radial Gap Varied

The effects of increasing axial gaps for three fixed radial gaps are compared in Fig. 33 for the conical extension with 45-deg conical half-angle. For convenience, Fig. 33a reproduces the results of Fig. 31a for zero radial gap exhibiting the asymmetrical profile noted for the largest axial gap (1.67 in.). For a radial gap of 0.85 in., the profile exhibits some modest nonsymmetry for intermediate axial gaps but has a significantly reduced core region (although reasonably symmetrical) for the large axial gap.

For the largest radial gap of 1.38 in., Fig. 33c, the profile behaves as just described for the radial gap of 0.85 in. except that the nonsymmetry of the profiles appears more exaggerated. It is

pointed out that all of the results presented in Figs. 31, 32, and 33 were obtained before the importance of extension roll orientation was discovered and hence these results are for random roll orientations.

The small geometrical model imperfections are believed to have an influence on the data only for combinations of the radial and axial gaps that force the flow to turn substantially to attach to the bellmouth. For smaller radial and axial gaps, asymmetries were never observed, implying that roll orientation was not important for these cases. The small gap configurations are the ones found in the bellmouth flow quality section that will satisfy flow quality criteria.

The bellmouth total pressure profile data presented in this section were obtained for the highest Mach number of 0.6. It is shown in the following that the profile data formulated as a percent of dynamic pressure are independent of bellmouth Mach number. It should be pointed out that data for the several Mach numbers were obtained without disturbing the configuration for model changes. Hence, asymmetries associated with geometric imperfection are expected to be constant for each Mach number for a specific configuration and, hence, represent a bias that cancels with inlet Mach number comparisons. The following results show this to be the case:

1. The effects of increasing axial gap for fixed radial gap of zero and fixed extension conical half-angle of 45 deg are shown in Fig. 34 for Mach numbers of 0.3 and 0.6. Figure 34a is a reproduction of Fig. 31b for convenience.
2. Comparing total pressure ratios for the two Mach numbers of Fig. 34 shows that the profiles of each individual configuration are similar. The results for a particular axial and radial gap from Fig. 34 are replotted on Fig. 35a for the three Mach numbers. Clearly, the profiles are related but not identical. These data are replotted in Fig. 35b as a fraction of dynamic pressure for each Mach number. The profiles for different Mach numbers become essentially identical in terms of this parameter, for this example, an asymmetric core.
3. The effects of Mach number on bellmouth pitot pressure profiles are shown in Fig. 36 for a configuration with large axial and radial gaps, which typically results in thickening of the bellmouth shear layers and correspondingly reduced core flow dimensions. It is observed that when presented as a fraction of plenum total pressure, the profiles for each Mach number are similar, but not identical. When the data are reformatted and presented as a percentage of dynamic pressure, the profiles for each Mach number are essentially identical. This same result was found in Fig. 35 and is representative of all data for this bellmouth for each extension; i.e., for identical geometry, identical bellmouth pitot pressure profiles as a fraction of dynamic pressure were obtained.

4.3.2 Bellmouth B (DR = 0.375)

The effect of increasing axial gap on bellmouth exit total pressure profiles for three radial gaps is illustrated in Fig. 37 for the 45-deg conical half-angle extension. Asymmetries in the apparent thickness of the shear layer from side-to-side as well as increasing thickness of the

shear layers with increasing axial gap are observed, which are similar to the features found for Bellmouth A. Figure 38 demonstrates that the side-to-side asymmetry is also a function of extension roll orientation for Bellmouth B, as was found for Bellmouth A.

The small geometrical differences associated with roll orientation seem to have an influence on the profiles only for cases with larger axial and radial gaps where significant regions of separated and recirculating flow exist between the bellmouth and extension. Small geometrical differences may have a large impact on the details of the reattachment of the extensive flow to the bellmouth for these cases.

For small radial and axial gaps, where candidates for acceptable flow quality are found, extension roll had no detectable effect, as was the case for Bellmouth A. A significant feature of all the profiles in Fig. 37, that did not appear for Bellmouth A, is the occurrence of a significant nonuniformity in the distribution of bellmouth total pressure in the expected core region.

On initial examination, this spatial variation of total pressure across the core has the appearance of total pressures losses associated with flow through the bellmouth. However, these variations are shown to be artifacts of a gradient total pressure in the subscale plenum and not losses in the bellmouth. These gradients become significant for the higher plenum velocities in this bellmouth compared to Bellmouth A. Figure 39 illustrates bellmouth pitot profiles for three roll orientations of the FOD vane section. The spatial gradient of total pressure in the bellmouth is found to be a strong function of vane orientation, nearly disappearing for a roll angle of zero deg. These results are believed to confirm that the spatial gradients observed in the bellmouth profiles are not total pressure losses associated with the flow through the bellmouth, but are caused by gradients of total pressure in the plenum introduced by the FOD screen section in the subscale plenum.

Direct evidence of plenum total pressure gradients is presented in Fig. 40 where radial profiles of the subscale plenum pitot pressure are shown at two axial locations (1 and 10 in. downstream of the FOD screen) in the plenum. The axial station immediately downstream of the vane section exhibits very large changes in pitot pressure, reflecting the presence of vane-induced disturbances. For the axial station further downstream near the bellmouth inlet, the very large gradients of pitot pressure have been "washed out," leaving a radial distribution of pitot pressure reminiscent in magnitude and spatial variations of the distribution of pitot found in the bellmouth core. This finding confirms that pitot pressure variations in the core of this bellmouth can be attributed to subscale plenum total pressure gradient.

Consequently, the variation in total pressure across the bellmouth exit is not considered in the assessment of flow quality attributed to the bellmouth itself. The results for Bellmouth B were presented in Figs. 37 to 39 for the highest Mach number (0.6) tested because of the more favorable uncertainty associated with the corresponding higher pressure and pressure difference. However, it has been found that Mach number does not have any significant effect on the bellmouth exit total pressure profiles. Figure 41 compares results from Fig. 37a with the corresponding data for M = 0.3. The total pressure profiles are seen to be similar.

When the results are reformulated as essentially local dynamic pressure ratioed to core dynamic pressure, the profiles are found to be essentially identical at all Mach numbers, as was found in Bellmouth A. This result is illustrated in Fig. 42 for both a symmetrical core distribution case, represented by axial gap = 0.0, and a very nonsymmetric core, represented by axial gap = 1.67. Such strict Mach number independence of the total pressure profiles only exists for constant geometry, in particular, constant extension roll orientation at larger gaps.

These characteristics of the total pressure profiles provide a basis for the bellmouth flow quality assessment described in the next section.

4.4 BELLMOUTH FLOW QUALITY

4.4.1 Distortion

The effects of introducing nonzero axial and radial gaps between the bellmouth inlet and extension outlet on the bellmouth exit flow quality are assessed by comparing distortion and turbulence parameters computed from the bellmouth total pressure profiles with criteria established in Section 3.2.2. The geometrical region over which the criteria are to be applied is determined for each family of extensions (or single extension) as the experimentally measured core for that member of the family with zero radial and axial gap, as described in Section 3.2.1. Schematic diagrams illustrating the process of determining this geometrical core flow region and applying the distortion criteria are presented in Fig. 43, and an example with no gaps is shown in Fig. 44.

It should be noted that this process yields, in effect, a differential and not an absolute measure of flow quality since distortion is compared to criteria over an *experimentally determined core* for the zero gap configuration. Thus, the distortions for the nonzero gap configurations are evaluated relative to the zero gap case as a baseline, which may have unrecognized degraded flow quality. This is considered to be a rational approach since the goal of this work is to determine the effect of gaps themselves on bellmouth flow-field quality without regard to other additive experimental or subscale facility peculiar contributions. That is, the absolute flow quality associated with the complete experimental rig is not necessary for present purposes.

The application of the procedure for evaluating the distortion parameter for representative total pressure profile data is illustrated in Fig. 45 for Bellmouth A, for a series of tests with increasing axial gaps at zero radial gap. Figure 45a, for zero axial and radial gap, shows the determination of the core region for this family of increasing axial gaps. The pitot pressure difference ratioed to dynamic pressure is used for establishing the boundary-layer edge, because this parameter provides good resolution and is more directly related to boundary-layer edge velocity ratio definition. For completeness, these zero radial and axial gap data are reformulated as pitot to plenum pressure ratio in Fig. 45b to show the boundary-layer edge definition in terms of this parameter. The boundary-layer edge found in Fig. 45a is reproduced in Figs. 45c and d for increased axial gaps. It is observed that these two profiles pass the distortion parameter criteria. Figure 45d, for the largest axial gap in this family of extension configurations, shows that total pressure profile data failed the criteria.

The maximum distortion parameter for each bellmouth/extension configuration tested was established as demonstrated in Fig. 45. A summary of the maximum distortion parameters so obtained is presented in Fig. 46. Figure 46a shows that modest axial gaps can be tolerated without violating the distortion criteria. For large radial and/or axial gaps, the maximum value of the distortion parameter generally increases and finally becomes large and multi-valued when nonsymmetries develop in the total pressure, and extension roll orientation is varied, as discussed in Section 4.3. Figure 46b shows that for zero radial gap, the axial gap cannot be increased beyond the smaller increments without violating the criteria. Results for the Bellmouth B are presented in Fig. 47 and generally follow the same trends observed in Figs. 46a and b.

4.4.2 Mach Number Effect on Distortion

A distortion criteria of 0.5 percent has been established from the historical bellmouth flow quality database at AEDC as to what is both desirable and attainable in the state-of-the-art turbine engine test cells.

Distortion, as conventionally defined by the turbine engine testing community, represents the maximum total pressure difference found in the core as a percent of the core total pressure and not of the core dynamic pressure. This definition serves the purposes of the testing community since distortion relative to the total pressure at the turbine engine inlet face is the parameter of significance to engine performance, and not the relative distortion as a fraction of the dynamic pressure. Consequently, the distortion criteria limits used for judging flow quality may be expected to be Mach number dependent and must be, therefore, established for the appropriate bellmouth Mach number.

The 0.5-percent distortion criterion was determined from the historical AEDC database for high subsonic bellmouth Mach numbers. This is the relevant Mach number range for evaluating bellmouth distortion since current generation engines operate with high subsonic compressor inlet Mach numbers in flight, and, consequently, these are the conditions normally supplied to the engine during direct-connect testing. The 0.5-percent numerical value for distortion criteria has been used as the appropriate standard-of-comparison for the subscale bellmouth data obtained at Mach number = 0.6 and presented in the previous section.

As mentioned above, distortion, as appropriately defined for test cell bellmouth flow quality purposes, is not intended to be, is not appropriate for, and does not yield useful results when applied at lower Mach numbers, because it becomes excessively generous in assigning flow quality. For example, as the Mach number is lowered to approximately 0.085 ((just below the lowest Mach number (0.1) tested)), the static-to-total pressure ratio has risen to 0.995 such that only a 0.5-percent difference exists between static and total pressure, numerically the same as the M = 0.6 distortion criteria. The pressure ratio at this Mach number (0.085) therefore would imply that no possible distortion, including 100 percent loss of dynamic pressure, could violate the M = 0.6 distortion criteria. The result clearly demonstrates that a high Mach number distortion criterion, defined as a percent of total pressure, is not useful for judging relative flow quality at low Mach numbers. In fact, for the subscale test, no instance was found where the classically defined distortion at M = 0.1 and M = 0.3 exceeded the high Mach number distortion criteria. At M = 0.1, even

the losses associated with the vortex would not be large enough to violate the M = 0.6 distortion criteria. Consequently, the classical distortion parameters have not been presented for the M = 0.1 and M = 0.3 subscale tests because of a lack of meaningful criteria at these conditions and because the predominant interest in full-scale turbine testing is at the higher Mach number.

Although not of significance for turbine engine testing, for more general applications, the *relative* distortion of bellmouth flow as a function of Mach number may be of interest. A rational definition for such a *relative* distortion, which might imply the usefulness of a Mach number independent distortion criteria, would be the maximum total pressure change in a region as a fraction of the theoretical maximum available change; such as pressure loss or change as a percent of flow dynamic pressure or, nearly, equivalently, as a percent of the difference between total and static pressures. Representative bellmouth total pressure profiles are presented in terms of such a relative distortion parameter in Figs. 35 and 36 with Mach number as a parameter. The significance of these comparisons, which was suggested previously, is that the pressure profiles are virtually identical for each Mach number when presented as a fraction of dynamic pressure. This result implies that the relative bellmouth distortion, in both magnitude and distribution, is also essentially equivalent for each Mach number. This is a general result that applies to all profile data acquired during these subscale tests. The Mach number independence suggested by these results was not wholly expected, especially for bellmouth flows exhibiting severe, nonsymmetric distortion.

4.4.3 Turbulence

A significant acoustic coupling between the rake and the freejet flow was observed as the rake entered and exited the bellmouth freejet during a traverse for all bellmouth/extension combinations tested. This coupling consisted of an audible "whistle" heard in the insulated control room, as well as increased turbulence levels indicated by the rake-mounted acoustic transducer when the rake either traversed through or was parked near the edges of the bellmouth core flow. The "whistle" disappeared when the rake moved away from these positions, indicating that the "whistle" is an artifact of the position of the rake and not associated with any inherent aerodynamic process related to the bellmouth/extension geometry. An unknown part of the increased turbulence exhibited by the acoustic pressure transducer with the rake in these positions must also be attributed to the presence of the rake itself. Unfortunately, this coupling was found in the region of the bellmouth flow near the edges of the core flow determined above in which distortion and turbulence are to be compared with criteria.

Since the unknown rake-induced apparent turbulence could not be reliably extracted from the acoustic pressure signal by a simple universally acceptable procedure, the turbulence level associated with the presence of bellmouth/extension gaps could alone not be evaluated. However, a lower limit for the turbulence in the bellmouth was determined from the acoustic data obtained while the rake was parked near the axis of the bellmouth. These turbulence data are presented in Fig. 48 and show that the level of turbulence is essentially independent of the presence of axial or radial gaps or the particular extension employed for a given bellmouth. The level of turbulence was affected by the tested bellmouth, the turbulence being consistently higher in the Bellmouth B.

To explore the reasons for the affect, the rake turbulence data are replotted in Fig. 49 as a function of the turbulence parameter measured in the facility air supply ducting just upstream of the subscale plenum model. These turbulence parameters on the bellmouth centerline and in the facility ducting are seen to correlate in Fig. 49, suggesting that the bellmouth turbulence may be a function of the general facility background turbulence and not associated with the bellmouth and extension configurations. More circumstantial evidence for this source of the bellmouth turbulence is shown in Fig. 50 where the bellmouth centerline turbulence data are replotted as a function of facility mass flow. The data for all gaps collapse essentially to a single function of facility mass flow rate, basically independent of the details of the axial and radial gaps of any extension. The indicated turbulence level is nearly proportional to facility flow rate, suggesting these turbulence data are an indication of background facility turbulence and are not necessarily related to turbulence induced by the bellmouth extensions and gaps. It is believed that the facility possesses large background turbulence partly because the air supply is throttled from about 3500 to 4000 psia to near atmosphere in the test cell. It has been observed that even steady-state, large volume pressure transducers externally mounted and plumbed into the cell to obtain facility operating parameters "jitter" significantly in response to the imposed turbulence at the highest facility mass flows. The perceived audible "noise" associated with operation of this facility at high mass flow is also severe.

In conclusion, it is believed that no useful turbulence data with respect to extensions and gaps can be obtained from the acoustic probe fixed near the bellmouth centerline. The magnitudes of the indicated turbulence are associated with the test cell itself and should not be compared with criteria to assess the effect of gaps. However, the acoustic pressure data may be amenable to further useful analysis by subtracting (perhaps digitally) the acoustic profiles obtained during traverses through the bellmouth freejet for zero gap and nonzero gap configurations. If the audible whistle and associated unknown turbulence associated with rake position were common for the configuration with zero and nonzero gaps, then the difference would be a measure of the increased turbulence for the nonzero gap configuration over the baseline configuration with zero gap. The high background turbulence associated with the facility mass flow would also be eliminated by this procedure. This difference parameter is probably the turbulence measure of interest for assessing the change in bellmouth turbulence caused by introducing gaps between the extension and bellmouth. This analysis remains for the future.

4.5 MEASUREMENT UNCERTAINTY

4.5.1 Pressure Measurements

The conventional parameter used for assessing bellmouth flow quality is the profile of the ratio of local pitot pressure and plenum total pressure over the bellmouth exit. The region over which the measurement uncertainty of the pressure ratio must be established and controlled for purposes of flow quality determination includes the bellmouth "core" flow and enough of the adjoining boundary layer to accurately define its edge, i.e., deep enough into the boundary layer so that the resulting boundary-layer total pressure loss encompasses several times the maximum allowable flow quality distortion or turbulence criteria. Usually, pressure profile data are also acquired over the remainder of the bellmouth exit, including the wall shear layer. For the current

work, boundary-layer profiles were obtained across the entire freejet into the cell static pressure region, although only the limited region just described is used for assessing flow quality in a specified bellmouth core region.

The region chosen, somewhat arbitrarily, for maintaining measurement uncertainty for flow quality evaluation purposes of the present results includes the bellmouth core and into the boundary layer to a distance where viscous losses were approximately 20 percent of the core dynamic pressure. This is the region over which the uncertainty of the measured pitot pressure ratio must be considered and maintained within a small fraction of the distortion and turbulence criteria to extract useful flow quality results from the data. The pressure range over these regions used to assess flow quality is shown in Fig. 51 for each bellmouth Mach number.

Since the evaluation of flow quality consists of *comparing* the pressure ratio parameters computed (1) within a single pressure data channel during a traverse across the bellmouth exit; (2) from channel-to-channel results during a traverse; and (3) from channel-to-channel observations among separate traverses, a comparative uncertainty analysis (Ref. 2) may be appropriate. If the uncertainty introduced into the elemental bias and random errors of the pressure measurement itself for those calibration steps between the Scanivalve secondary standard and ultimate "truth" is small, the uncertainties in the computed pressure ratio may be negligible. This may occur since the small neglected calibration errors in the pressure calibrator are introduced equally into all pressure data channels so that the corresponding errors in the pressure *ratio* may be negligible.

A conservative estimate of the maximum estimated elemental bias and random errors in the calibration steps between the Scanivalve system secondary standard and the "truth" is ±0.02, ±0.001 psia, respectively. These values were derived from laboratory calibration and from routine field observations between the Scanivalve secondary standard and other calibrated precision instruments sensing the same pressure, normally atmospheric pressure. The maximum propagated uncertainty in pressure ratio caused by introducing the same constant elemental error of the Scanivalve secondary standard into each of the ZOC 14 sensors is 0.003 percent. This is at least an order-of-magnitude smaller than the computed uncertainty in the pressure ratio parameter arising from the observed interchannel drift of individual sensors, following calibration of the ZOC 14 module with the Scanivalve secondary standard, and hence, can be neglected. Consequently, a comparative type uncertainty analysis is appropriate where the elemental errors are derived from observed channel-to-channel differences between the sensors when sensing the same pressure.

The Scanivalve ZOC unit channel-to-channel elemental errors measured for several operating conditions ranging from short-term, temperature-stabilized conditions to long-term situations with known thermal drift are summarized in Fig. 51. As is normally the case with this class of instrumentation, the bias errors are greater than the random errors. The corresponding uncertainty for the derived pressure ratio parameters computed by propagating the elemental errors through the data reduction equation are also listed in Fig. 51. It is observed that for short-term thermally stabilized transducer calibration and operating conditions, the uncertainty in the pressure ratio parameter is small relative to distortion criteria to be introduced in a later section, indicating that the data are of high quality relative to the intended use of evaluating bellmouth

flow quality. The elemental instrument errors associated with the fluctuating component of the Kulite pressure data have been estimated to be approximately ±15 percent of reading.

4.5.2 Probe Position Measurements

The uncertainty in the indicated rake (i.e., probe) position can have a significant detrimental effect on the evaluation of bellmouth flow quality, since a drift in the indicated position could be misinterpreted as thickening of the bellmouth boundary layer into the core region with subsequent apparent increase in flow distortion.

The rake position potentiometer was numerically recalibrated for each set of traverse data using the known relative position of the mechanical rake stops and the bellmouth exit to minimize this source of error. Further, when the relative position of the rake stops and the bellmouth was disturbed, such as during configuration changes, corrections could be determined from the symmetry of the pressure profiles as the probes approached the projected wall location on opposite sides of the bellmouth. The residual positional uncertainty consisting of about equal bias and random contributions is ±0.03 in. The quality of the positional data is considered good for purposes of evaluating the distortion and turbulence parameters in these bellmouths.

4.5.3 Flow Quality Parameters

The distortion parameter uncertainty near the edge of the "core" flow region of interest is controlled by errors introduced in determining the edge of this core flow region. This is a result of the fluctuations in the steady-state total pressure ratio in response to flow turbulence combined with errors in the rake position during continuous traverses. The elemental errors in the pressure measurements themselves contributed negligibly to the distortion measurement uncertainty at the core edge. Since negligible distortion was found in the central regions of bellmouth flows for these subscale tests, the maximum absolute distortion parameter always occurs at the edge of the core as bellmouth boundary-layer or inviscid flow distortion encroach into the core region as gaps are increased.

Therefore, the uncertainty in distortion parameter near the edge of the core, estimated to be approximately ±0.001 in the distortion parameter, is the appropriate measure of the quality of the distortion parameter measurements. This uncertainty is about 20 percent of the 0.5-percent maximum allowable distortion parameters according to the established criteria. In the core region, away from the edge, the effect of core edge determination diminishes significantly, and finally the distortion parameter uncertainty is controlled by errors in the pressure measurements themselves. The distortion parameter uncertainty drops to about an order-of-magnitude less than for the core edge region. The uncertainty introduced into computed turbulence parameters by propagating individual elemental errors through the data reduction relationships is completely dominated by the uncertainty in the Kulite pressure transducer data and hence is taken to be equivalent. The uncertainty in the computed distortion and turbulence parameters are summarized in Fig. 51.

4.6 TURBULENCE EFFECTS ON FAST-RESPONSE PROBE RAKE PRESSURE RESULTS

The traversing pitot probe rake system was designed for reasonably fast time response to permit continuous traversing with negligible pressure lag for typical freejet pitot pressure profiles, and for detecting the passage of vortices from the accompanying sudden pressure pulse. As a consequence, the probes are more responsive to the level of turbulence in the facility flow than to a conventional 40-probe, steady-state rake used for evaluation in full-scale turbine engine test cells.

On initial inspection, these turbulence-driven fluctuations in the pressure data acquired by the Scanivalve system can be misinterpreted as random errors in the overall data acquisition process. To illustrate the effect of facility turbulence on the pressure data acquired with the Scanivalve data system, the response of several probes to a steady-state facility operating condition is shown in Fig. 52. The responses of two rake-mounted pitot probes parked near the center of the bellmouth exit (designated p9 and p6) are shown in Fig. 52, along with the response of the plenum wall static pressure (p12), and that of a rake-mounted pitot probe parked in a very high turbulence region in the bellmouth shear layer (p8). Also shown is the response of a Scanivalve channel plumbed through the test cell wall and sensing steady atmospheric pressure (p1) with no turbulence input and the response of a rake-mounted Kulite transducer directly sensing the turbulence input to a pitot probe located near the bellmouth axis (designated k2).

The very small randomness exhibited by channel p1 represents the fundamental random instrumentation error of the Scanivalve data acquisition system and is consistent with the precision index presented in Fig. 51. Recall that channel p1 has no applied turbulent forcing function since it senses steady-state atmospheric pressure. Therefore, this result demonstrates that no unknown contributors to instrumentation randomness (for example, transducer acceleration) are influencing the data from any other Scanivalve channels, since all such channels are commonly mounted in a single pressure transducer module (designated ZOC 14) with channel p1. However, the other Scanivalve channels depicted on Fig. 52 are plumbed to locations inside the test cell and are consequentially exposed to test cell or bellmouth shear layer acoustic turbulence. The apparent high levels of randomness in these internally plumbed channels reflect the test cell acoustic turbulence or bellmouth shear layer turbulence. The fluctuations are attenuated due to viscous damping associated with the individual tubing system of each channel.

Channel p9 exhibits the greatest attenuation of the acoustic turbulence input (k2) caused by high viscous damping arising from very small tubing and orifice diameters. This channel was chosen for the majority of the data analysis because of the high attenuation of flow turbulence. Channel p6 exhibits much less attenuation of the acoustic turbulence as a result of having the largest diameter and shortest tubing length of the rake-mounted pitot probes. Channel p8 has a tubing configuration similar to channel p6 but exhibits a higher turbulent response than p12 since it is located in the higher turbulence shear layer. Channel p12 exhibits an intermediate attenuation of the test cell acoustic turbulence reflecting moderate diameter but rather long tubing required to reach the plenum area.

The steady-state ratio of bellmouth pitot pressure to plenum pressure forms the primary parameter used to evaluate flow distortion. The response of such a pressure ratio to test cell turbulence (designated p9/p12) for the two channels (p9 and p12) was used almost exclusively to evaluate flow distortion, which is also illustrated in Fig. 52. The *steady-state* pressure ratio profiles required for evaluating the flow distortion parameter are extracted from the fluctuating response to test cell turbulence, represented by p9/12, by locally time-averaging the fluctuating data as the rake traverses the bellmouth exit. A corresponding turbulence parameter is evaluated directly from the acoustic pressure data, represented by k2, as shown in Fig. 52.

5.0 RECOMMENDATIONS FOR FURTHER STUDY

It is recommended that additional effort, as funds are available, should be conducted on the following:

1. Determine the inherent Test Cell R1D turbulence,
2. Develop a low Mach number bellmouth distortion criteria, and
3. Determine if there is a gap effect hidden in the whistle, using digital analysis techniques to subtract the effect of the whistle.

6.0 GUIDELINES

The measured flow quality and observations made during the parametric investigaion of axial gap, radial gap, and extension angle enabled the development of general guidelines for bellmouth extension configuration. Comparisons between the results and established flow quality criteria formed the basis of the guidelines. The results are subject to such previously described issues as the rake acoustic interactions. The following are guidelines for determining a geometry for a bellmouth extension to eliminate the possibility of an inlet vortice.

1. A cone half-angle of less than 60 deg is acceptable with an angle of 45 deg or less recommended. A survey of AEDC turbine engine test cells revealed that the 45-deg extension could be accomodated without impacting entry into the plenum.
2. A radial gap of zero should preferrably be used only with axial gaps of zero; i.e., the extension exit plane should be mated tangent to but not necessarily sealed at the bellmouth inlet plane.
3. Figure 53 shows a range of acceptable radial and axial gaps for a 45-deg cone half-angle for two bellmouth inlet to plenum diameter ratios. The values given in this figure have been scaled to a full-size test cell. Radial and axial gap combinations in the hatched area are not recommended.

7. 0 SUMMARY

A technology program was conducted during FY93 and FY94 in Test Cell R1D concerning bellmouth flow quality. The purpose of the effort was to:

1. Determine if total pressure losses at the bellmouth exit were caused by inlet vortices.
2. Evaluate the conical extension method of eliminating these bellmouth-induced vortices.
3. Develop design guidelines for bellmouth extensions that address such parameters as radial gap, axial gap, and extension angle.

During the conduct of the experiment, it was shown, using flow visualization (combined smoke generator with laser light illumination), that inlet vortices were present in the subscale bellmouth. It was also shown that the bellmouth inlet vortices could be eliminated by the use of a 45-deg conical bellmouth extension attached to the bellmouth inlet. Additional testing results, using a variety of bellmouth extension angles and radial and axial gaps, were used to determine a range of possible combinations that can be used to eliminate the possibility of inlet vortices. An assessment of the impact of these diffierent bellmouth configurations on bellmouth flow quality was also made. These flow quality assessments included the effect of distortion and turbulence on the performance of the bellmouths.

The FOD screen and screen support were shown to induce a total pressure profile at the bellmouth entrance, which was also present at the bellmouth exit at mass flows corresponding to high power engine operation. Guidelines for use in determining a bellmouth extension configuration were developed based on the subscale testing that was accomplished during this technology effort.

REFERENCES

1. Society of Automotive Engineers, Inc. "Inlet Total-Pressure Considerations for Gas Turbine Engines." Aerospace Information Report 1419, May 1983.

2. R. B. Abernethy and J.W. Thompson, Jr. "Handbook Uncertainty in Gas Turbine Measurements." AEDC-TR-73-5, February 1973.

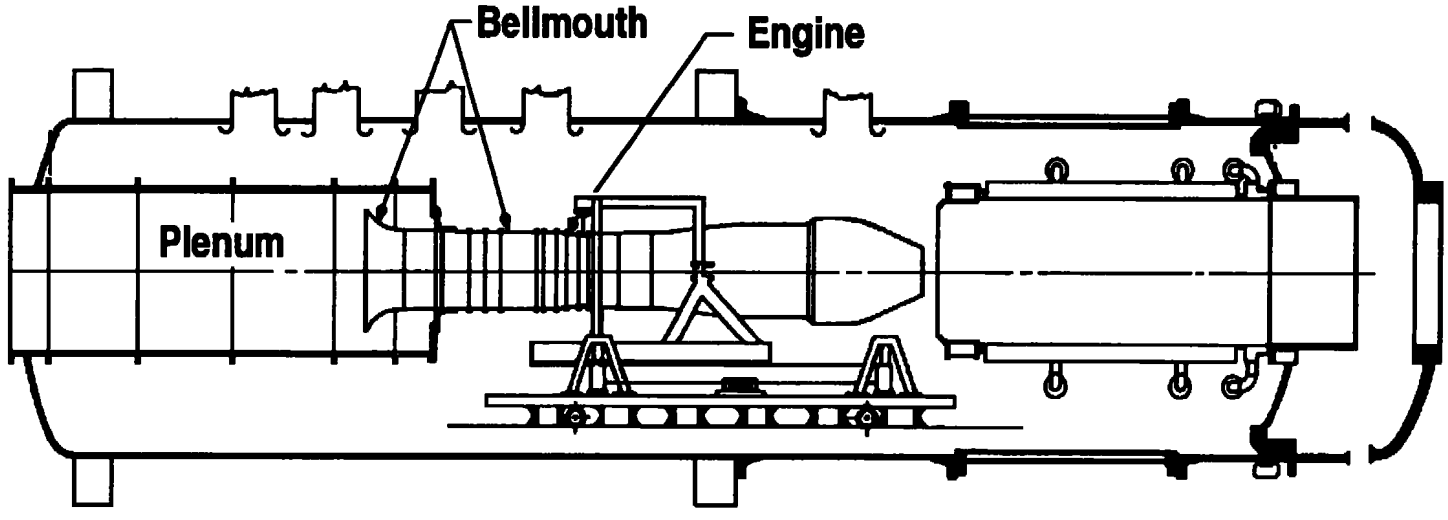

Figure 1. Schematic of bellmouth and engine installation in a typical, full-scale propulsion development test cell.

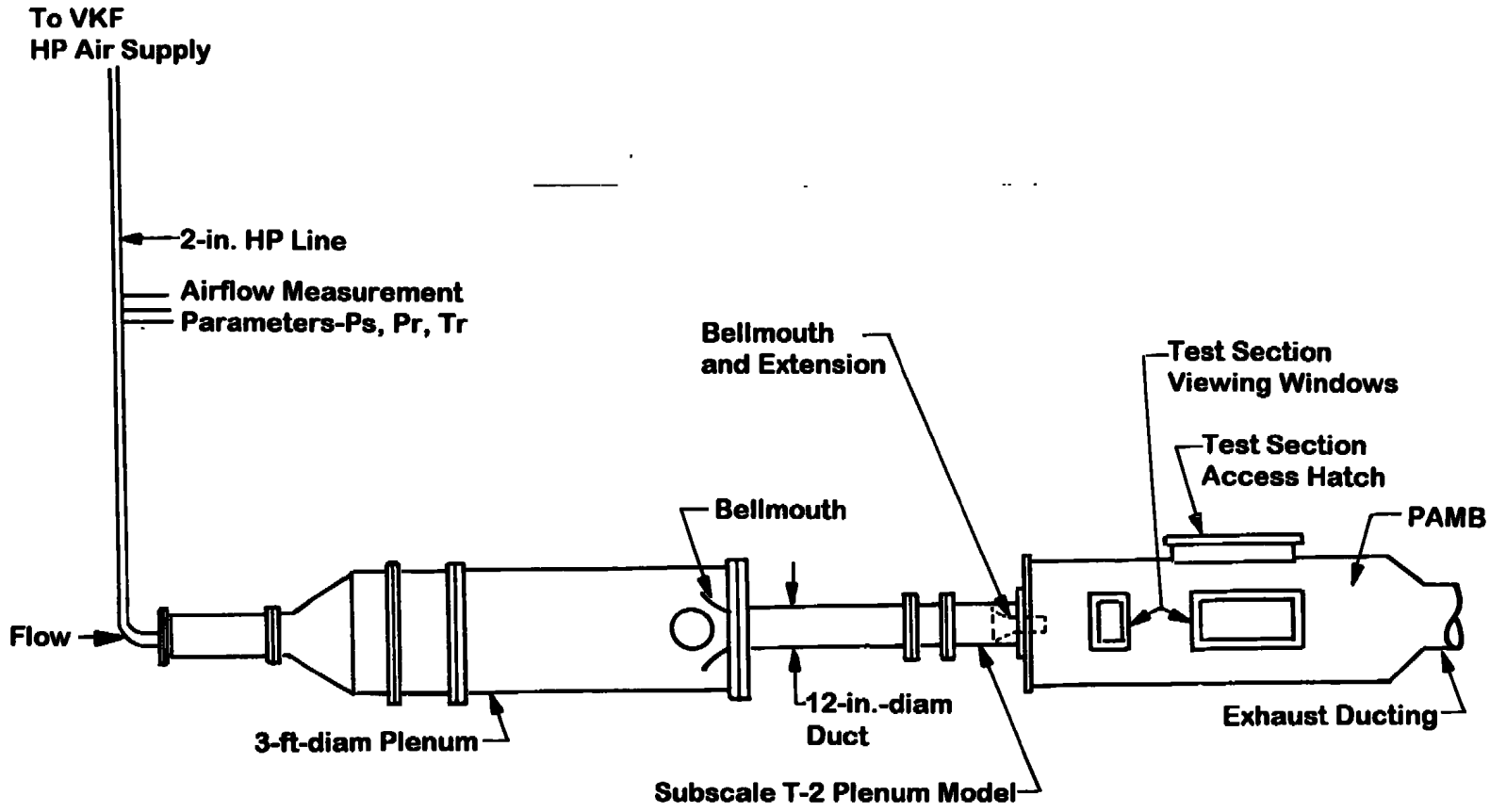

Figure 2. Schematic of Icing Research Cell R1D.

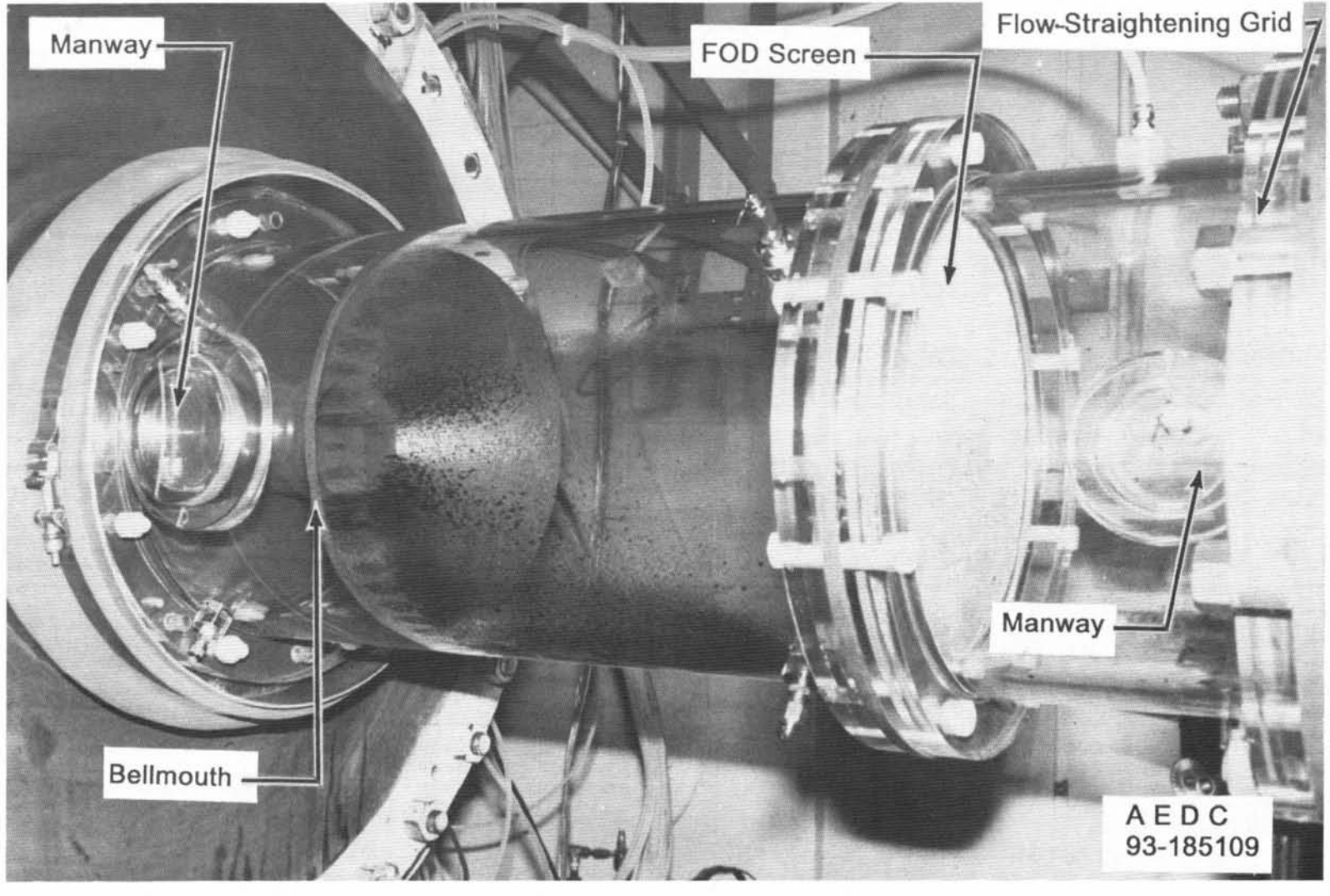

Figure 3. Subscale T-2 plenum model in R1D.

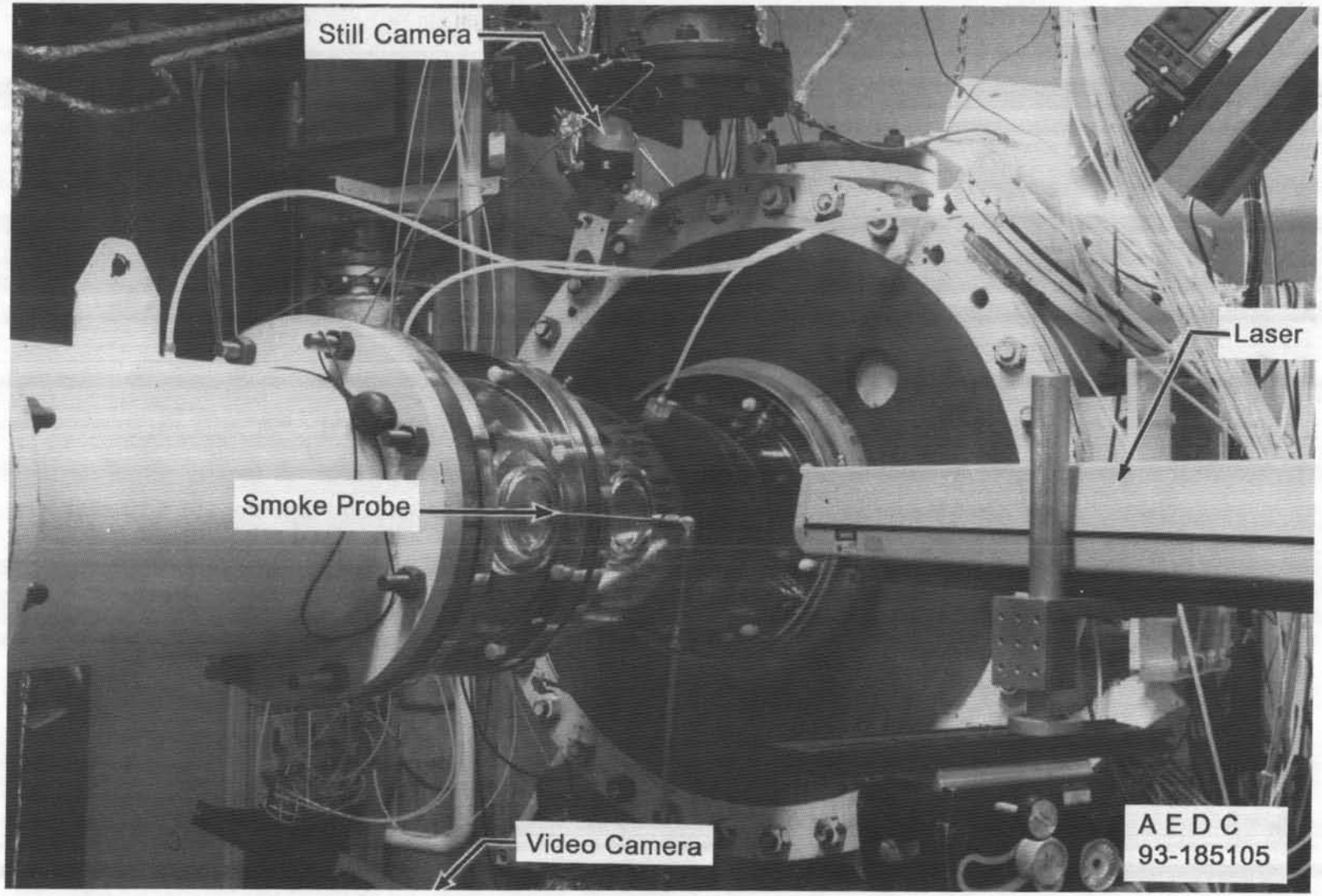

Figure 4. Instrumentation for subscale model.

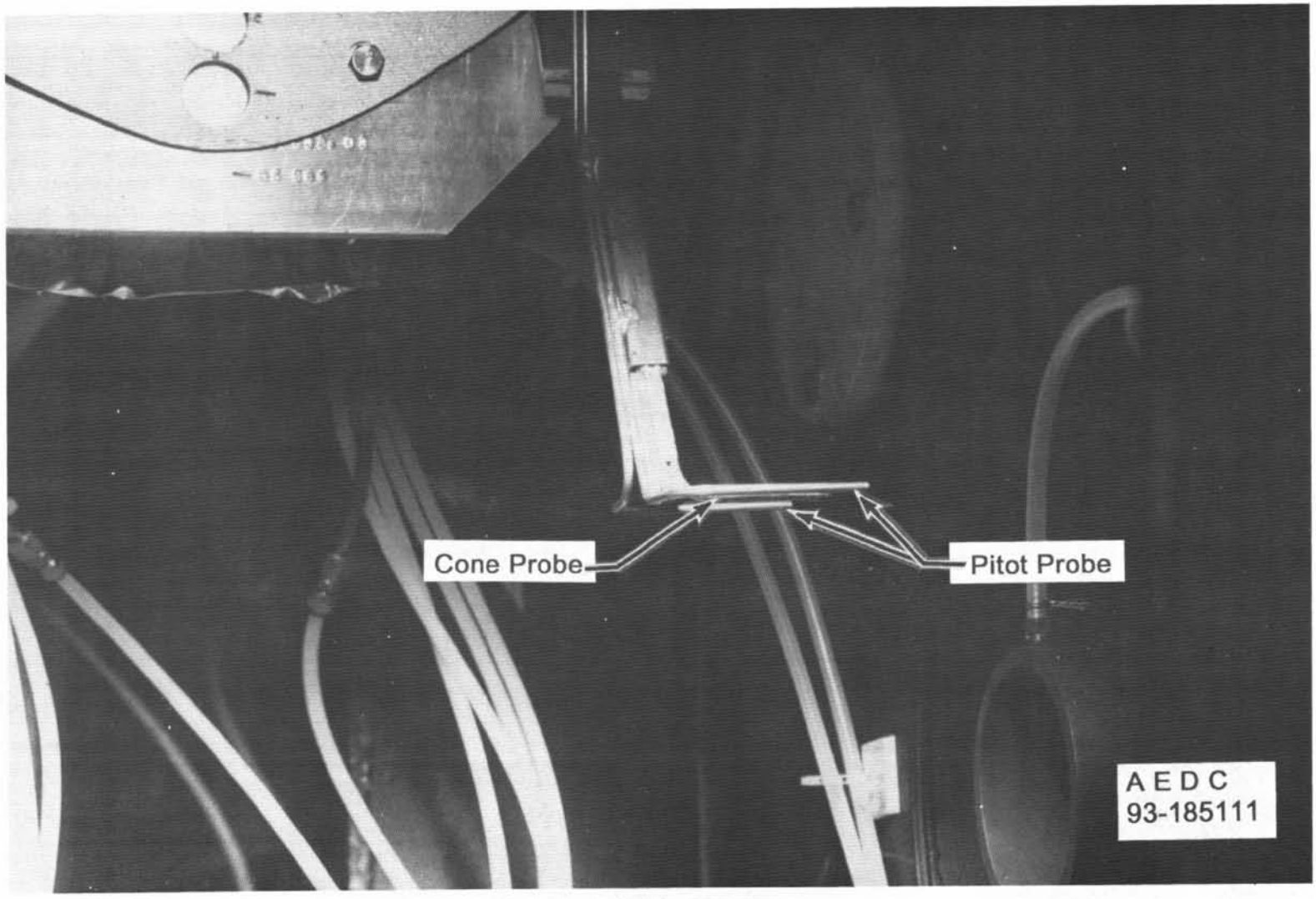

Figure 5. Cone and pitot probes on traversing rake.

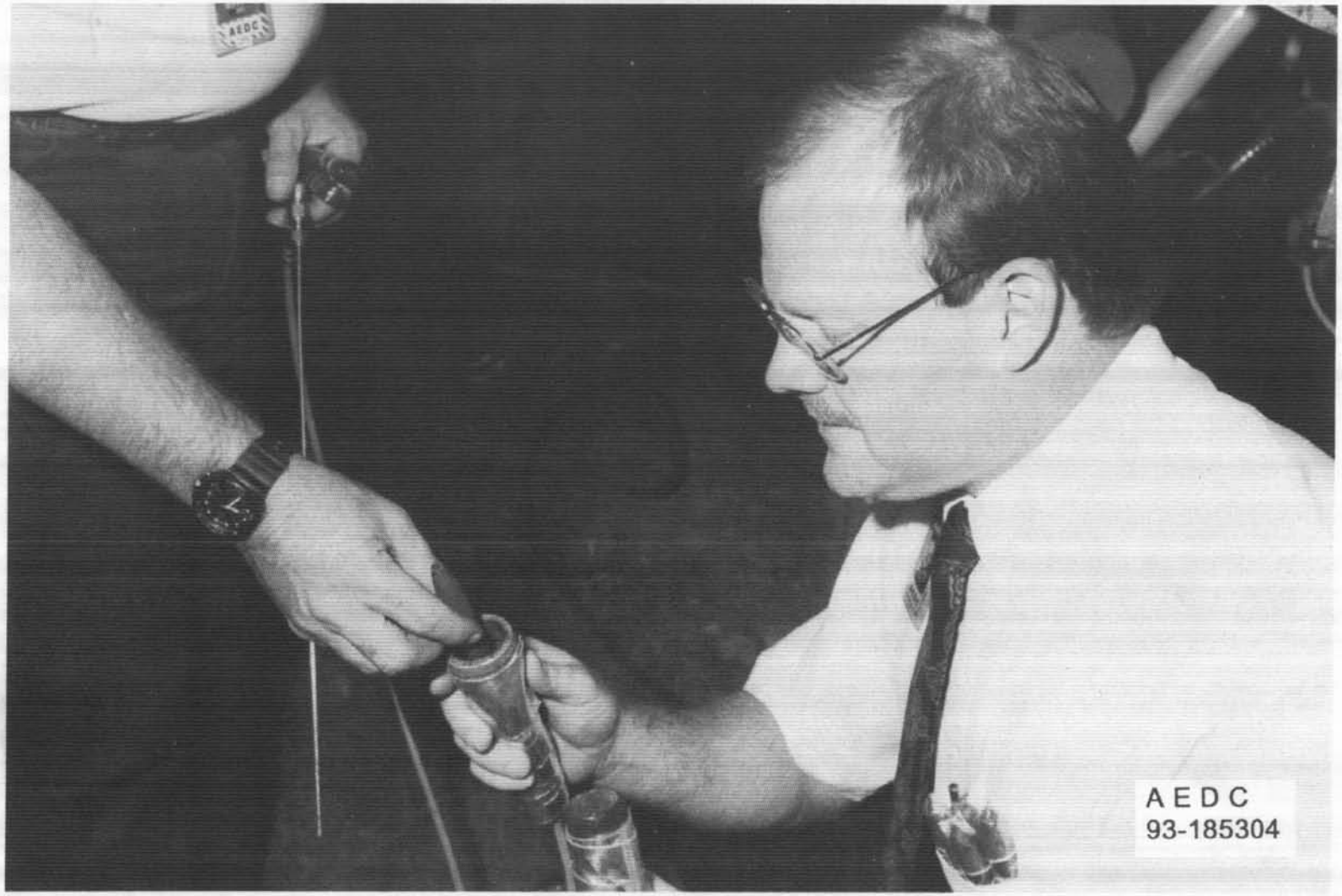

Figure 6. Smoke generator.

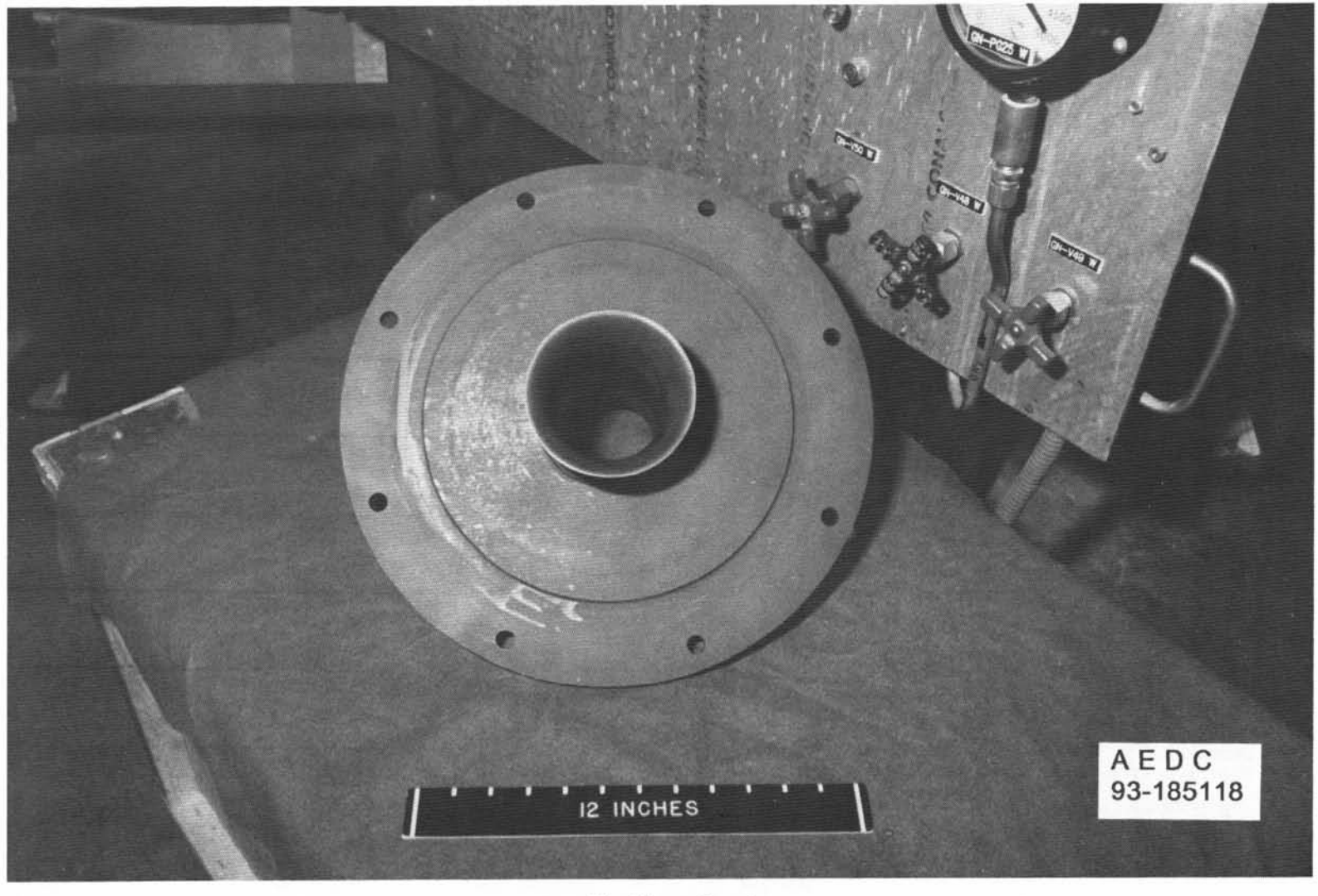

a. Configuration A

Figure 7. 1/6th scale model of Configuration A bellmouth.

Bellmouth Elliptical Contour Dim. X	+0.010 Dim. Y -0.000 I.D.
0	3.117
0.167	3.120
0.333	3.132
0.500	3.151
0.667	3.179
0.833	3.215
1.000	3.261
1.167	3.318
1.333	3.387
1.500	3.470
1.667	3.572
1.833	3.699
2.000	3.866
2.167	4.122
2.258	4.517

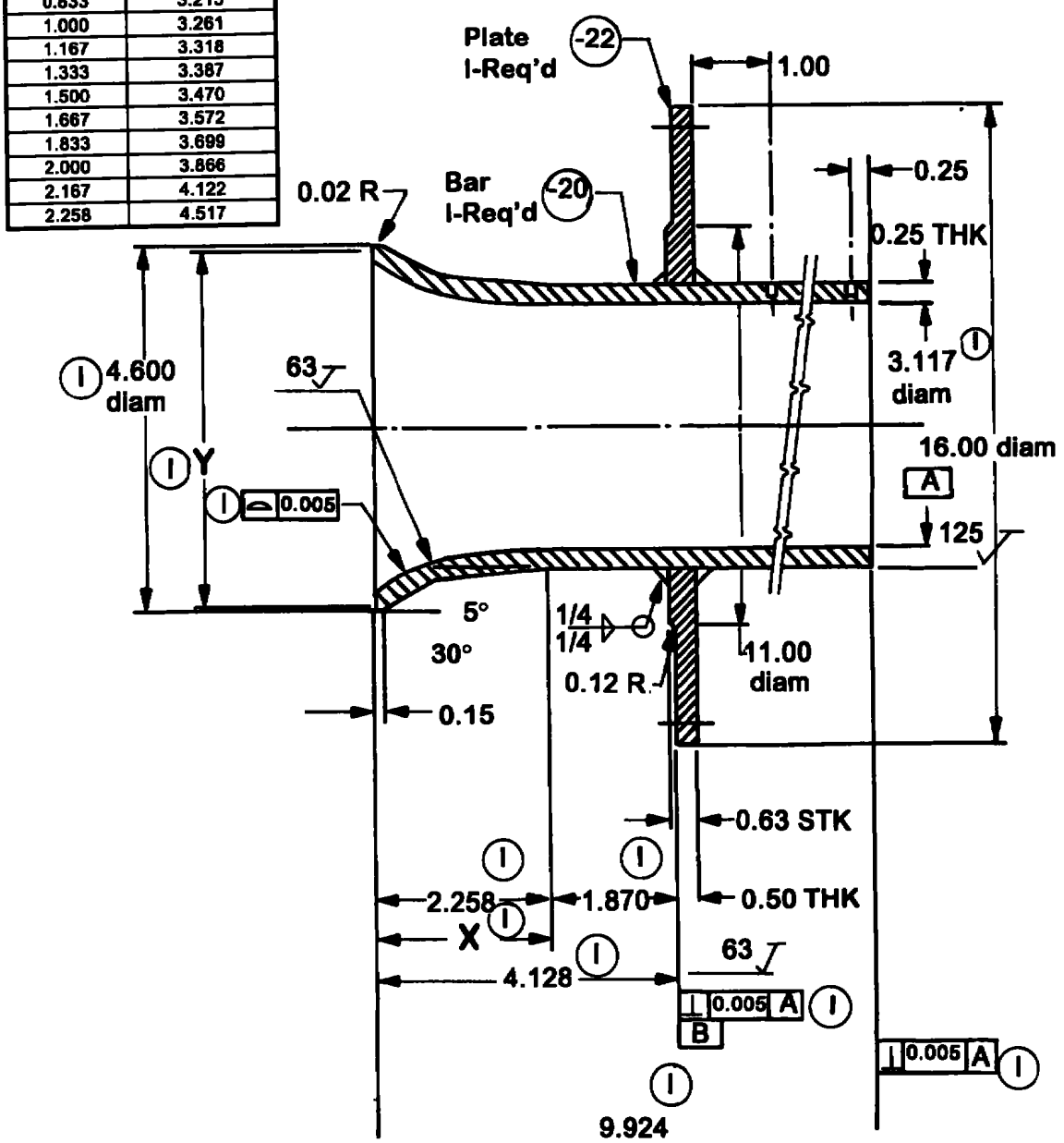

b. Bellmouth A

Figure 7. Concluded.

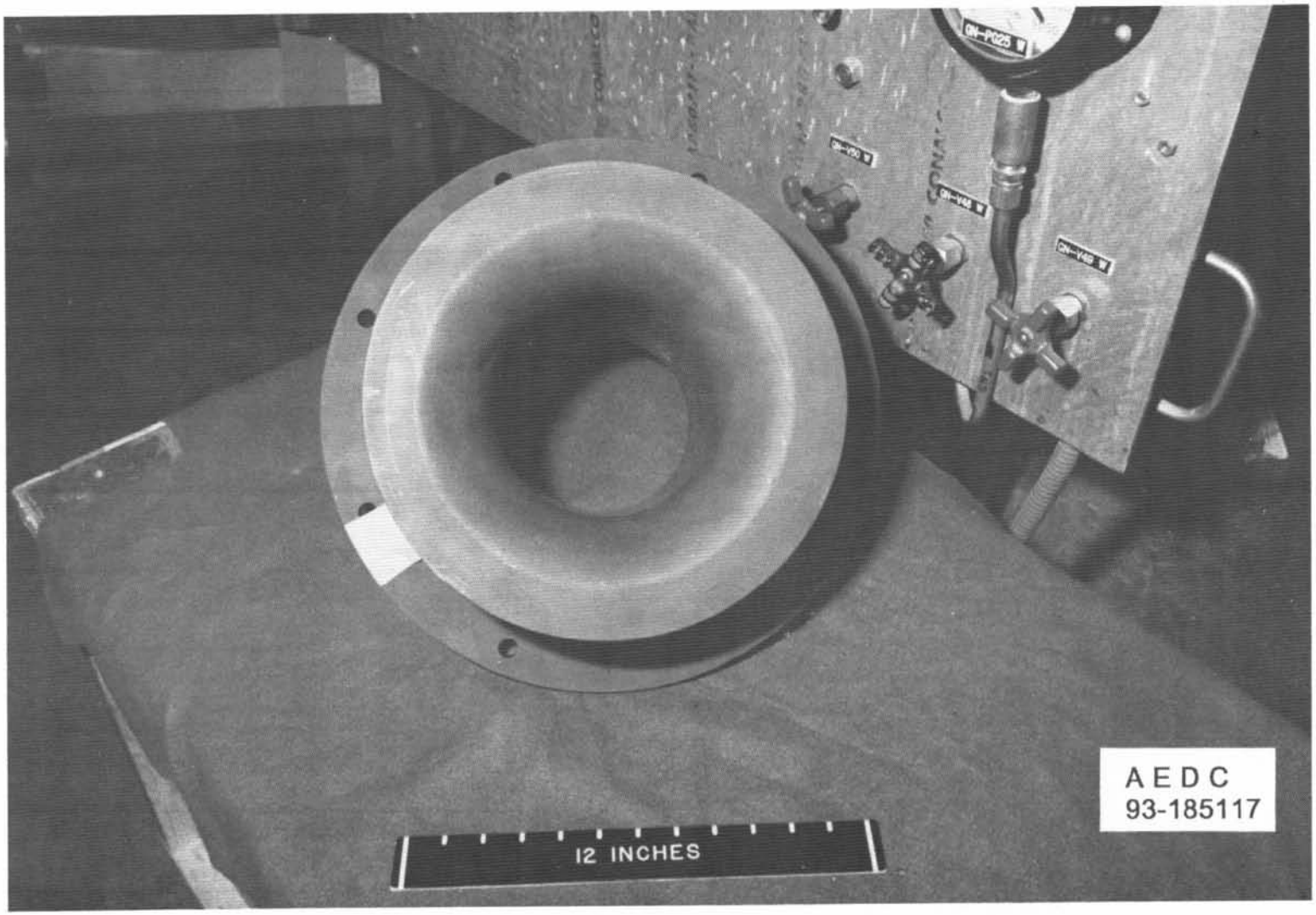

a. Configuration C

Figure 8. 1/6th scale model of Configuration C bellmouth.

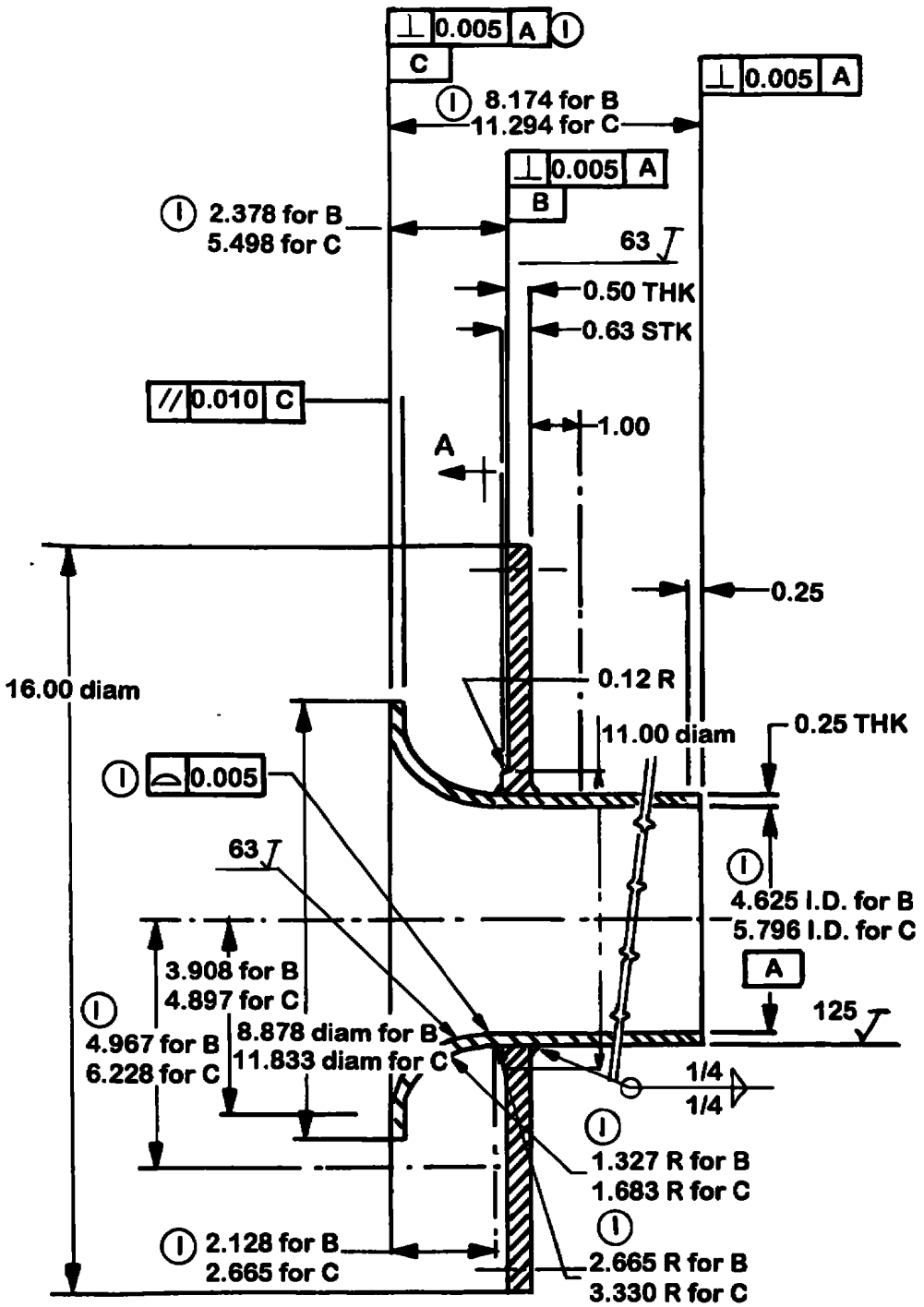

b. Bellmouths B and C
Figure 8. Concluded.

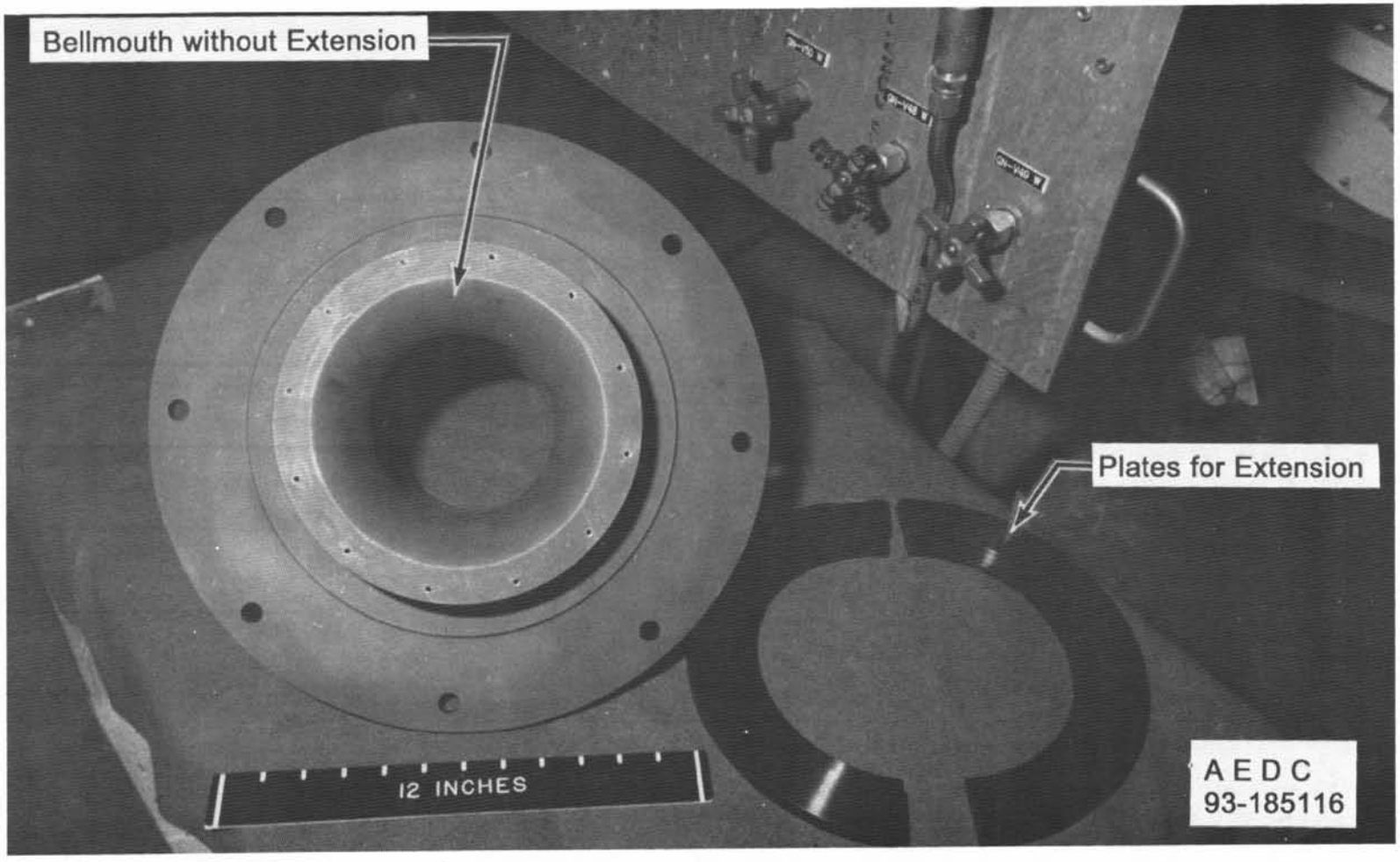

a. Configuration B

Figure 9. 1/8th scale model of Configuration B bellmouth and extension (90 deg).

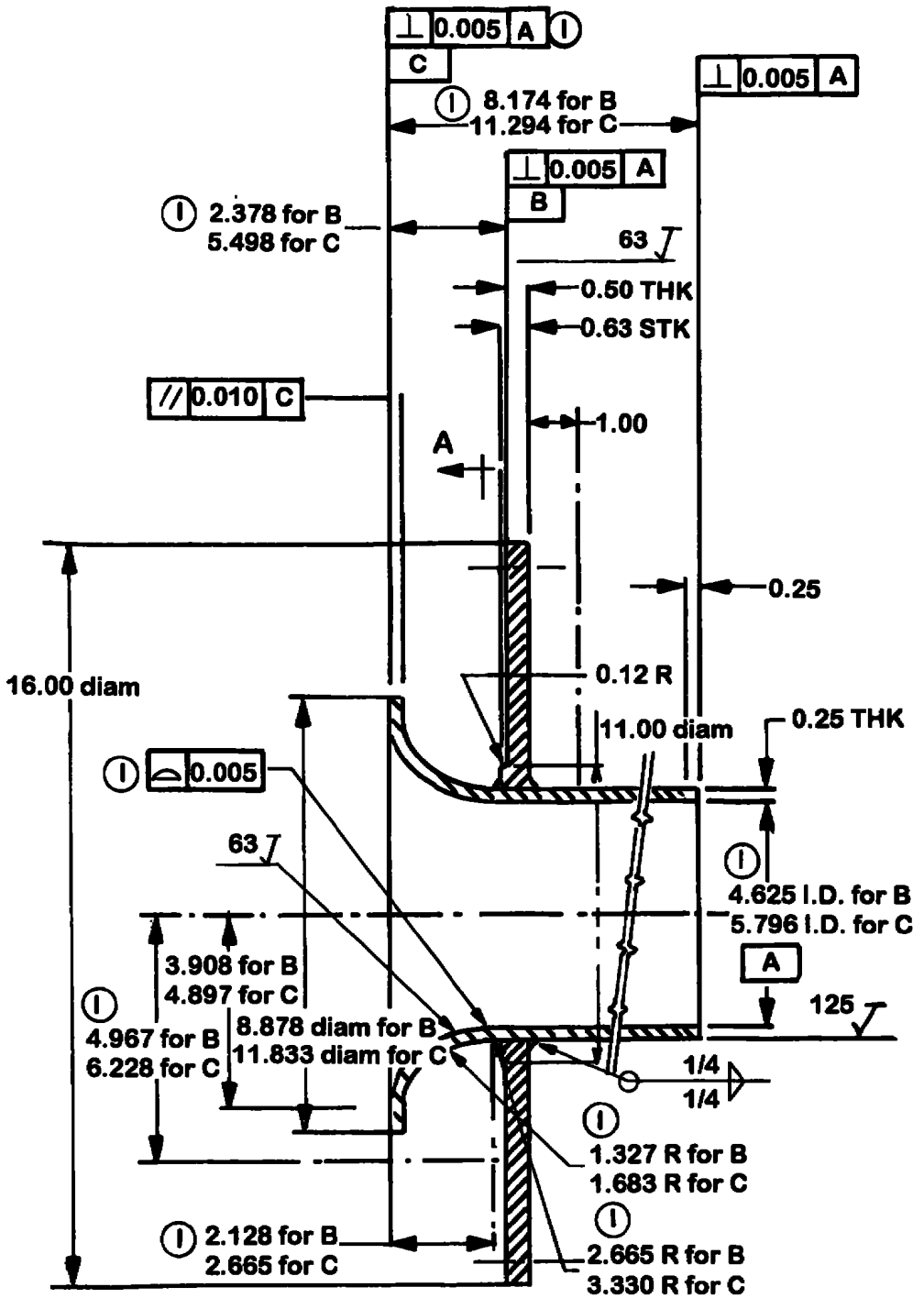

b. Bellmouths B and C
Figure 9. Concluded.

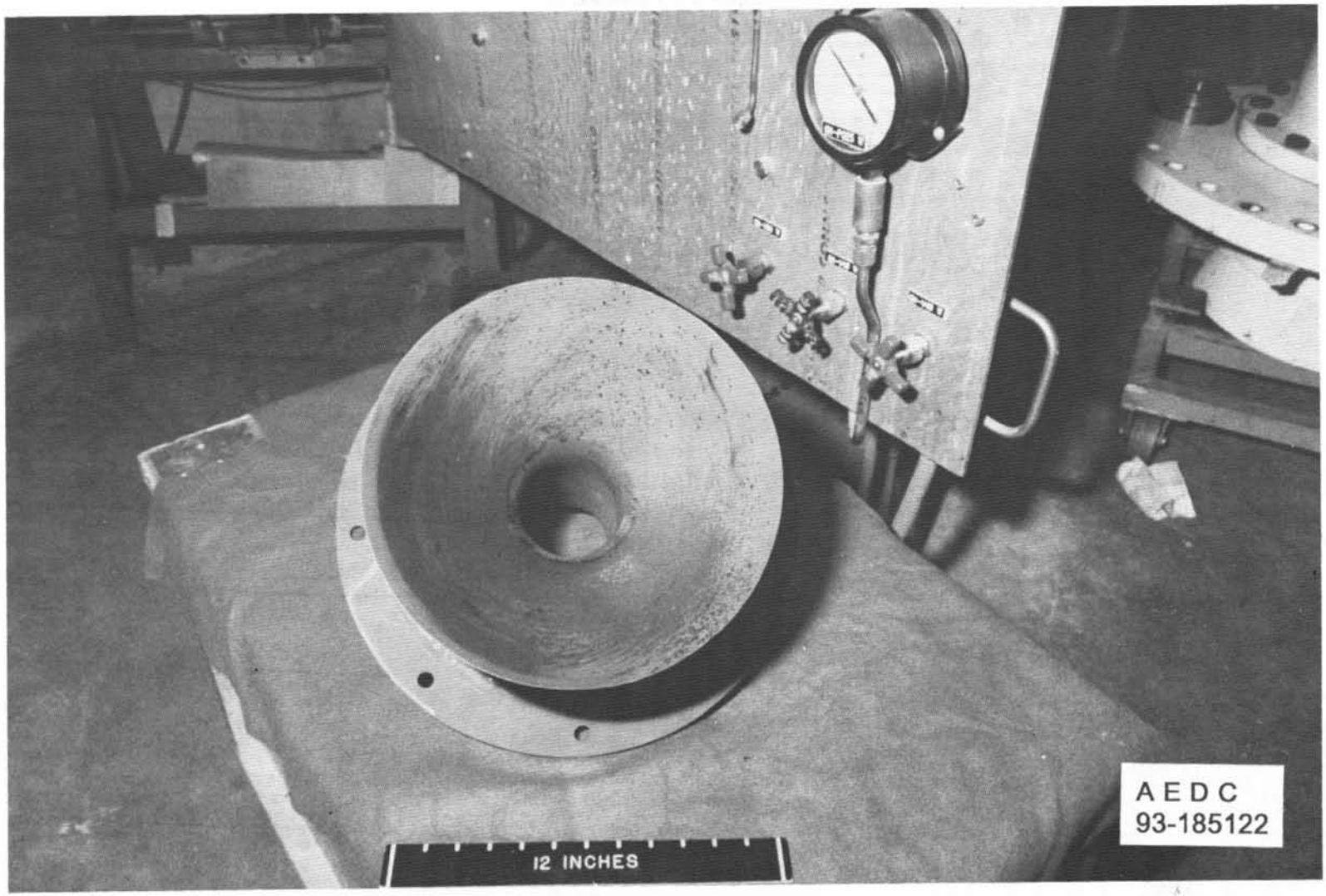

a. Configuration A

Figure 10. 1/6th scale model of Configuration A bellmouth with 45-deg extension.

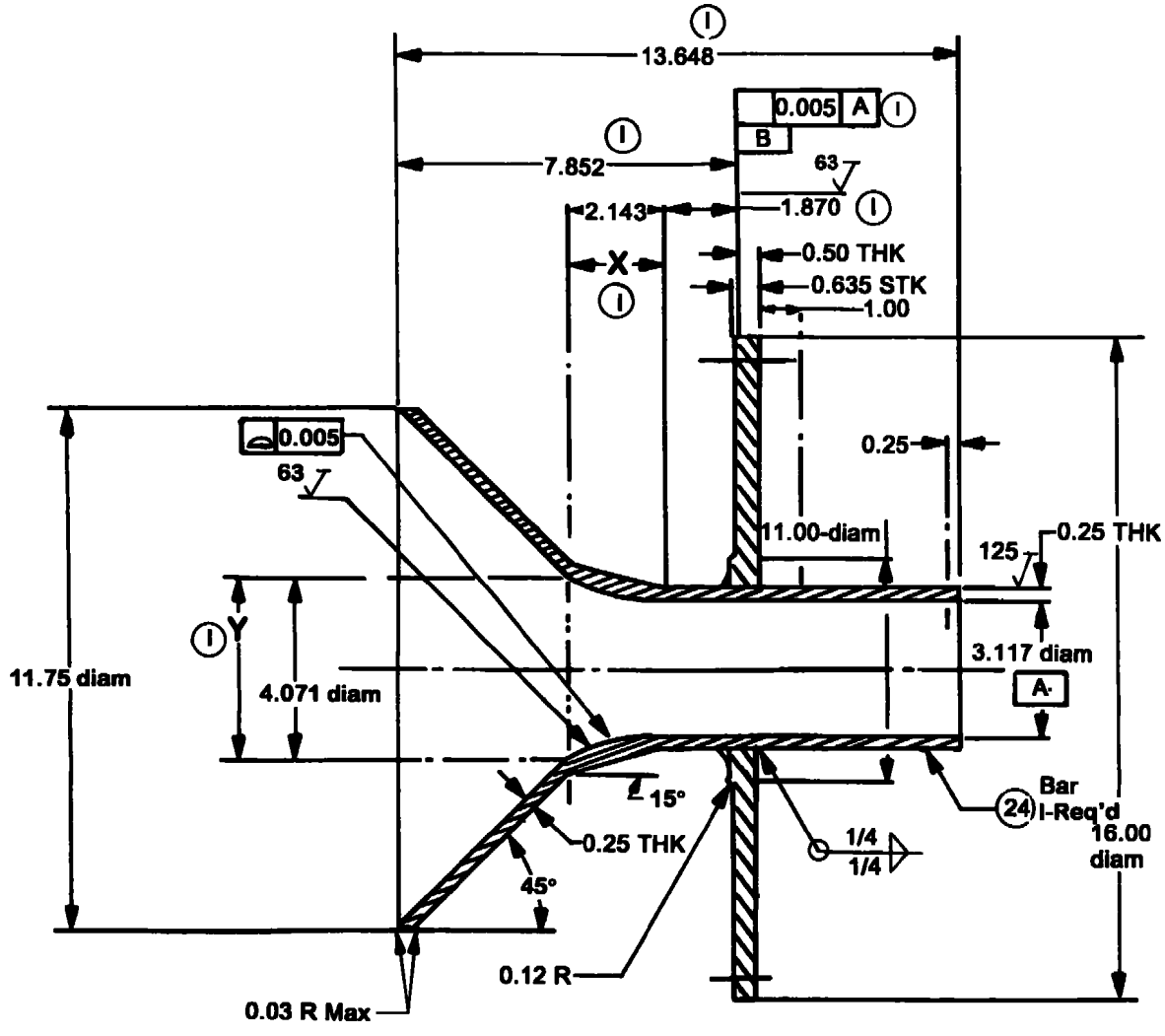

Bellmouth Elliptical Contour Dim. X	+0.010 Dim. Y -0.000 I.D.
0	3.117
0.167	3.120
0.333	3.132
0.500	3.151
0.667	3.179
0.833	3.215
1.000	3.261
1.167	3.318
1.333	3.387
1.500	3.470
1.667	3.572
1.833	3.699
2.000	3.866
2.143	4.071

b. Bellmouth A with sealed 45-deg cone extension
Figure 10. Concluded.

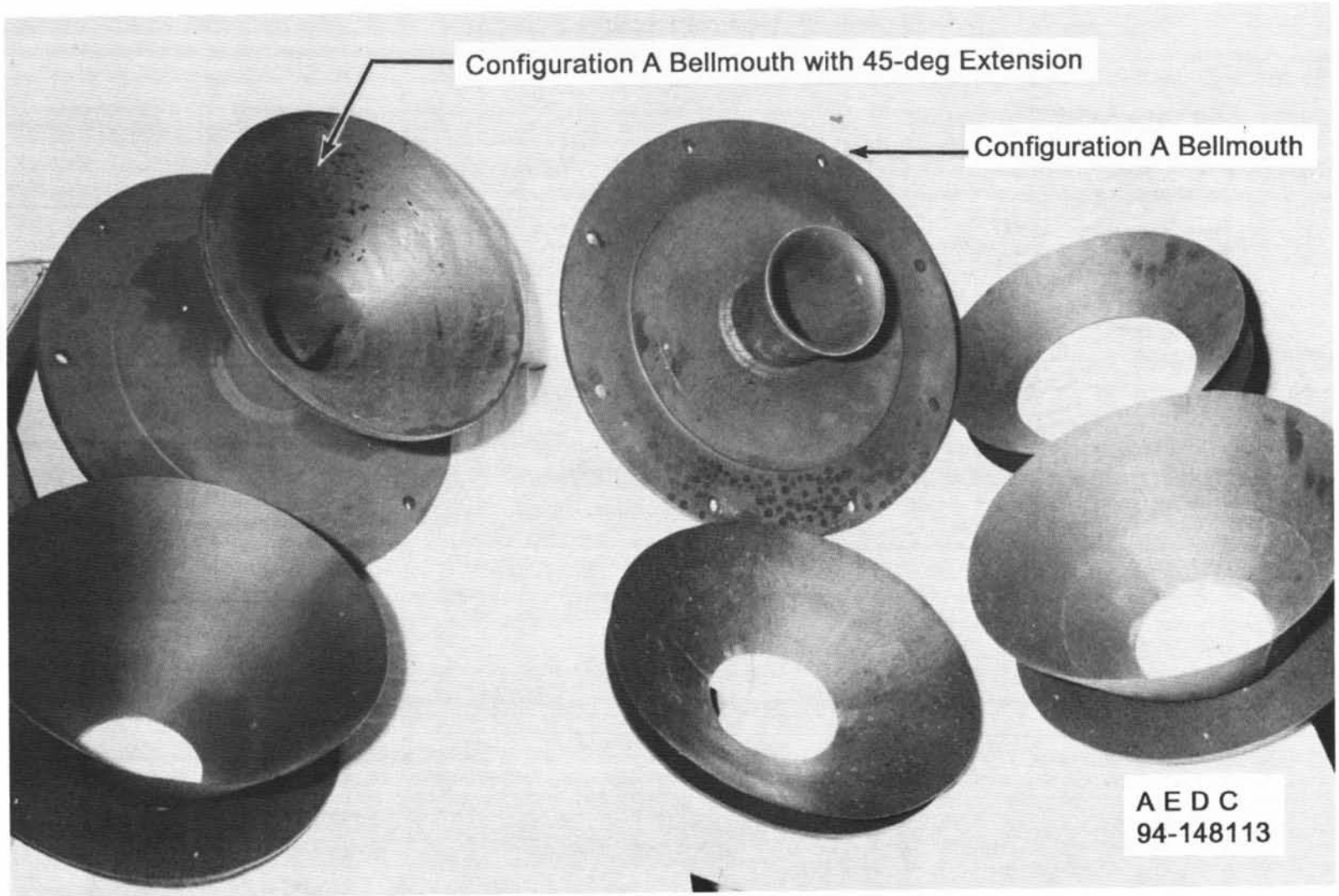

a. Several extensions

Figure 11. Bellmouth extensions.

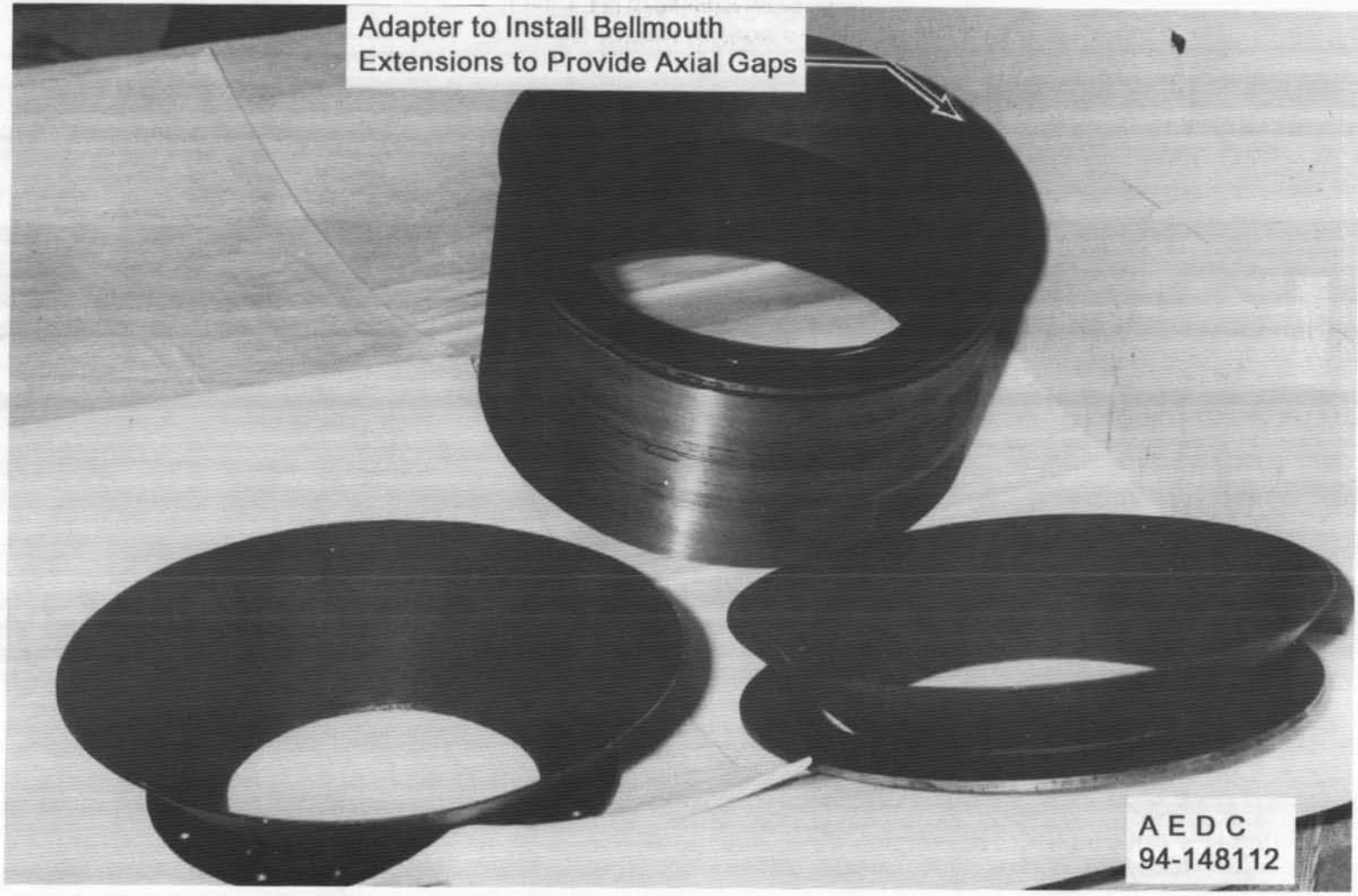

b. Adapter and additional extensions
Figure 11. Continued.

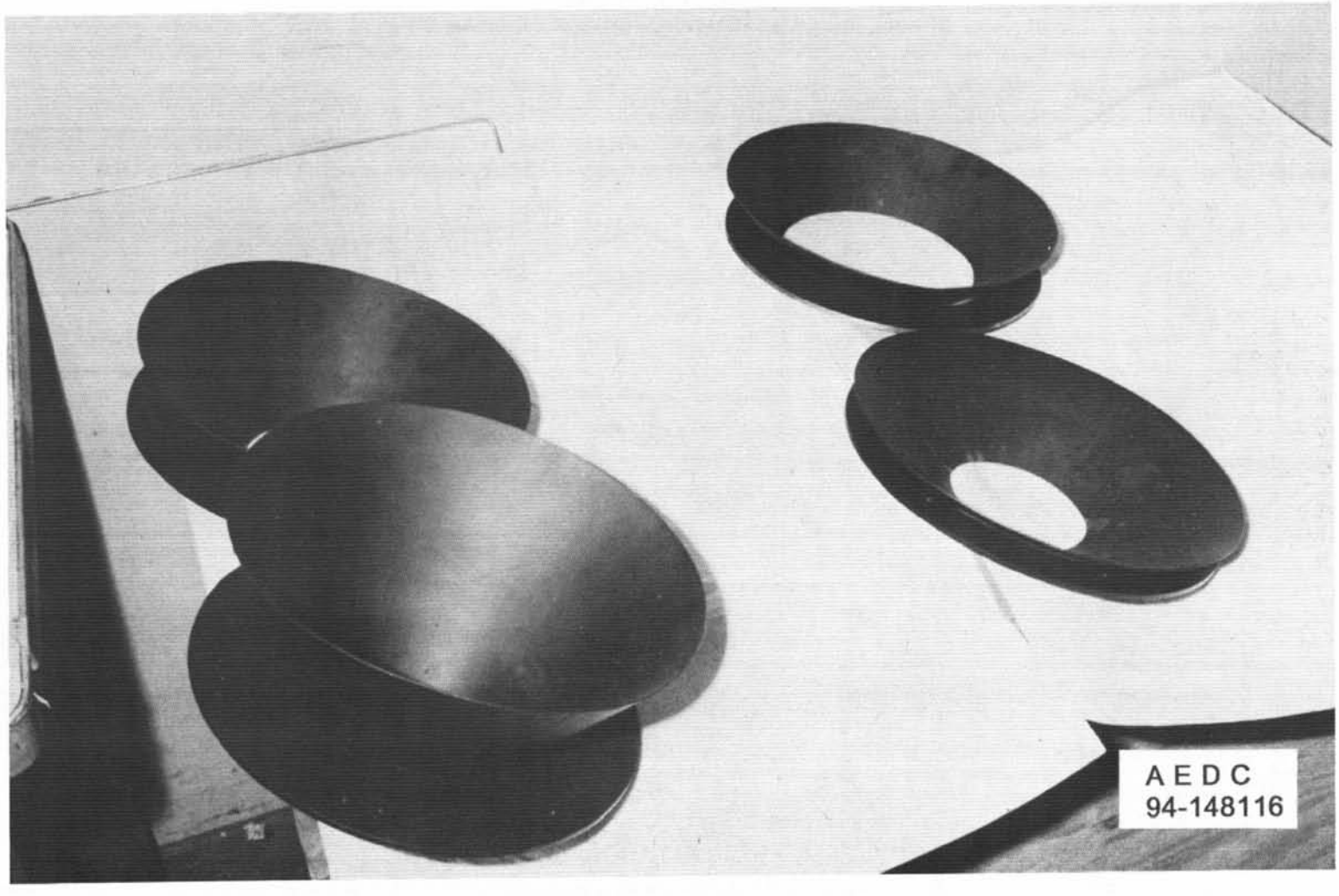

c. More extensions
Figure 11. Continued.

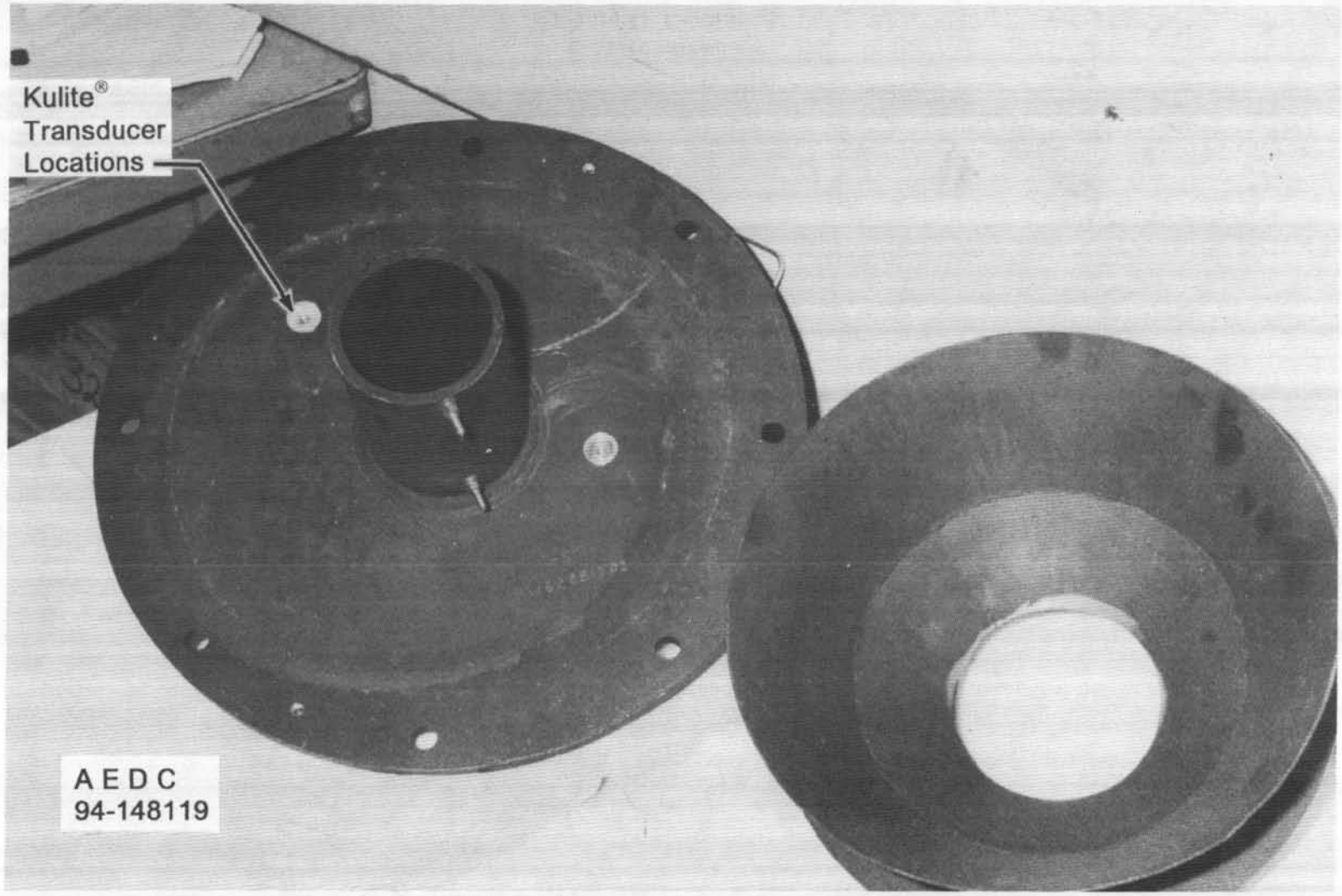

d. 30/45-deg extension and rear view of bellmouth
Figure 11. Continued.

Part No.	A	B	C	D	E	F
-2	5.90	2.97	4.14	45°	7.90	0.84
-4	804	1.90	2.62	45°	9.27	0.43
-6	6.97	2.44	3.38	45°	8.35	0.50
-8	4.20	3.82	5.34	45°	7.12	1.27
-10	4.20	2.23	4.36	60°	8.98	1.19
-12	3.79	6.94	7.97	30°	6.73	2.40

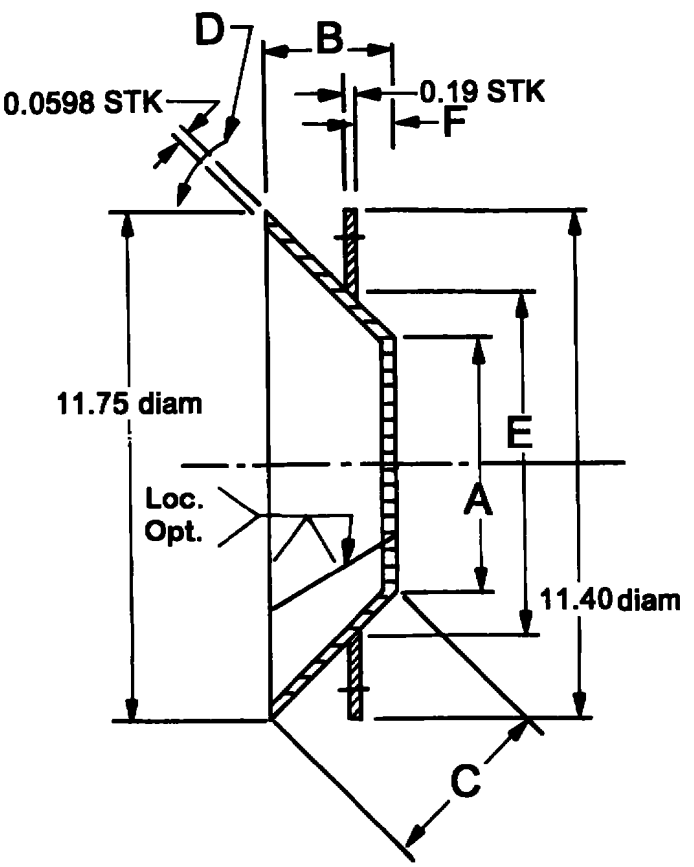

e. Cone extensions used with Bellmouths A and B
Figure 11. Continued.

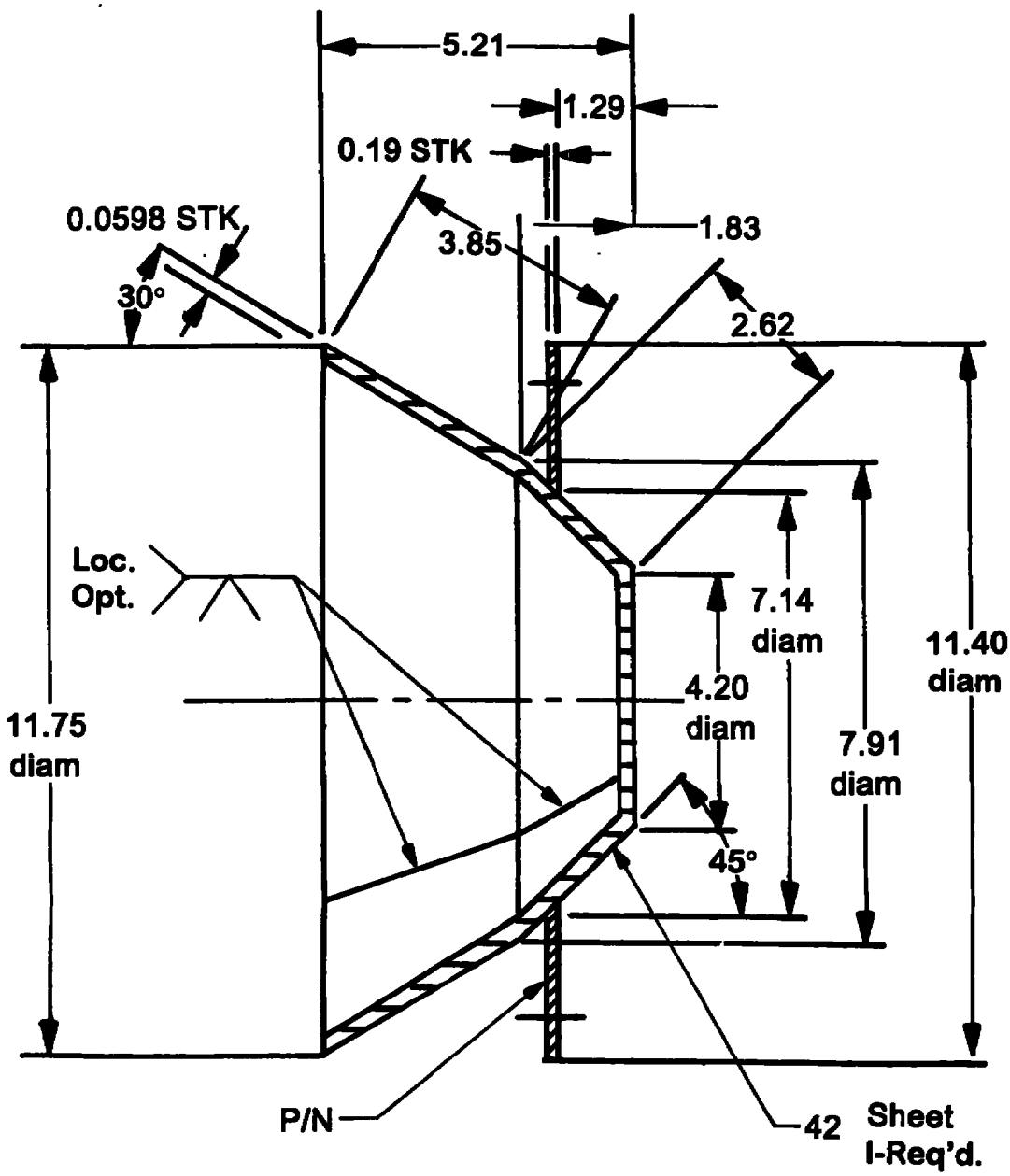

f. 30/45-deg cone extension
Figure 11. Concluded.

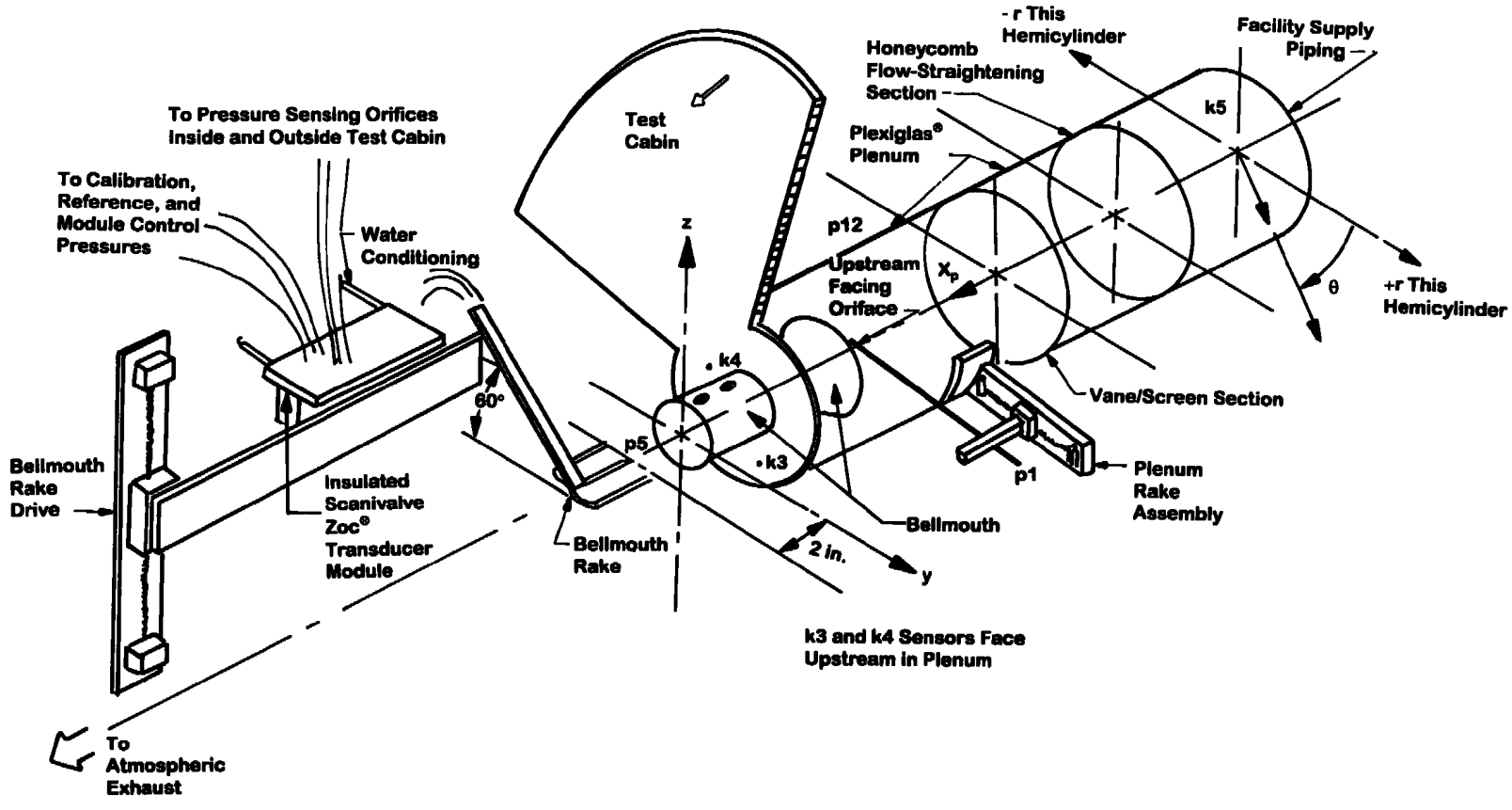

Figure 12. Installation schematic.

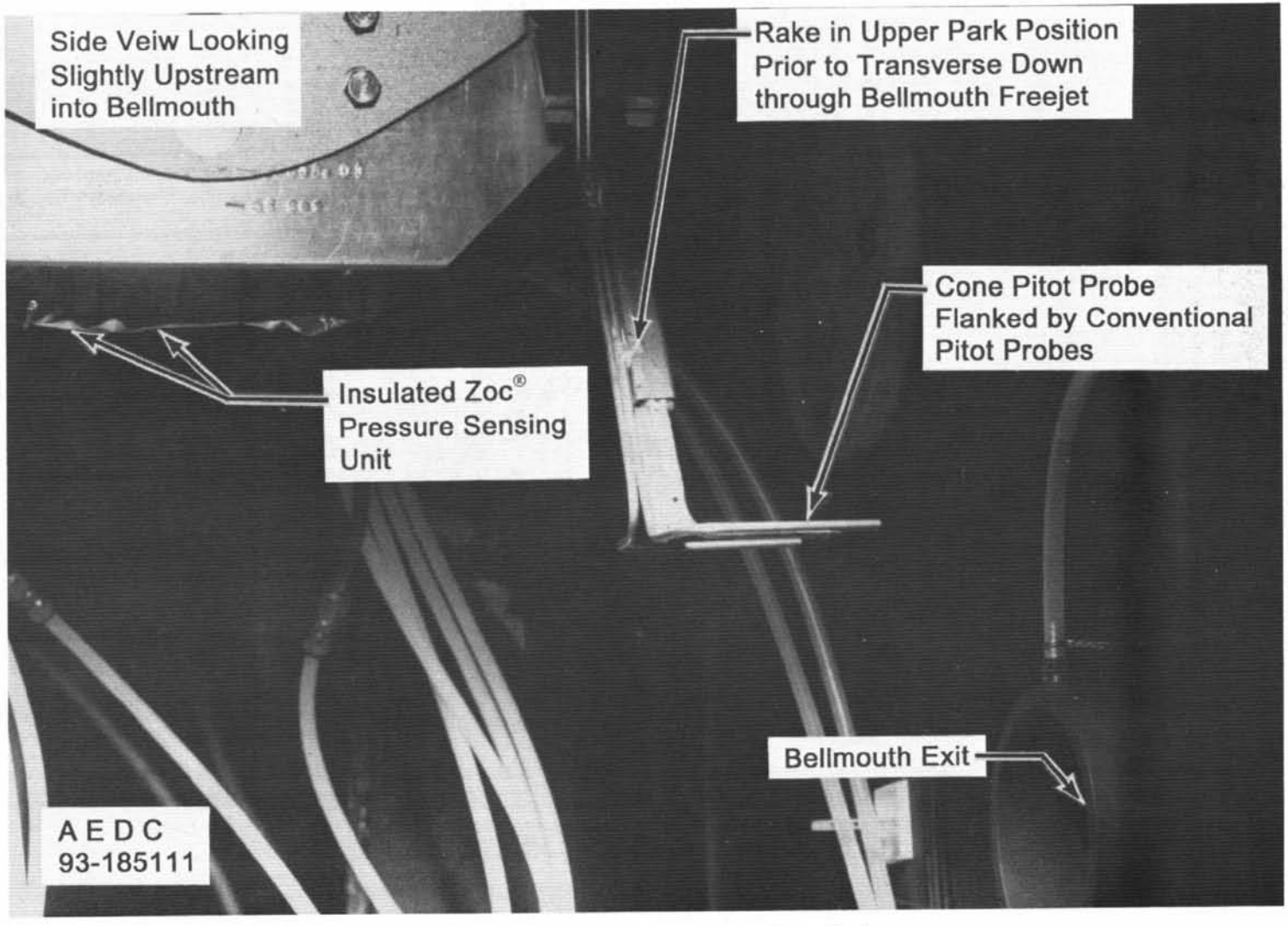

Figure 13. Phase 1 rake/bellmouth installation.

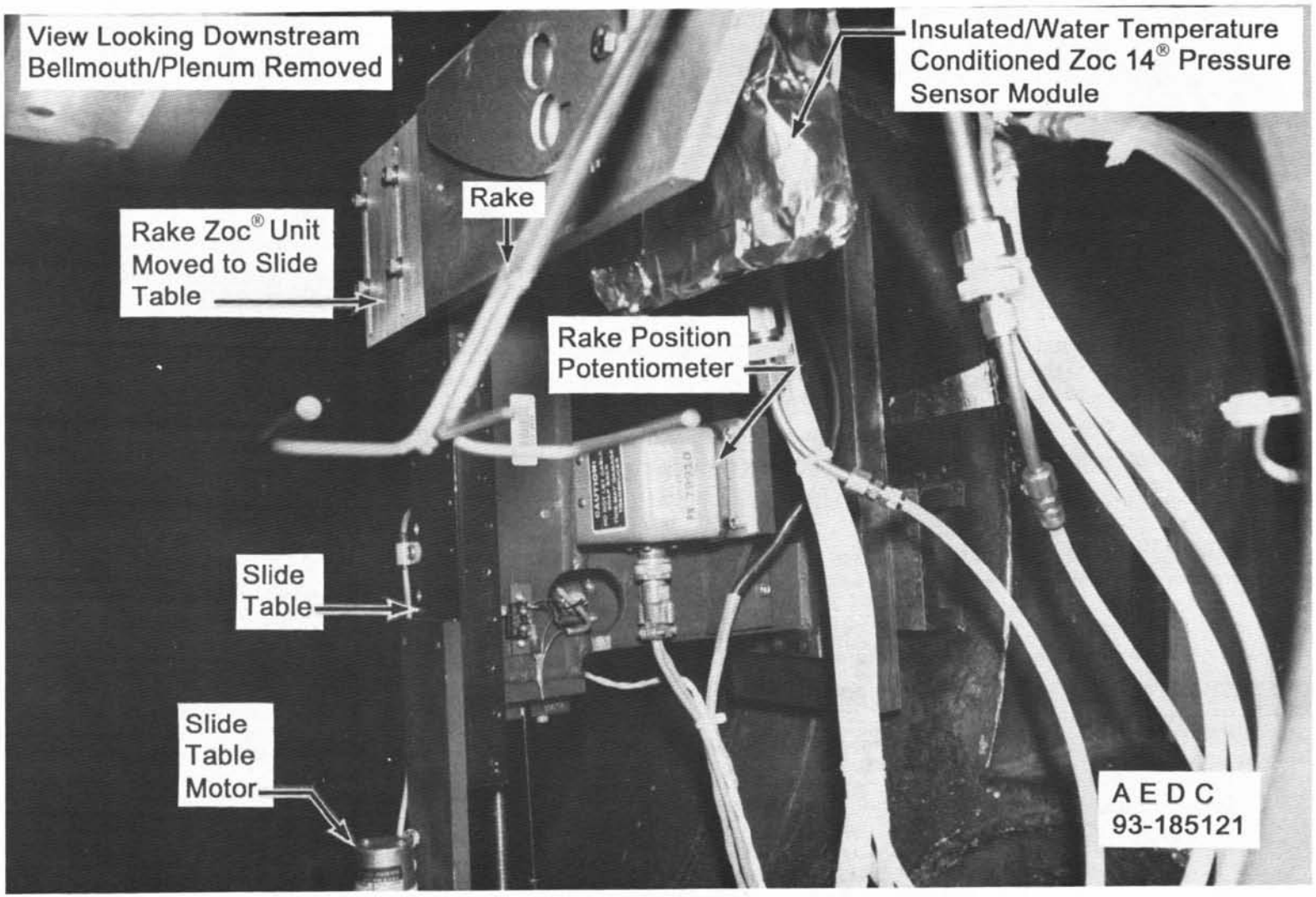

Figure 14. Phase 1 rake/slide table installation.

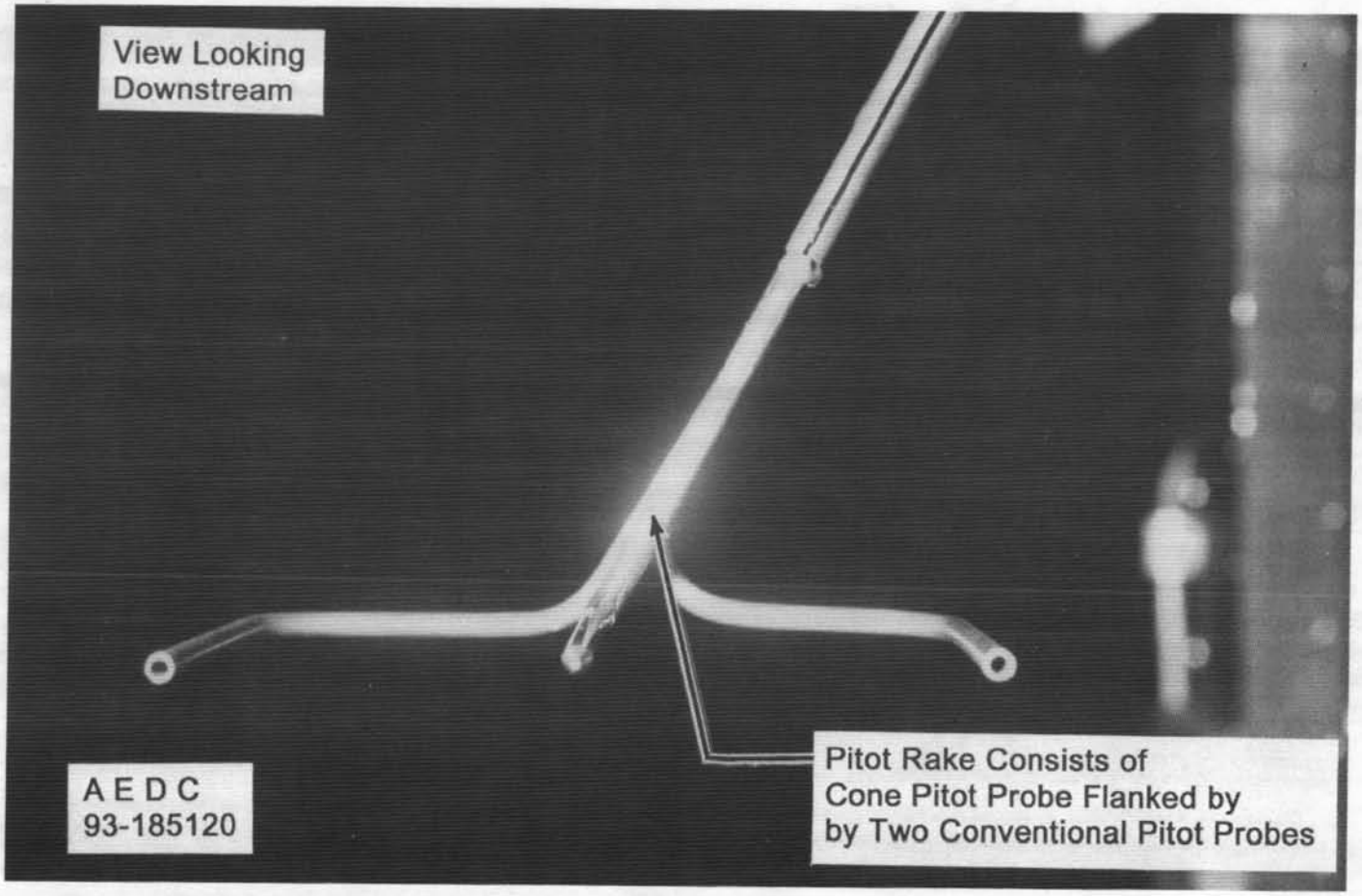

Figure 15. Phase 1 rake.

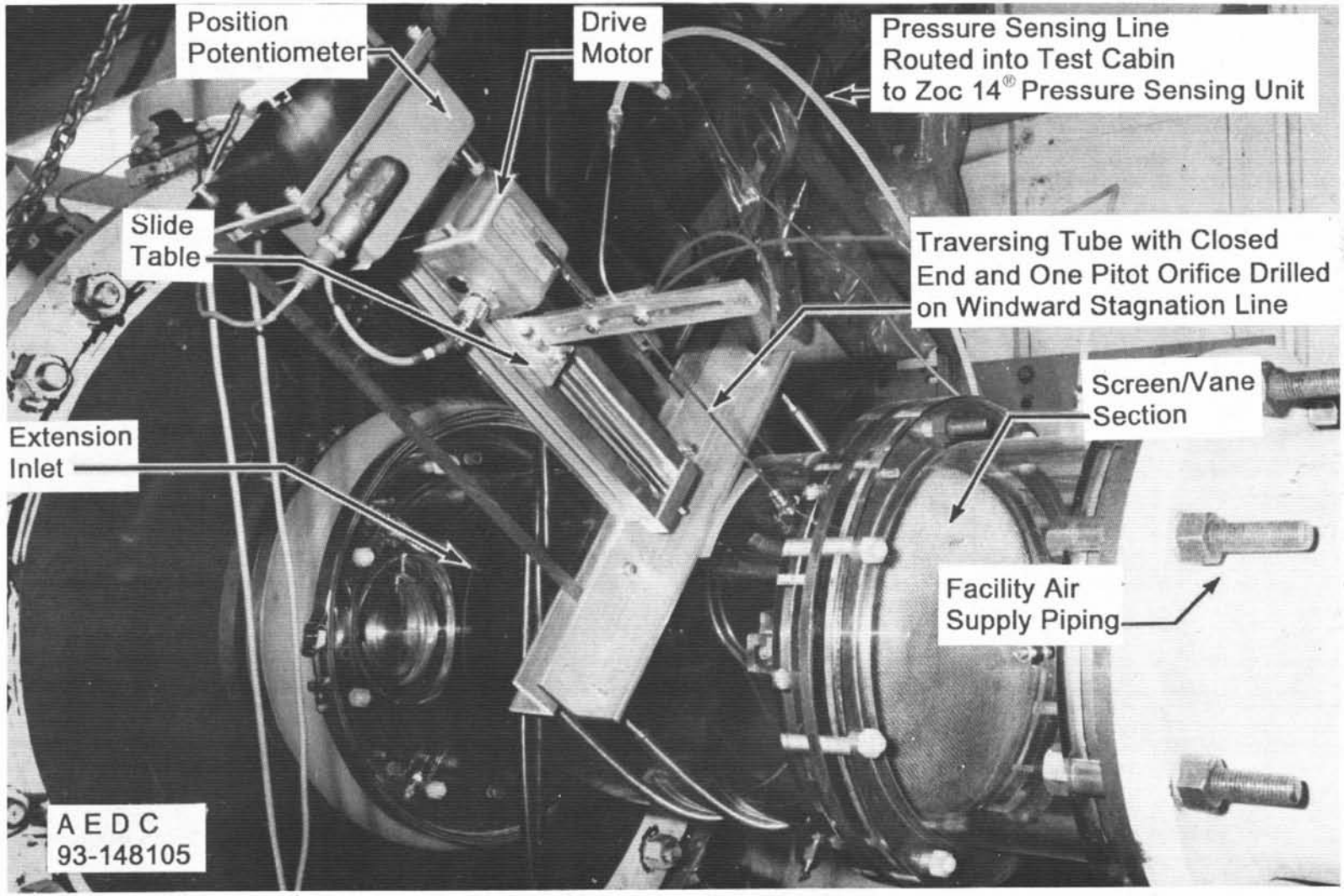

Figure 16. Plenum probe rake system.

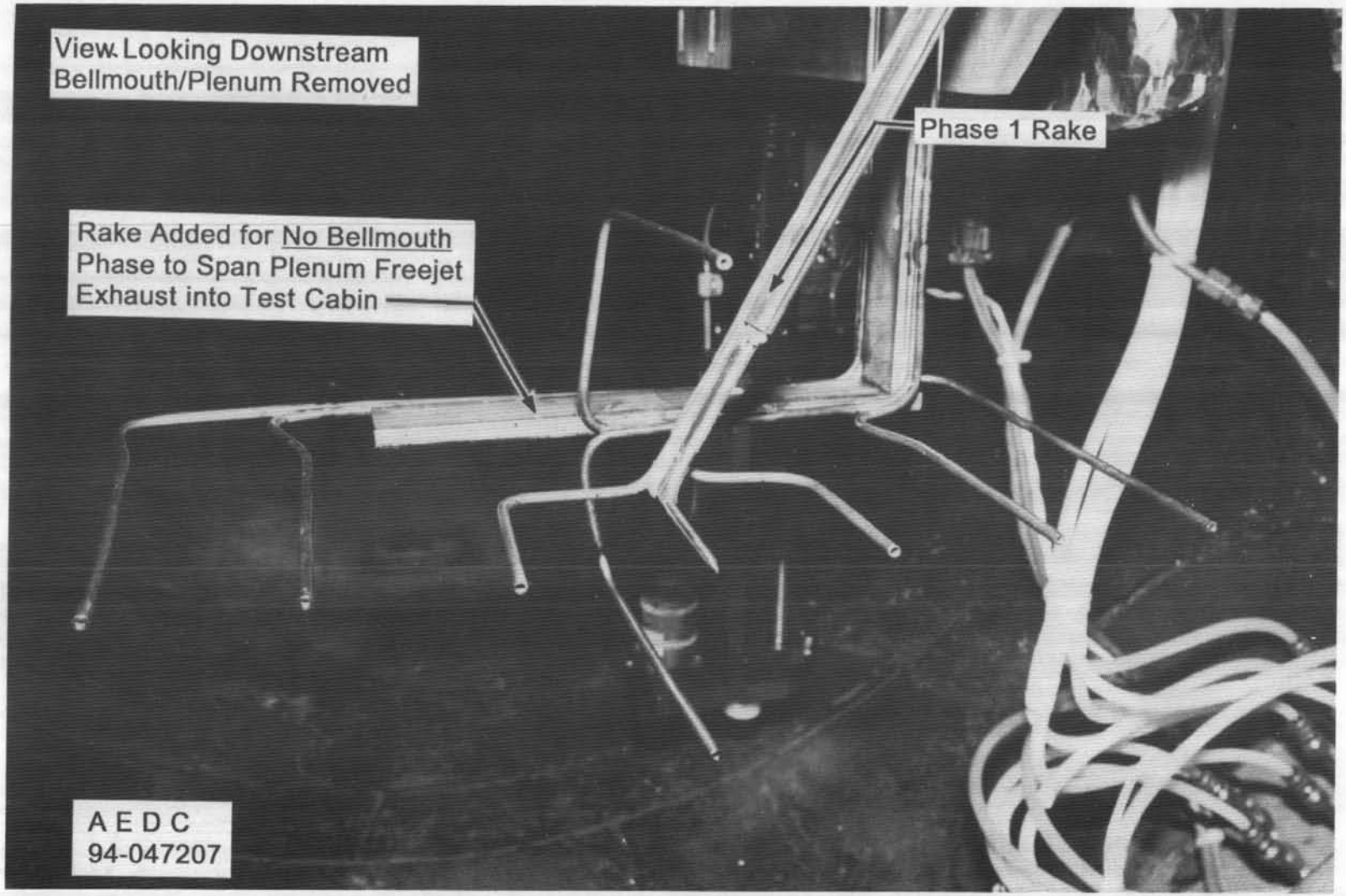

Figure 17. "No bellmouth" phase rake installation.

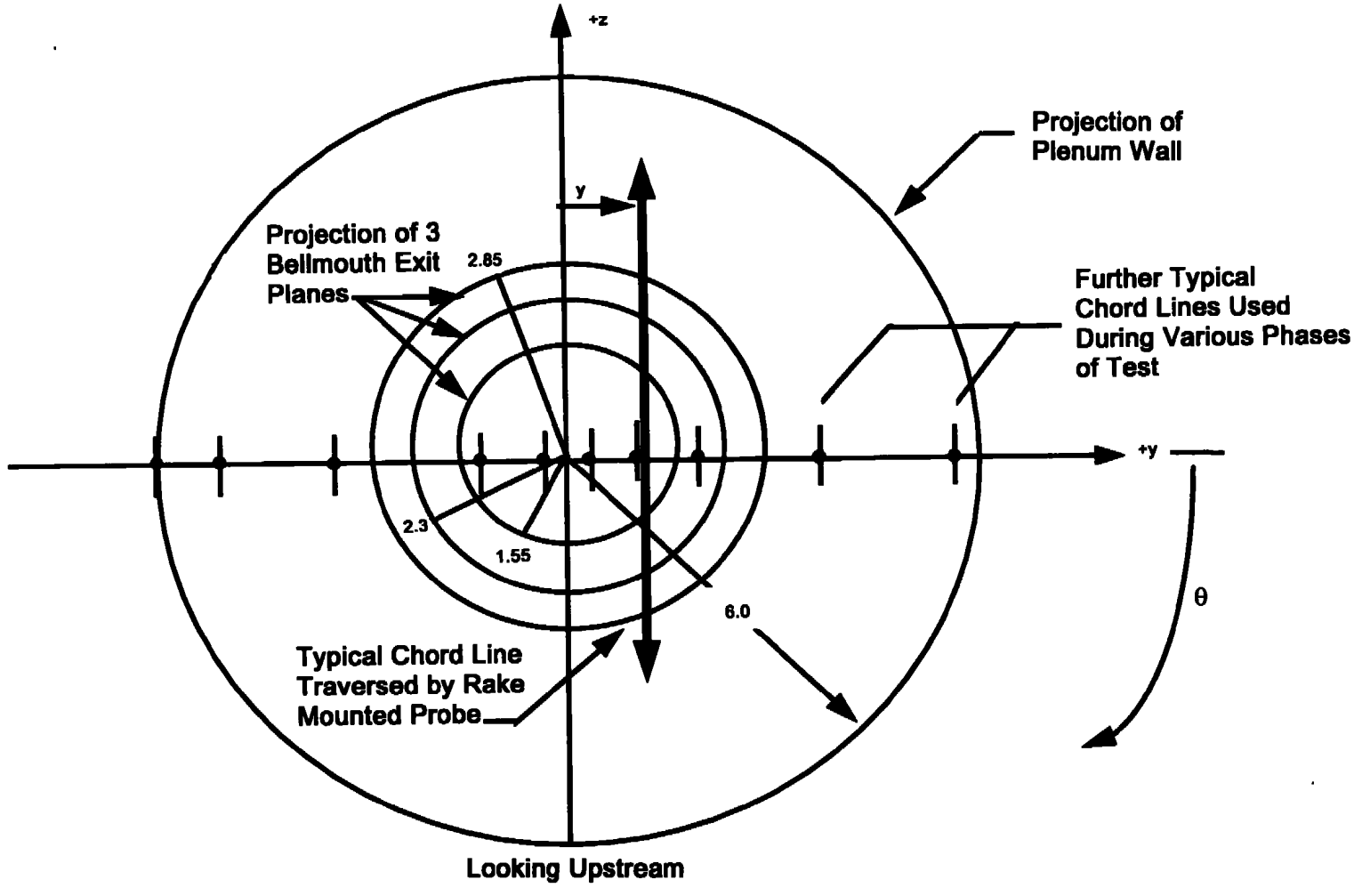

Figure 18. Diagram of chord lines traversed by rake.

Pressure Source

Channel Identification		Bellmouth Phase 1	Bellmouth Phase 2	y, in	z, in.
Scanivalve®	P_1	Plenum Pitot/Atmosphere	Same		
	P_2	Upstream Bellmouth	Same		
	P_3	Atmosphere	Same		
	P_4	Test Cell Supply Pipe	Pitot	1 15	0
	P_5	Cell Static	Pitot	-0.45	0.4
	P_6	Pitot	Same	-1.35	0
	P_7	Cell Static	Same		
	P_8	Pitot	Same	2.05	0
	P_9	Cone Pitot	Same	0.4	0
	P_{10}	Upstream Plenum	Same		
	P_{11}	Downstream Bellmouth	Same		
	P_{12}	Downstream Plenum	Same		
	P_{13}	Cone Static	Same		
	P_{14}	Cone Static	Same		
	P_{15}	Cone Static	Same		
	P_{16}	Cone Static	Same		
Kulite®	K_1		Rake Pitot	1.15	0.25
	K_2		Rake Pitot	-0.45	0.15
	K_3		Plenum End Wall	4.5*	60**
	K_4		Plenum End Wall	3.5*	210**
	K_5		Test Cell Supply Pipe	(8.12 in. Upstream of Plenum Model)	

* r, in.
** θ, deg

a. Bellmouth phases

Figure 19. Pressure orifice identification and location.

Channel Identification		Pressure Source	y, in.	z, in.
Scanivalve®	P_1	Plenum Pitot/Atmosphere		
	P_2	Pitot	5.65	0
	P_3	Pitot	3.90	0
	P_4	Pitot	-3.1	0
	P_5	Pitot	-4.85	0
	P_6	Pitot	-1.35	0
	P_7	Cell		
	P^8	Pitot		
	P_9	Cone Pitot	2.15	0
	P_{10}	Pitot	0.4	0
	P_{11}	Pitot	0.4	2.75
	P_{12}	Downstream Plenum	0.4	-1.87
	P_{13}	Cone Static		
	P_{14}	Cone Static		
	P_{15}	Cone Static		
	P_{16}	Cone Static		

b. "No bellmouth" phase
Figure 19. Concluded.

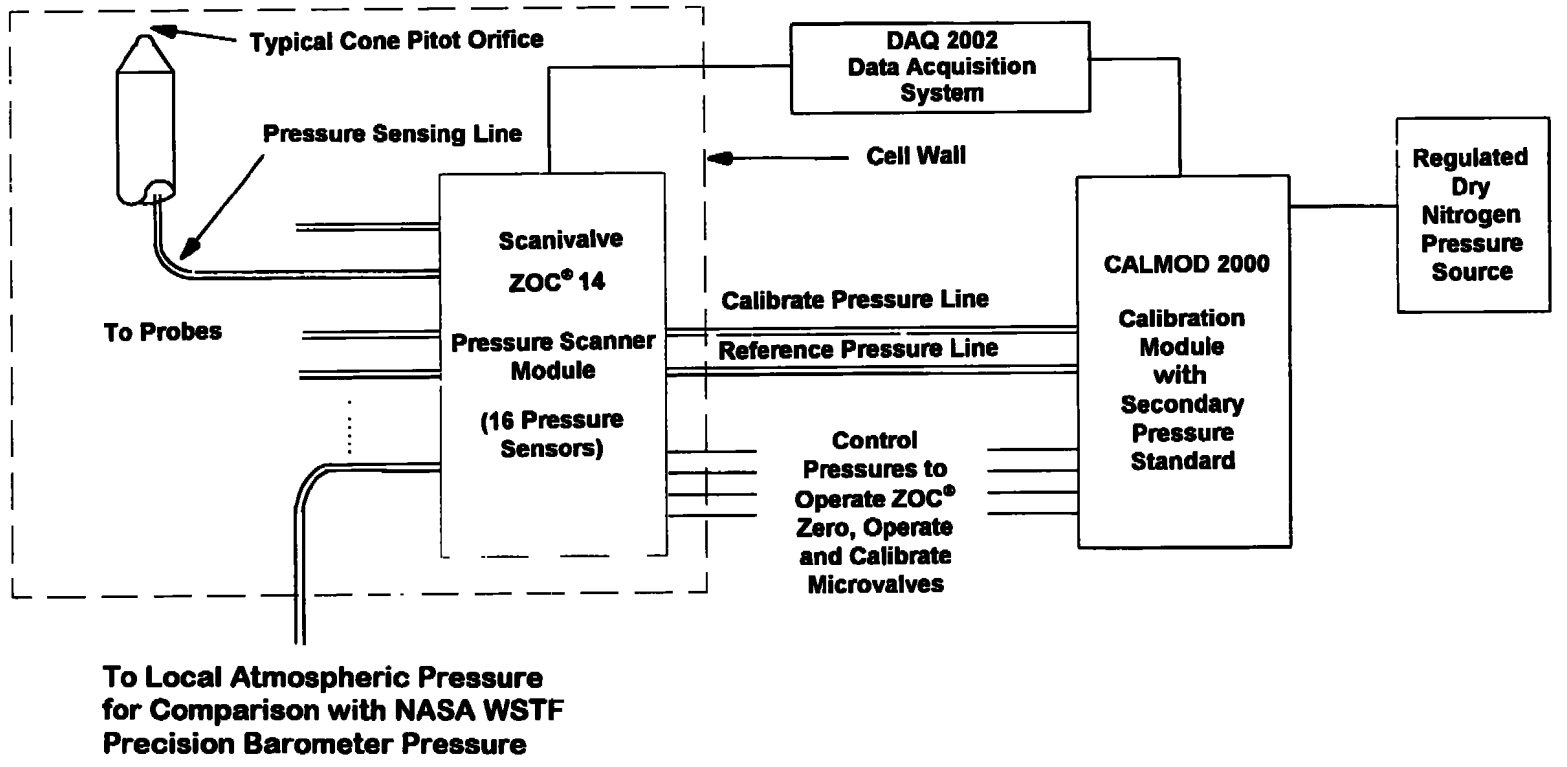

Figure 20. Pressure system schematic.

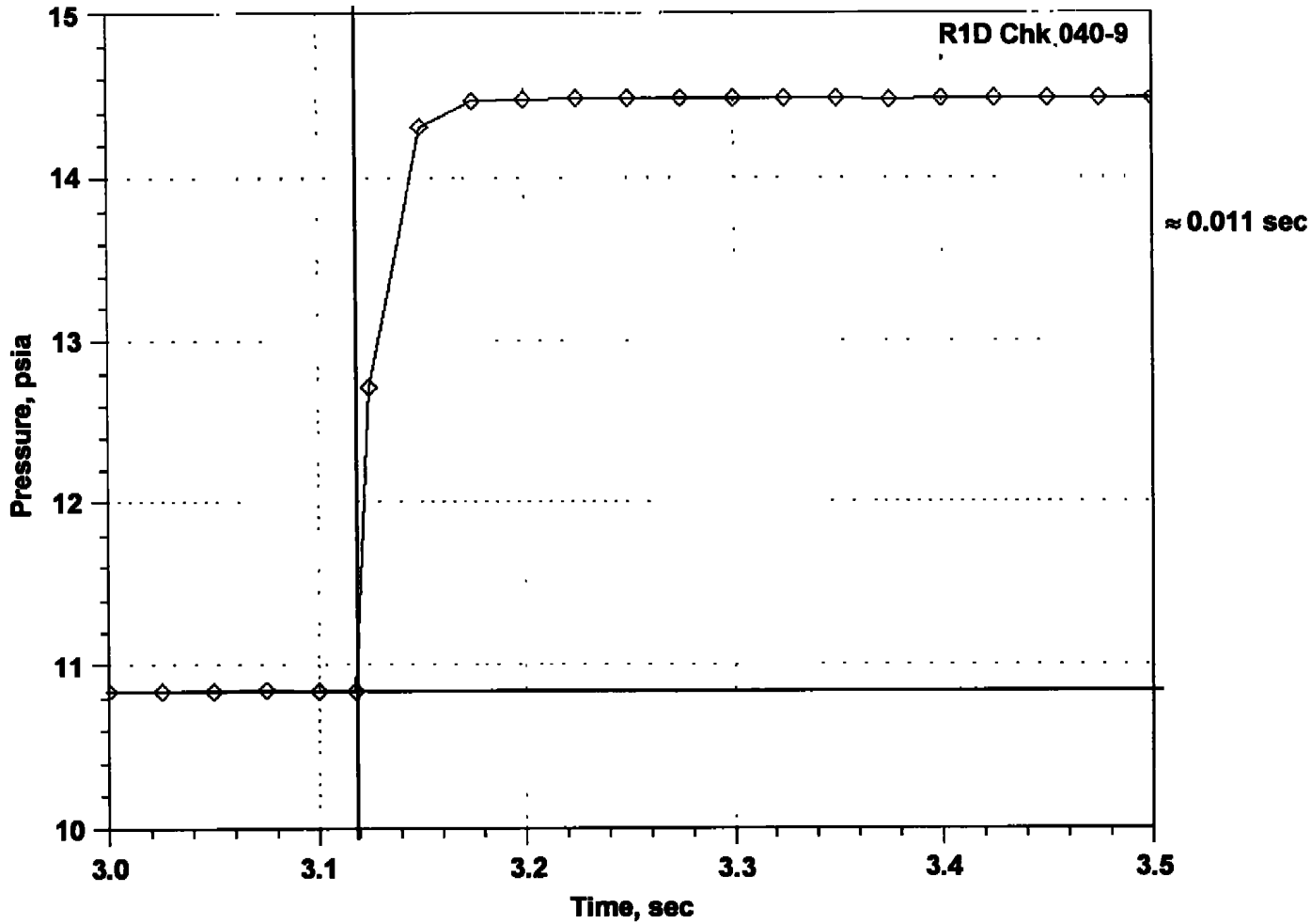

Figure 21. Pressure system time response.

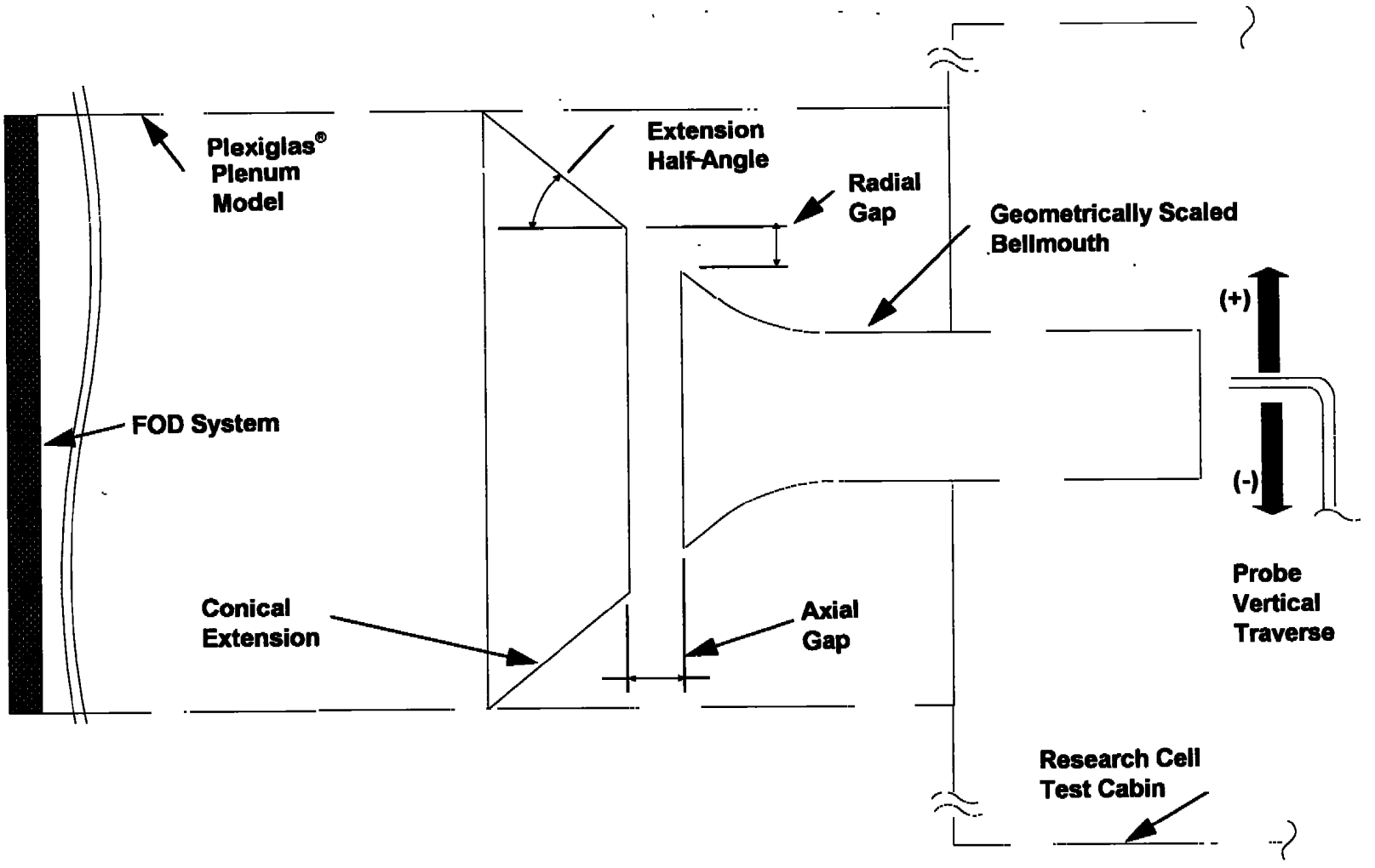

Figure 22. Schematic elevation view of subscale plenum model.

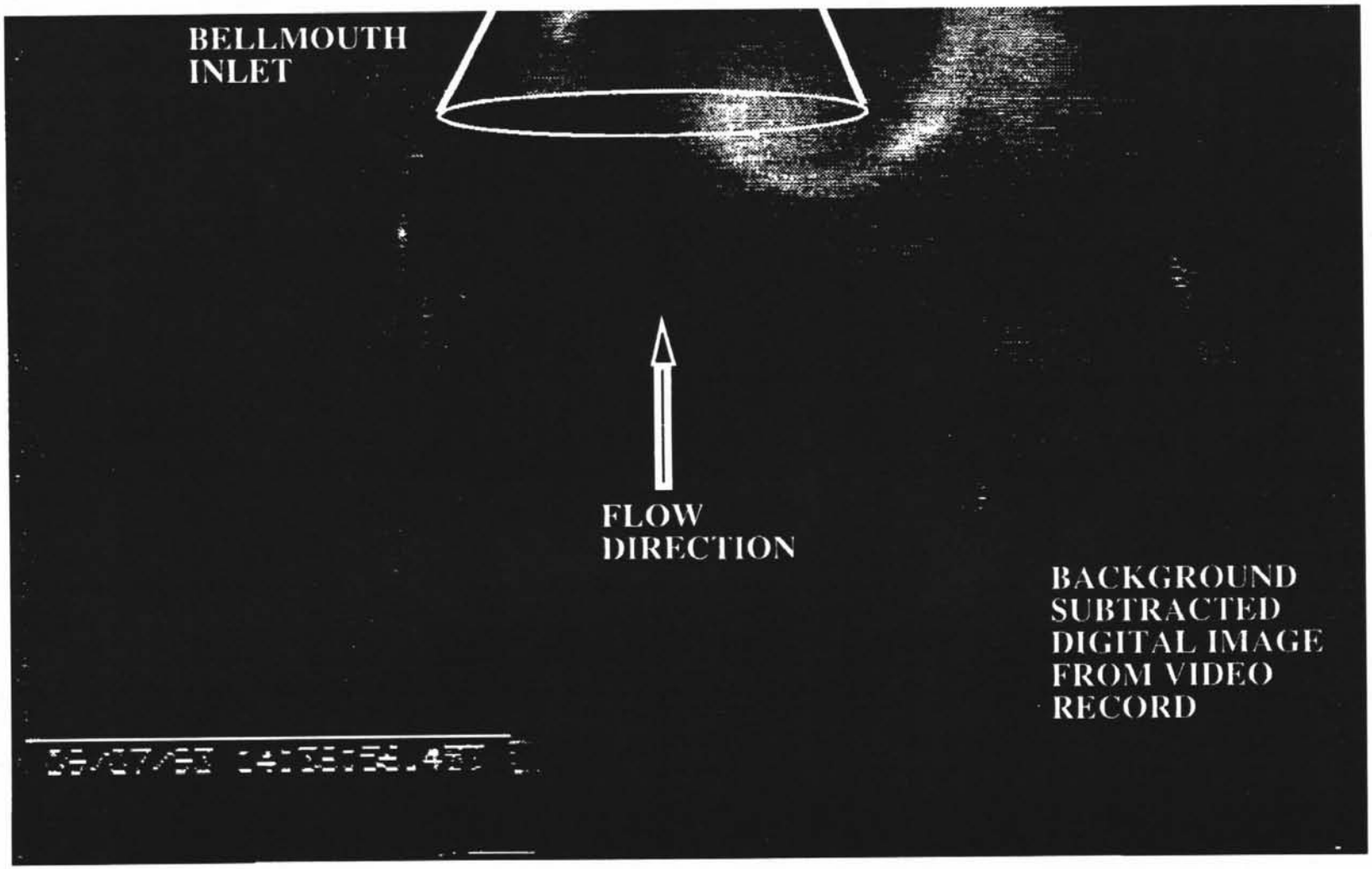

Figure 23. Image of vortex at subscale bellmouth inlet produced with the smoke/laser visualization.

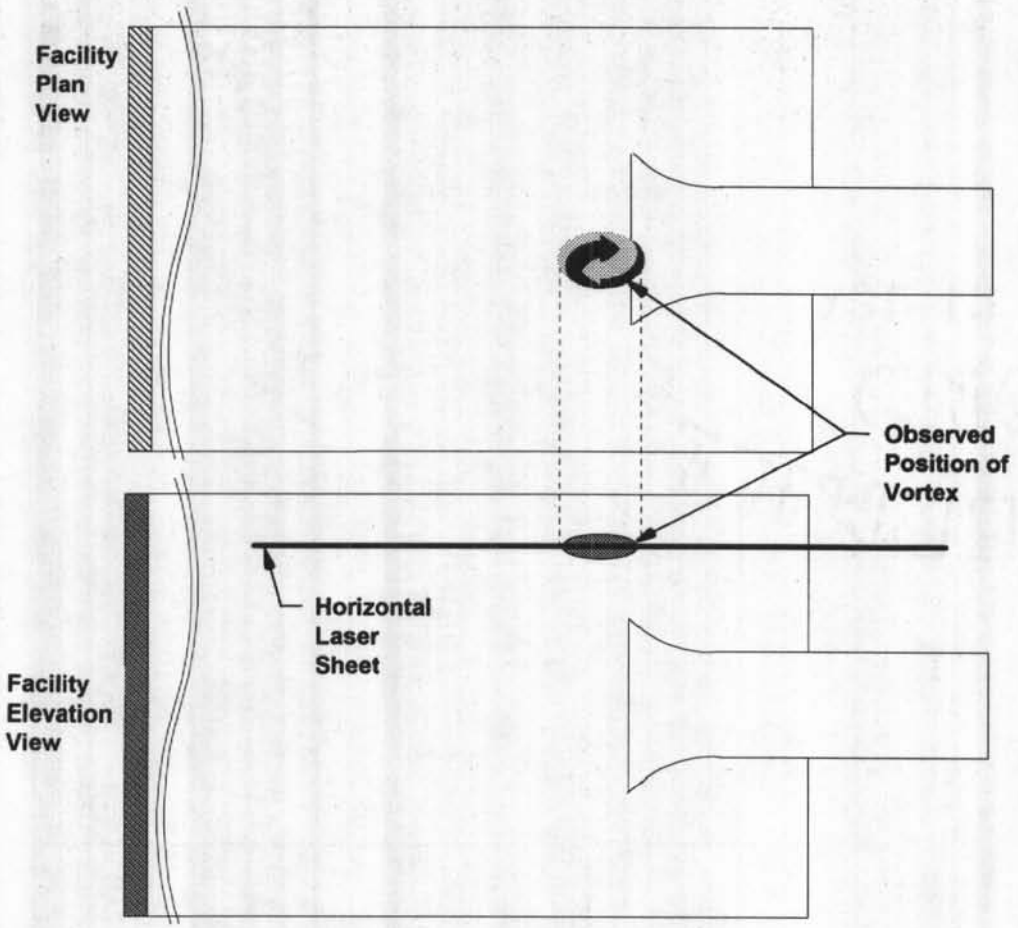

Figure 24. Schematic diagram of vortex at subscale bellmouth inlet.

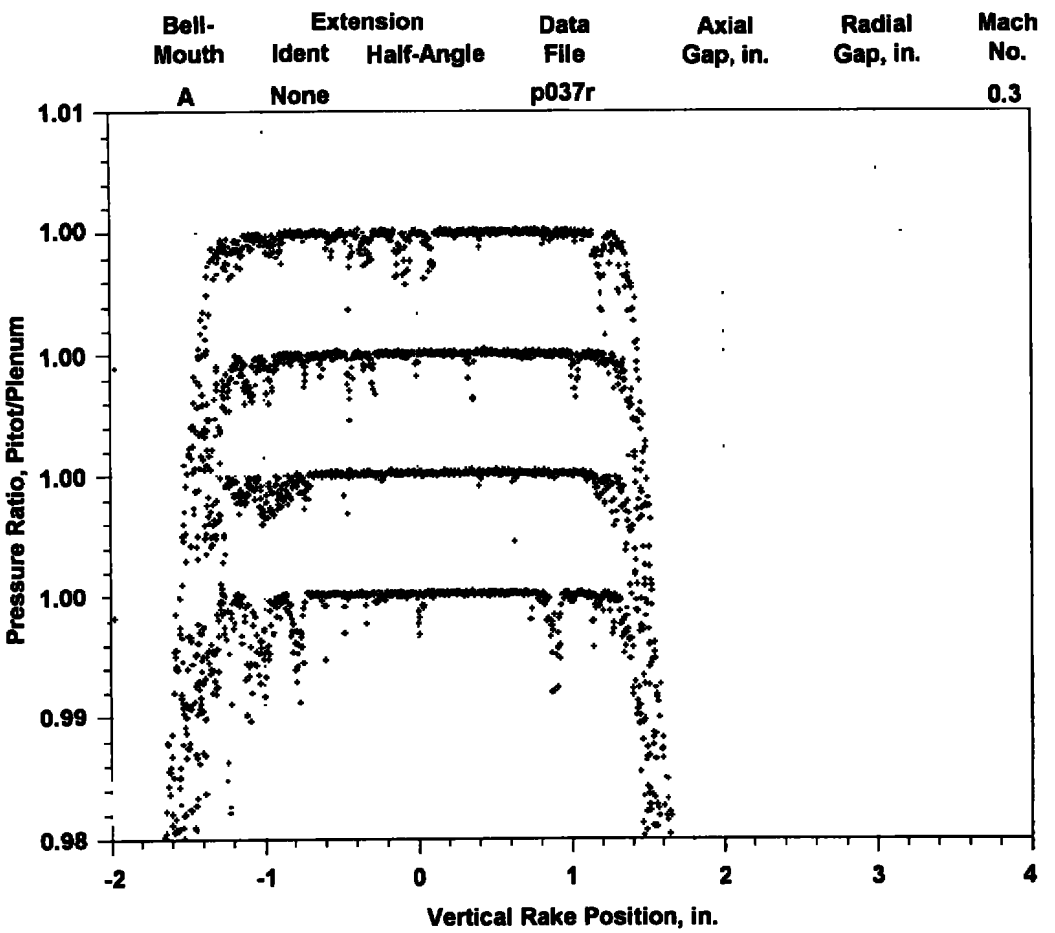

Figure 25. Comparison of total pressure profiles for several "repeat" traverses in Bellmouth A without extension.

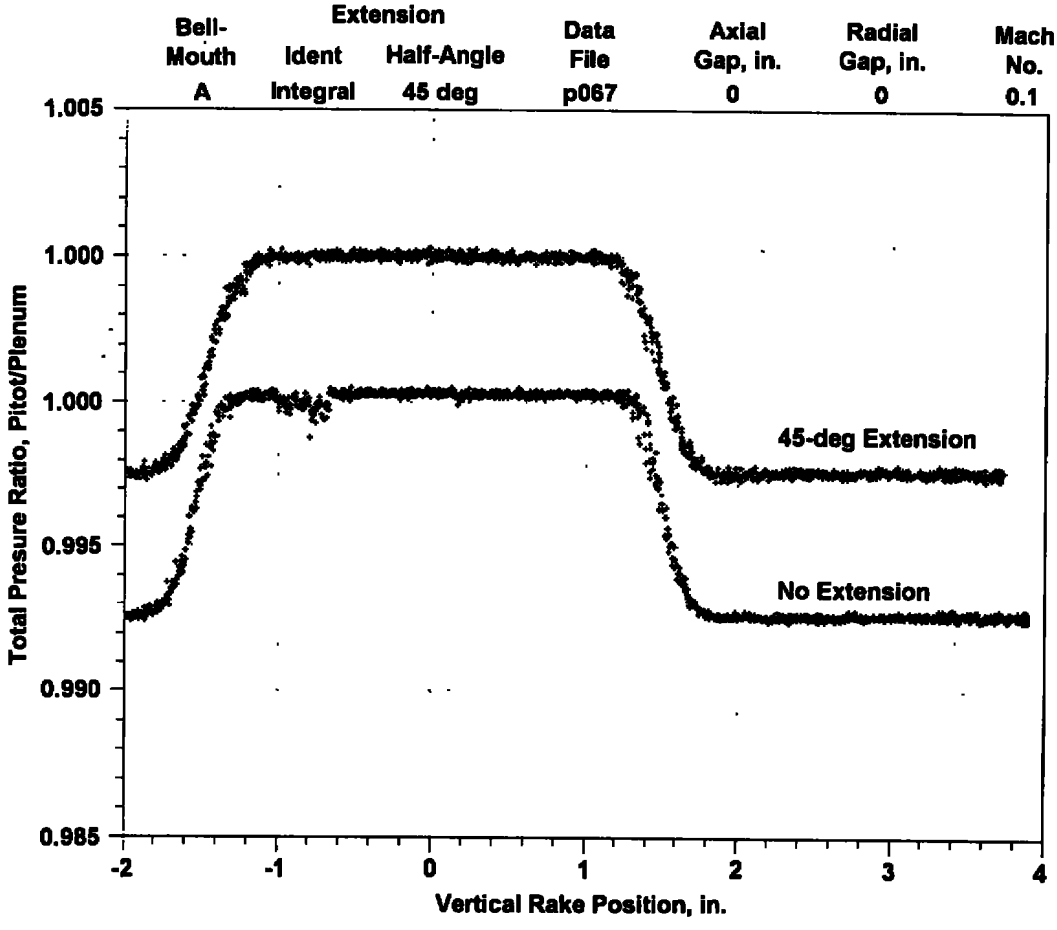

a. M = 0.1

Figure 26. Effect of extension on total pressure profiles in Bellmouth A.

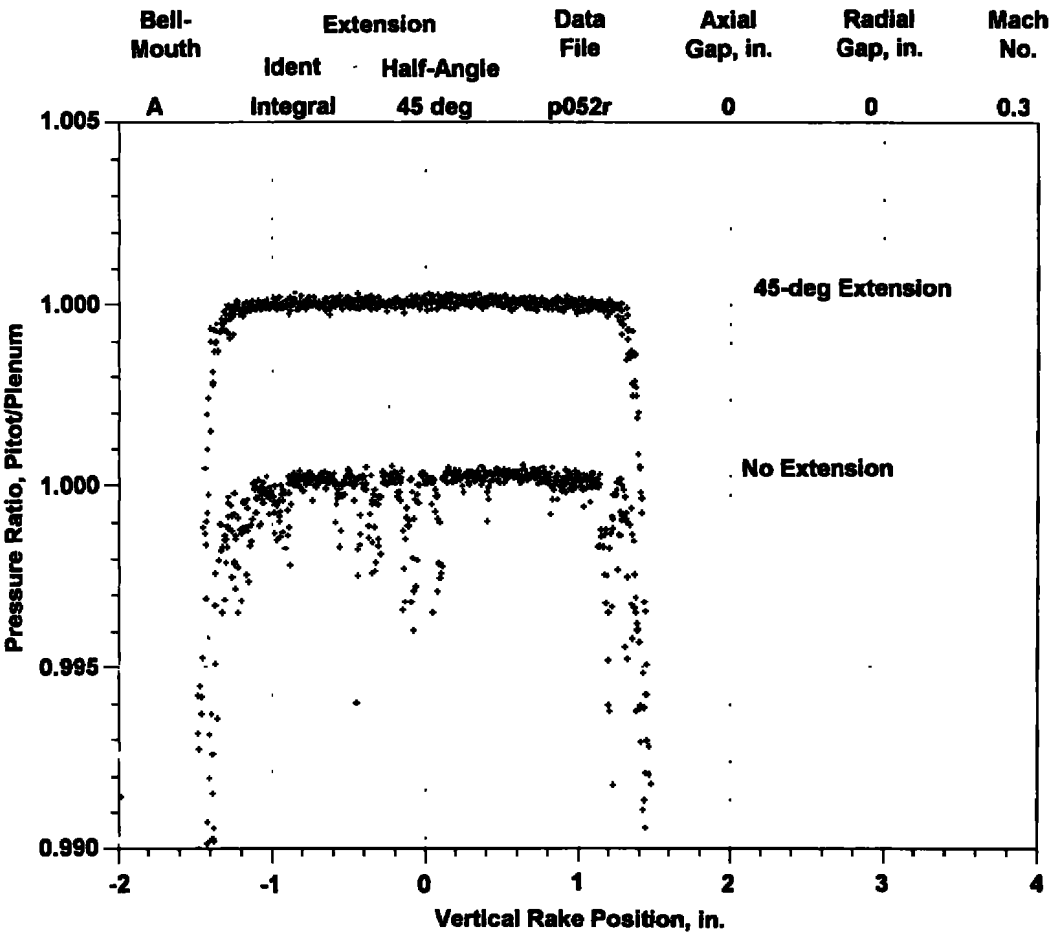

b. M = 0.3

Figure 26. Continued.

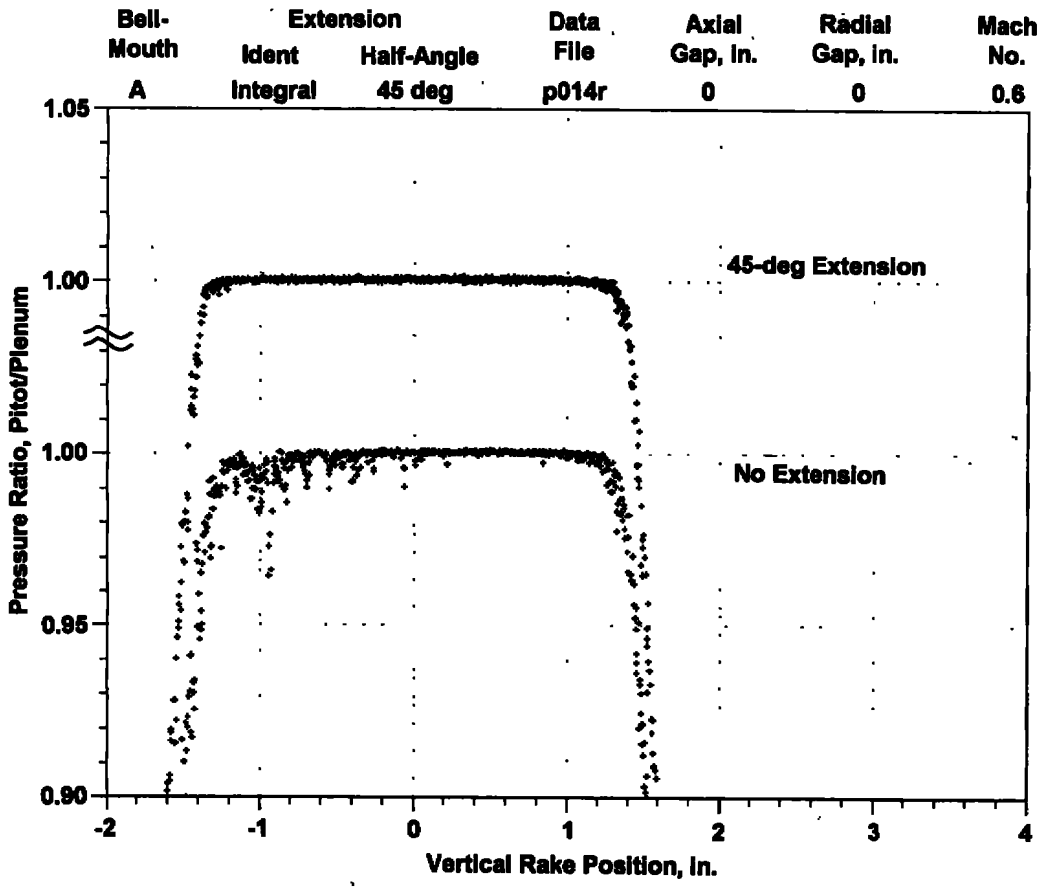

c. M = 0.6

Figure 26. Concluded.

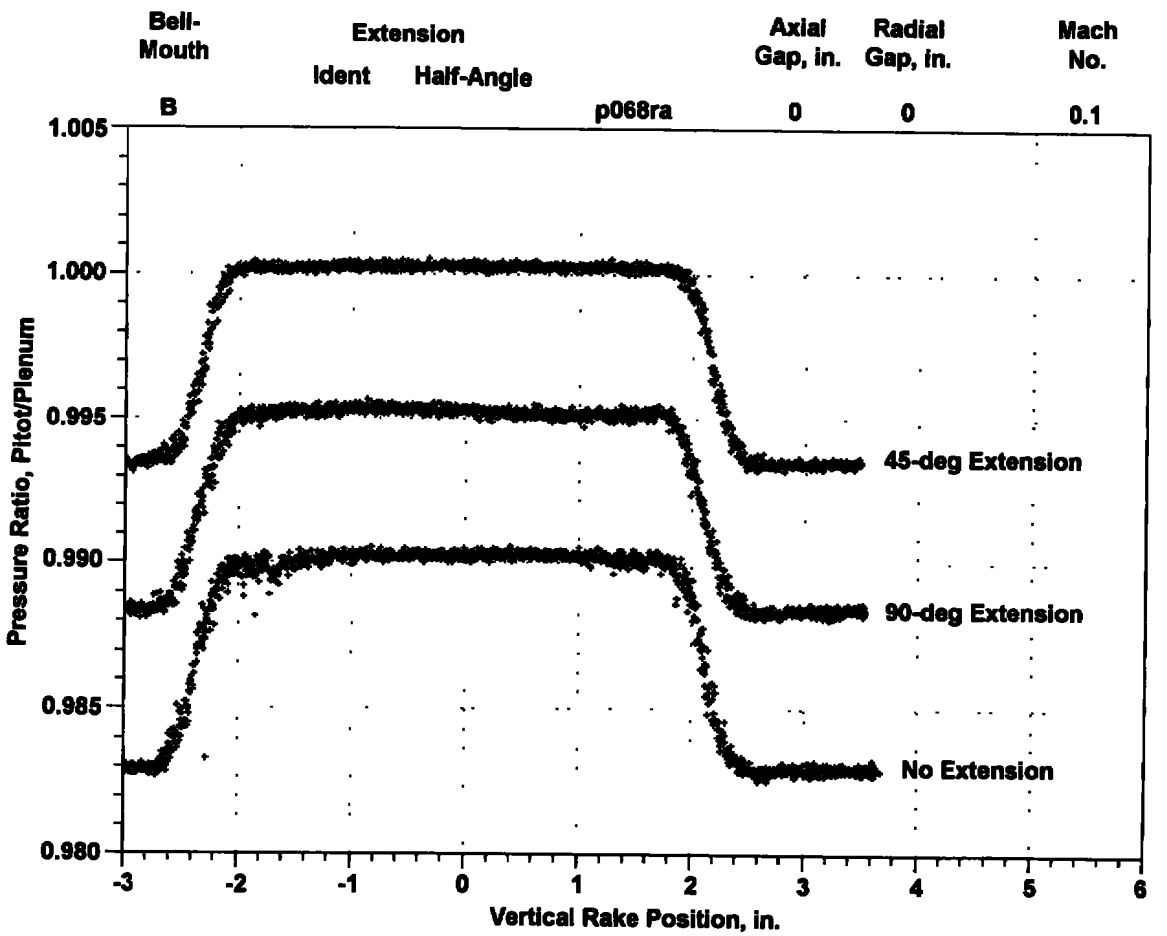

a. M = 0.1

Figure 27. Effect of extensions on total pressure profiles in Bellmouth B.

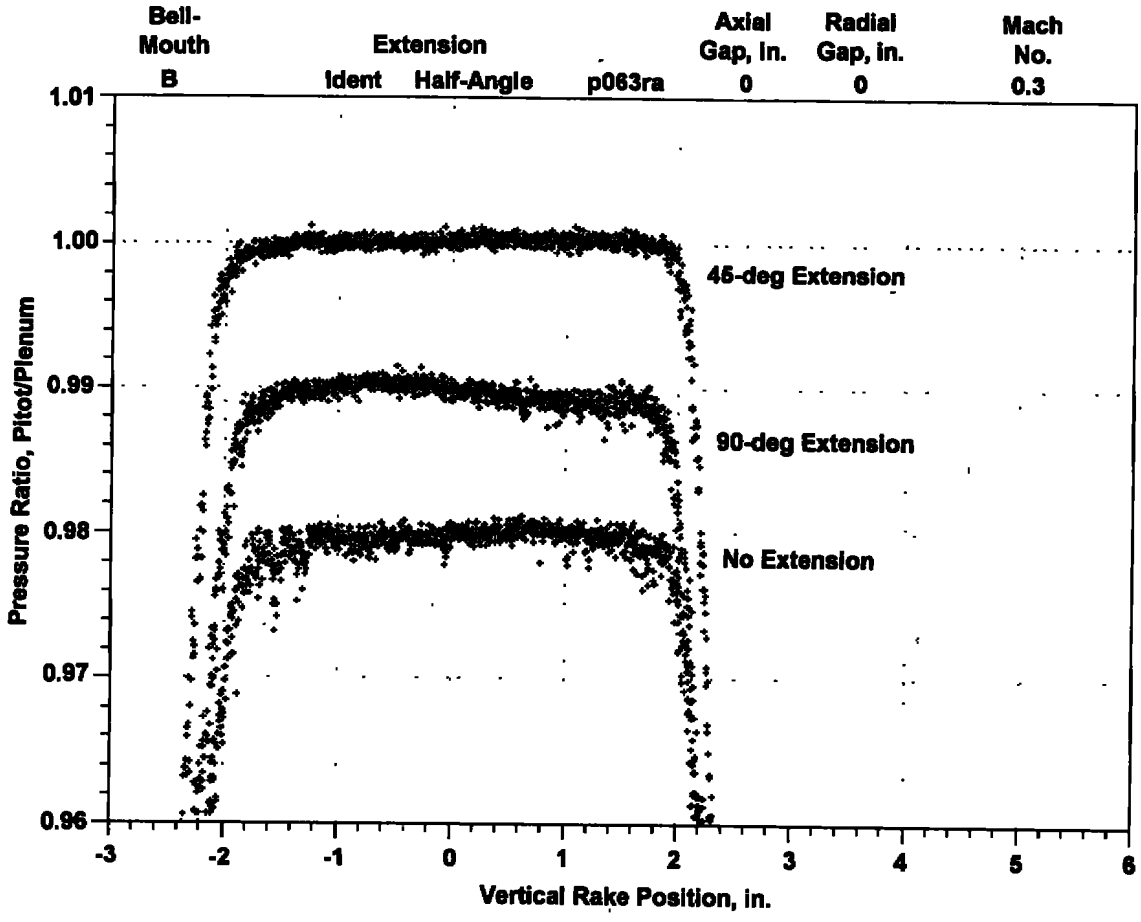

b. M = 0.3

Figure 27. Continued.

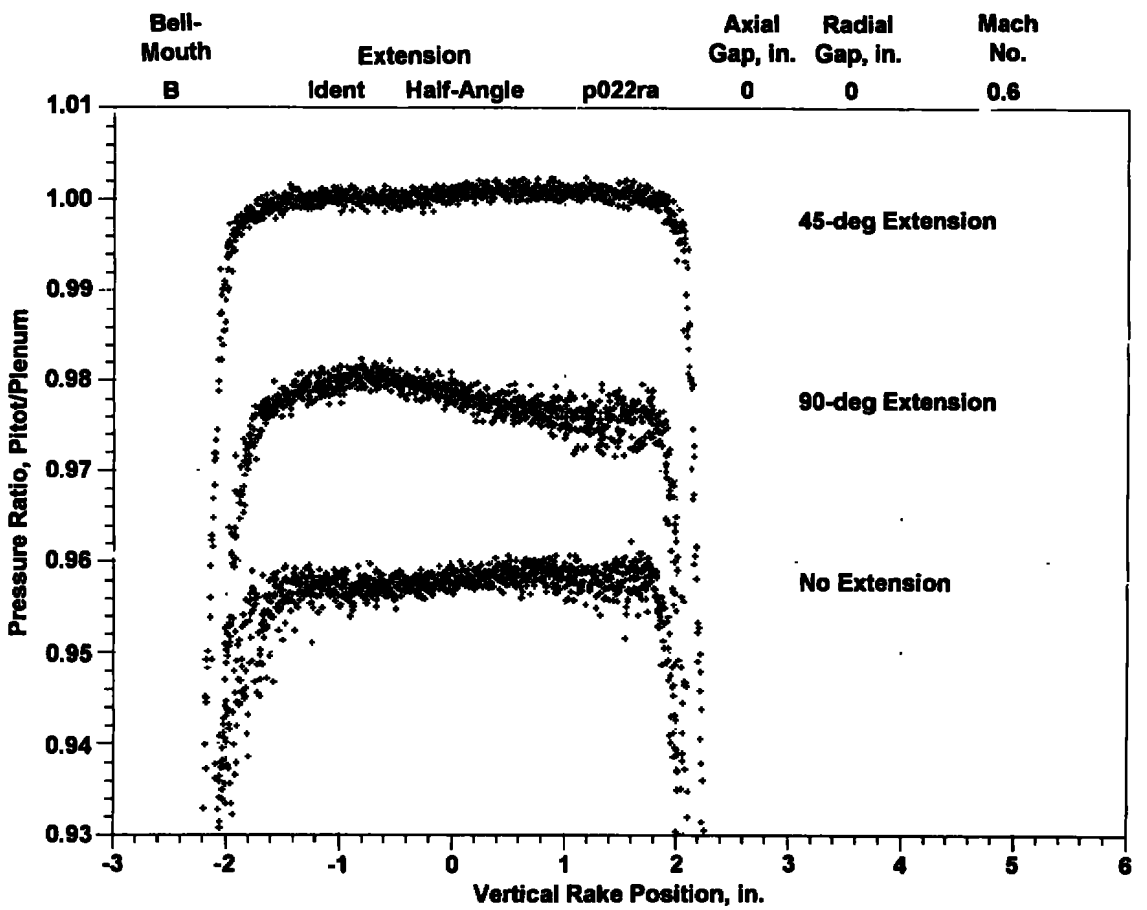

c. M = 0.6

Figure 27. Concluded.

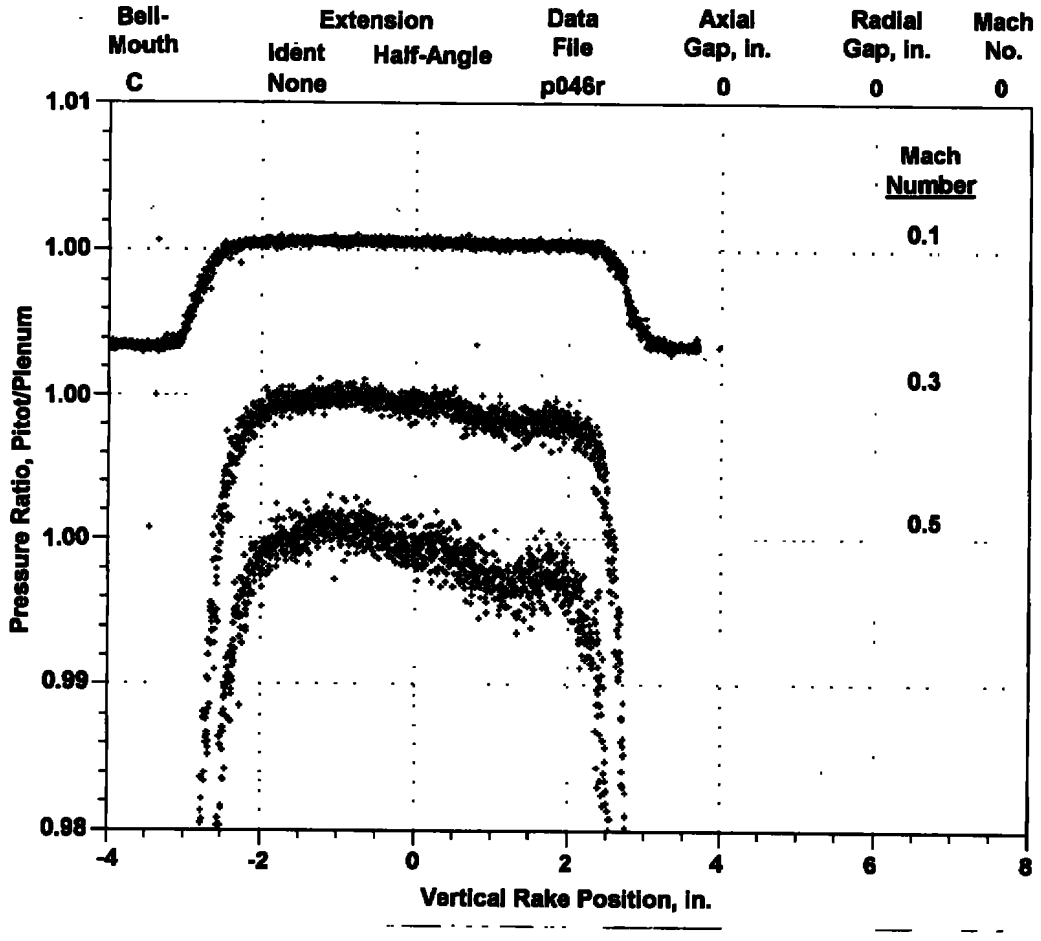

a. Total pressure ratio parameter

Figure 28. Comparison of total pressure profiles for several Mach numbers in Bell-mouth C.

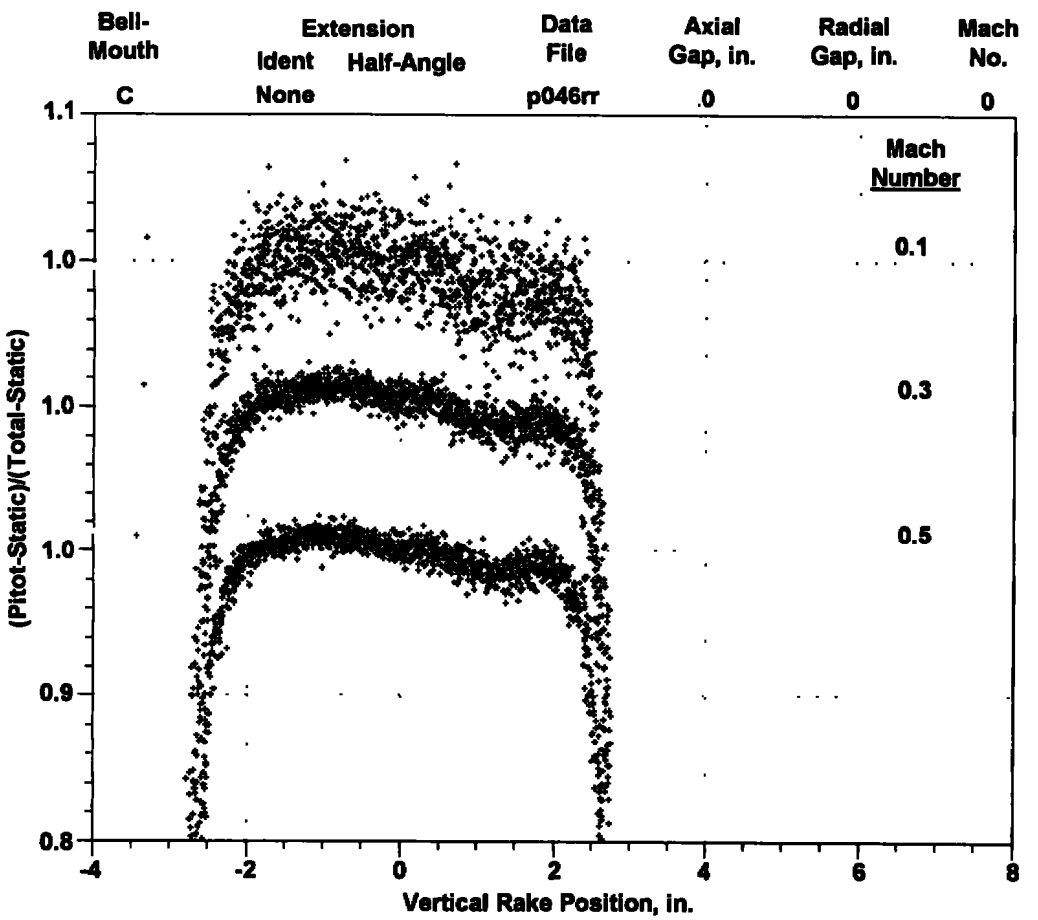

b. Dynamic pressure ratio parameter
Figure 28. Concluded.

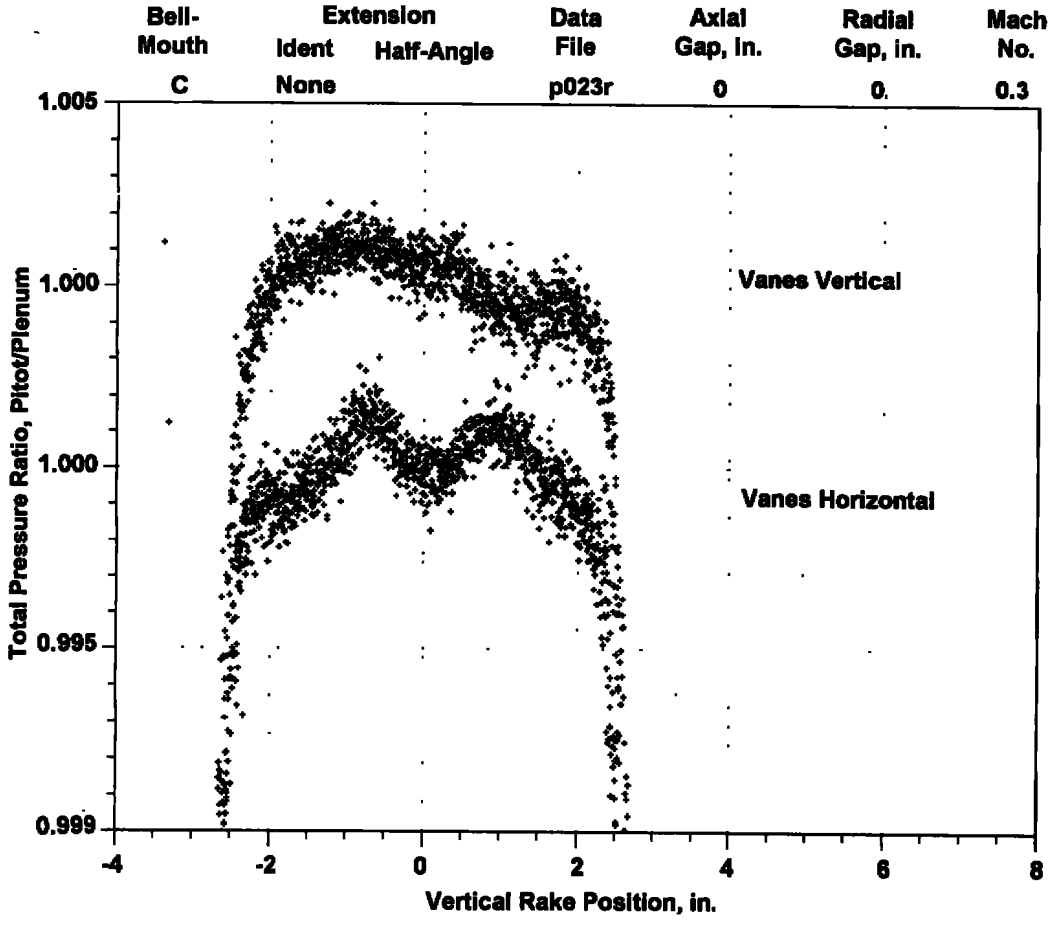

Figure 29. Effect of FOD screen/vane orientation on total pressure profiles in Bell-mouth C.

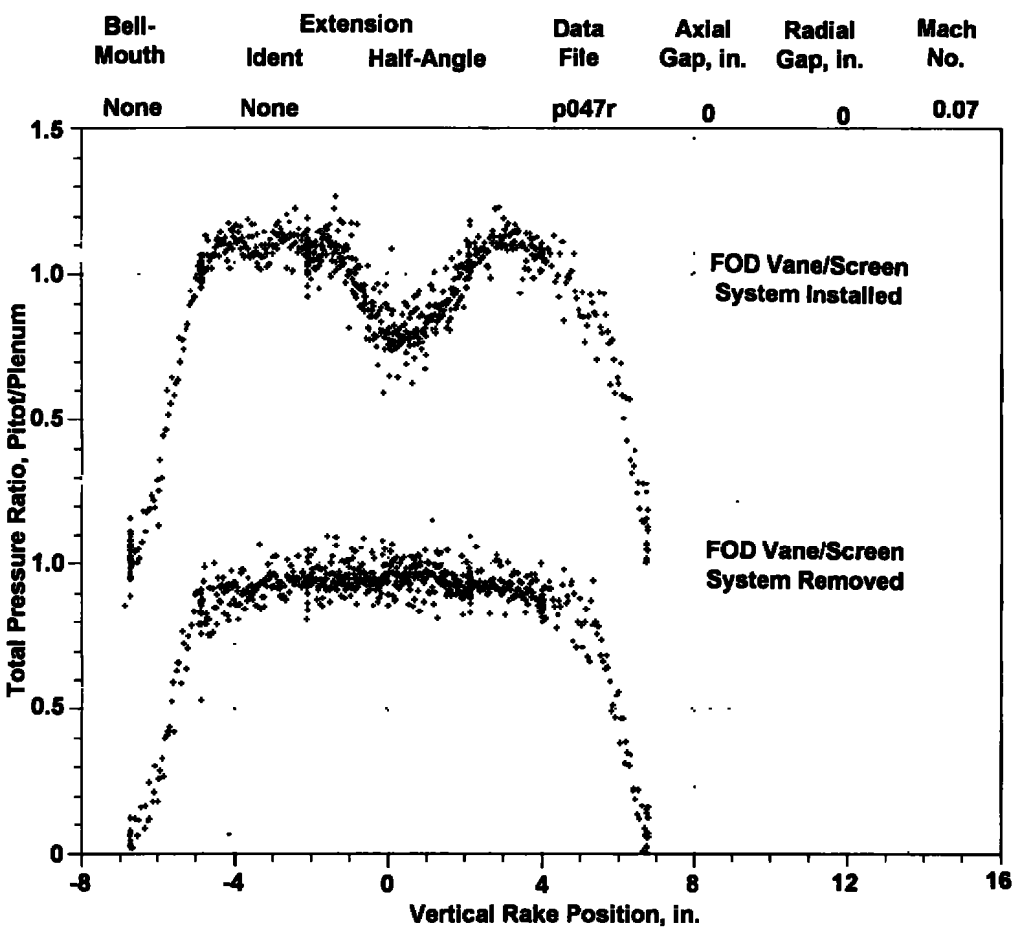

Figure 30. Effect of flow-straightening vanes on plenum total pressure profiles with bellmouth removed.

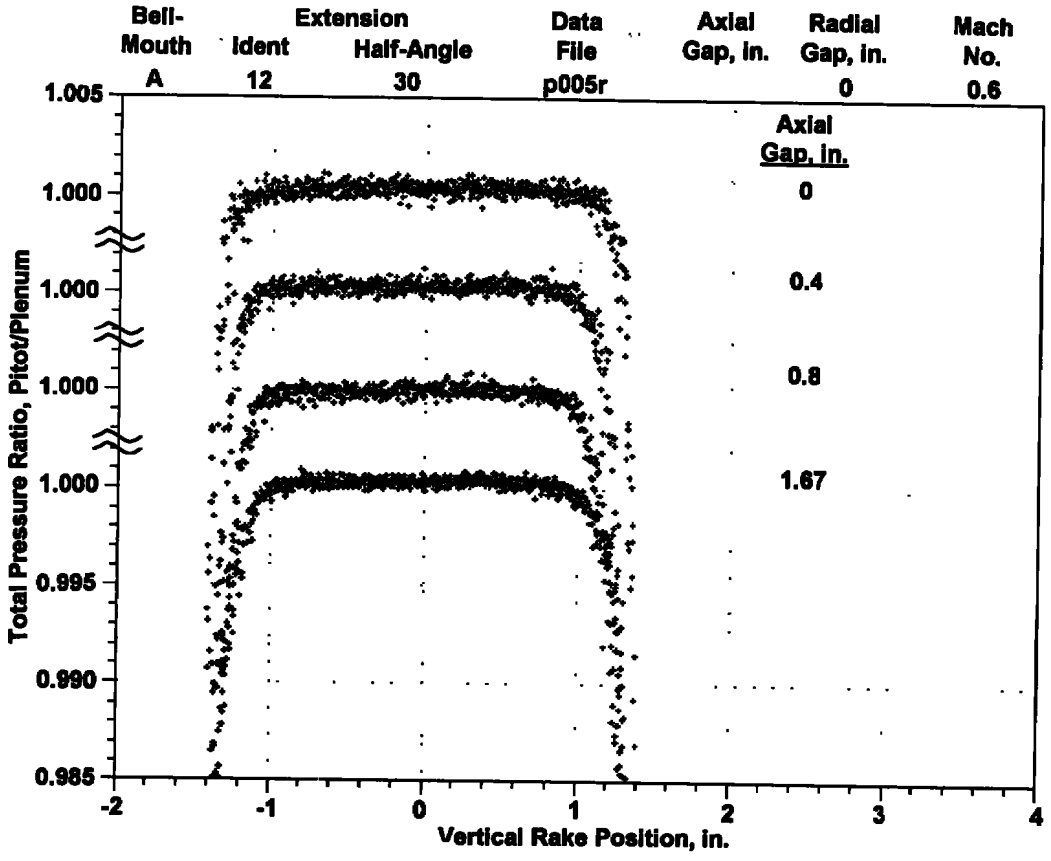

a. Extension half-angle, θ = 30 deg

Figure 31. Effect of increasing axial gap on total pressure profiles in Bellmouth A for zero radial gap.

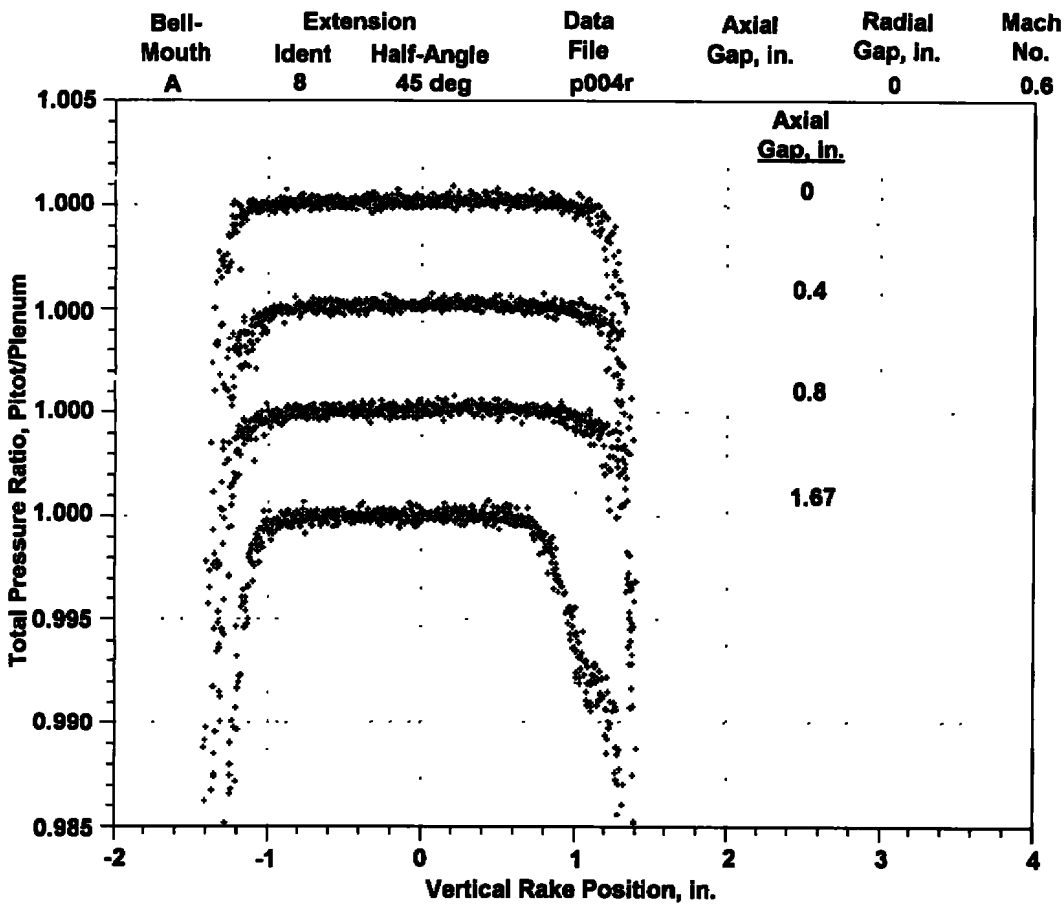

b. Extension half-angle, θ = 45 deg
Figure 31. Continued.

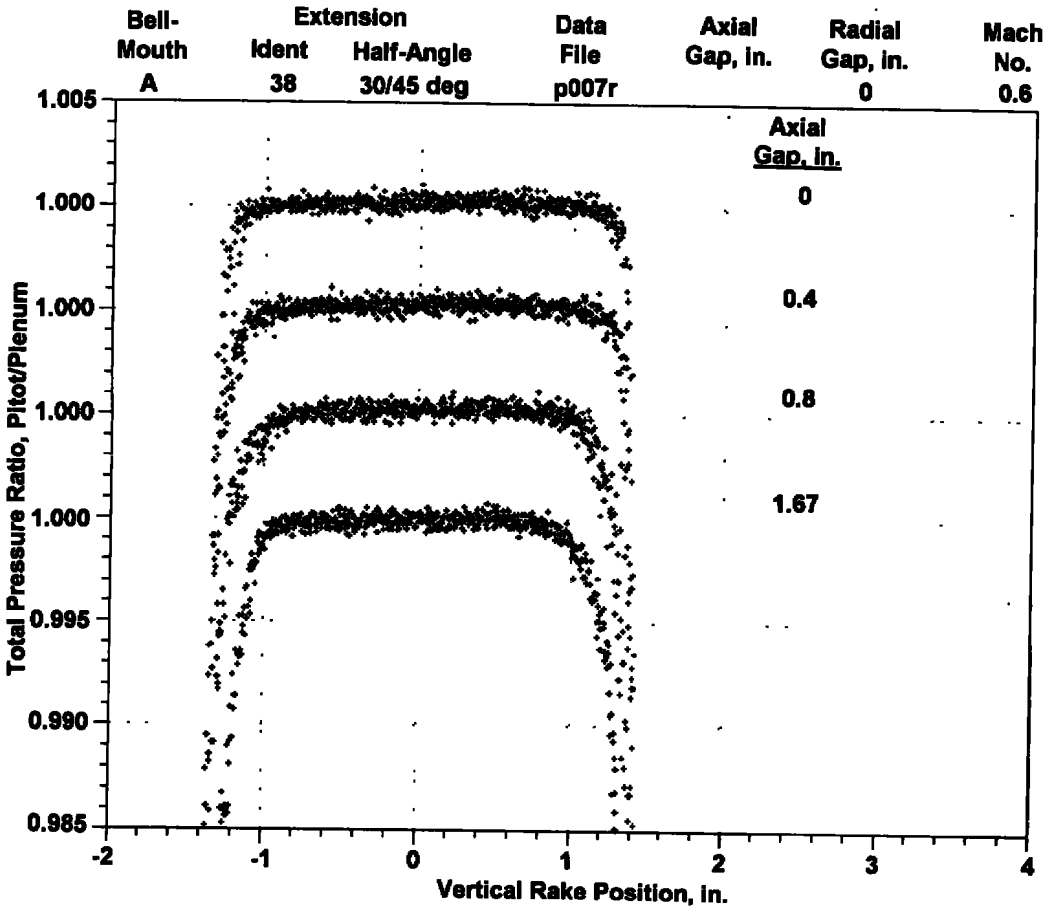

c. Extension half-angle, θ = 30/45 deg
Figure 31. Continued.

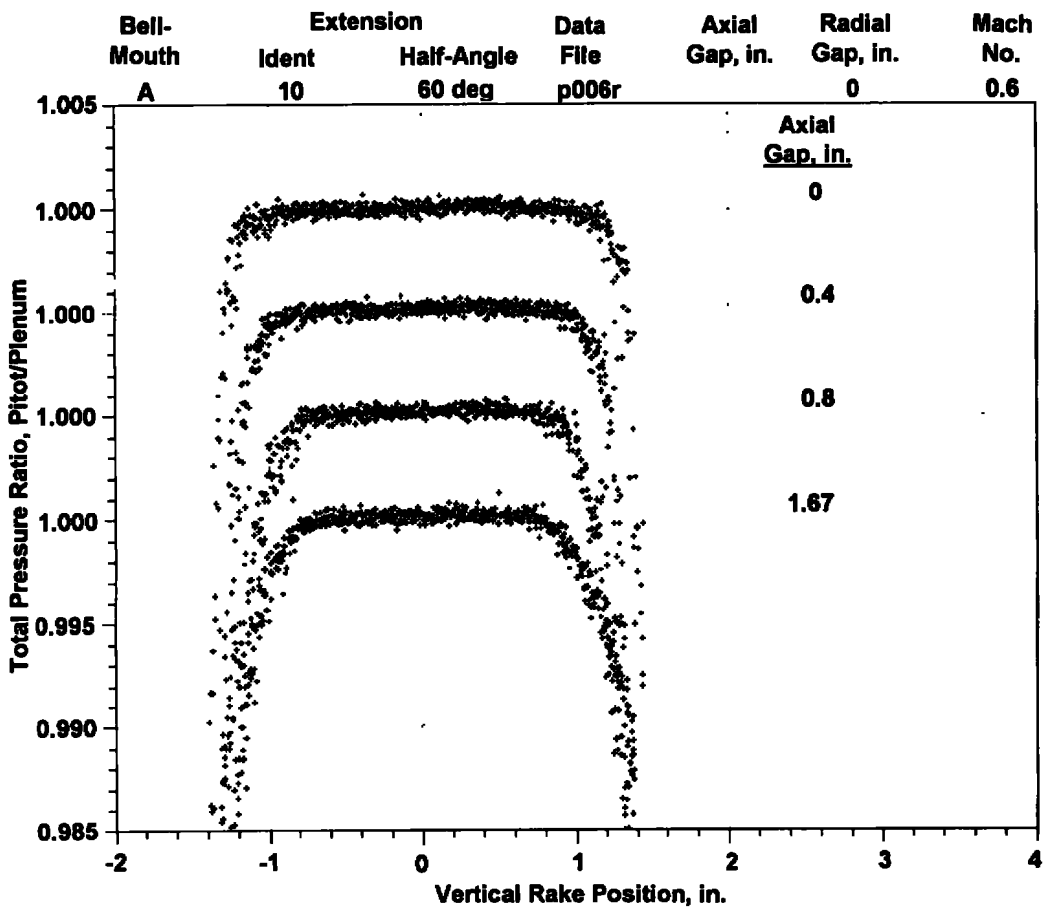

d. Extension half-angle, θ = 60 deg

Figure 31. Concluded.

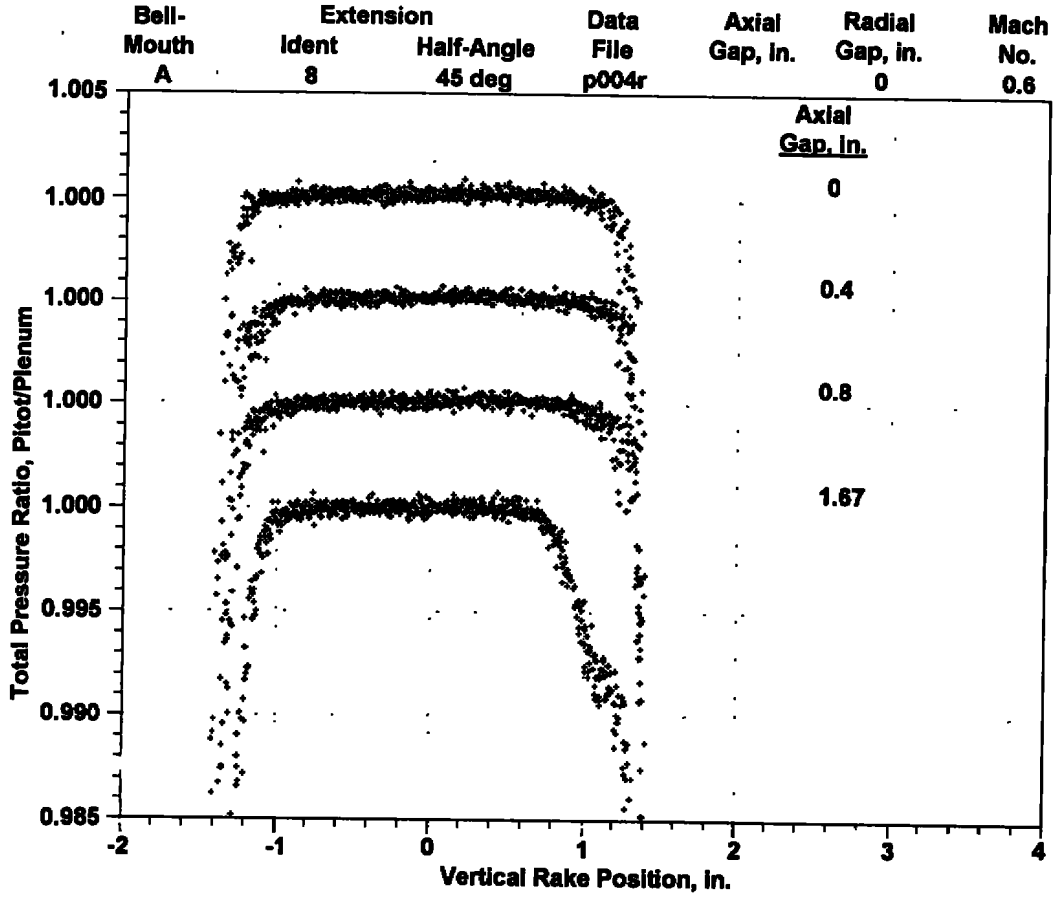

a. Fixed extension roll orientation baseline

Figure 32. Effect of extension roll orientation on total pressure profiles in Bell-mouth A for large axial gap and zero radial gap.

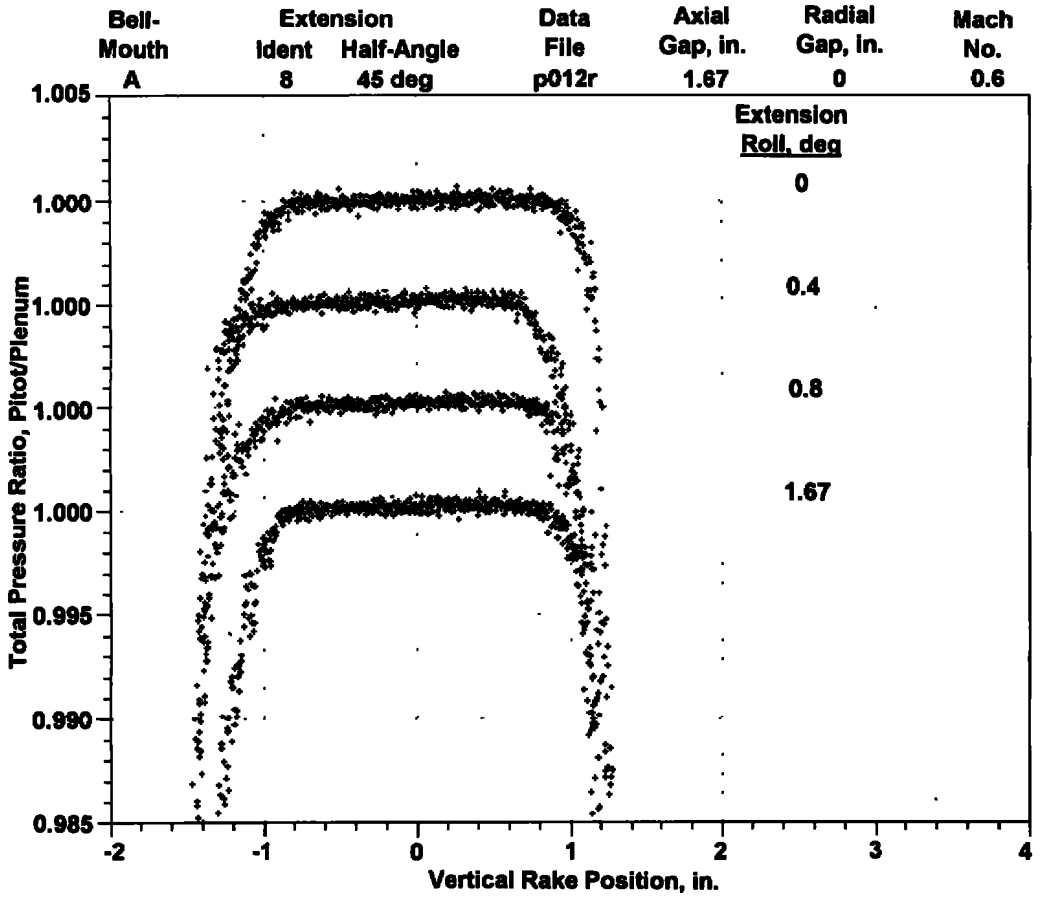

b.Variable extension roll orientation, axial grap = 1.67 in.
Figure 32. Concluded.

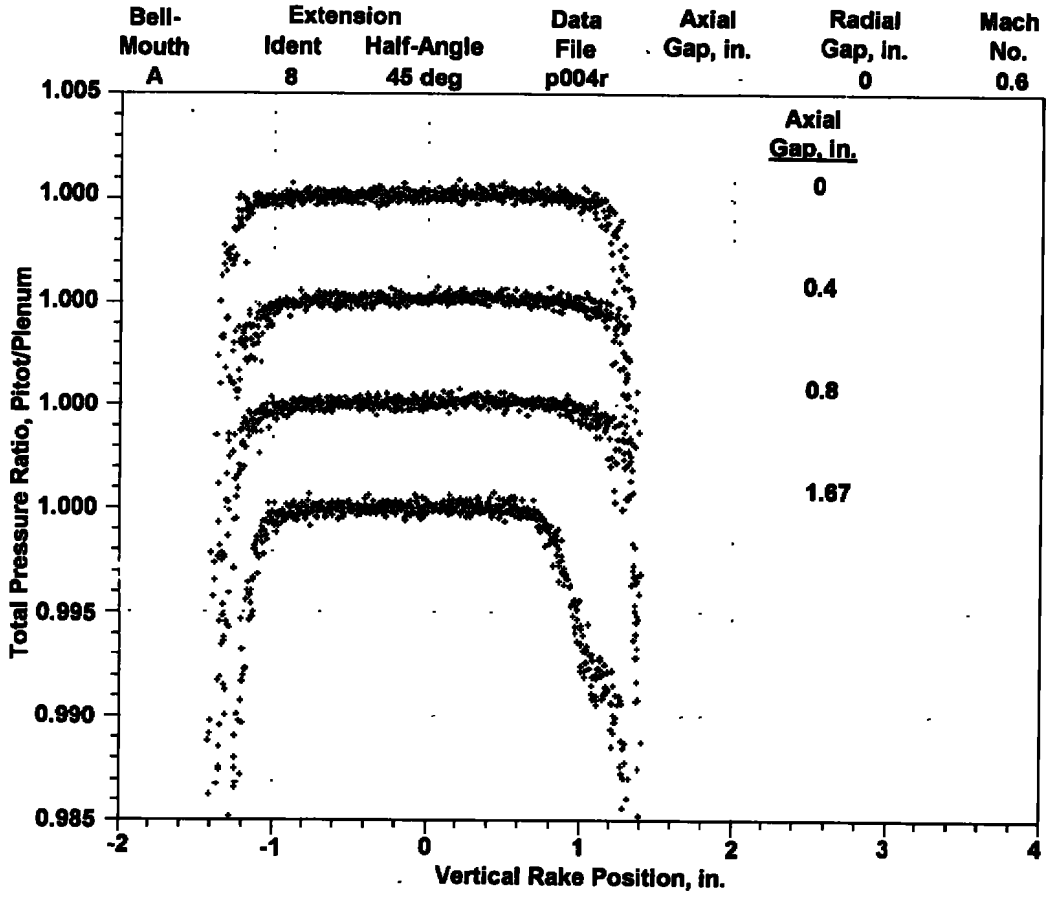

a. Radial gap = 0

Figure 33. Effect of increasing axial gaps on total pressure profiles in Bellmouth A for 45-deg half-angle extension.

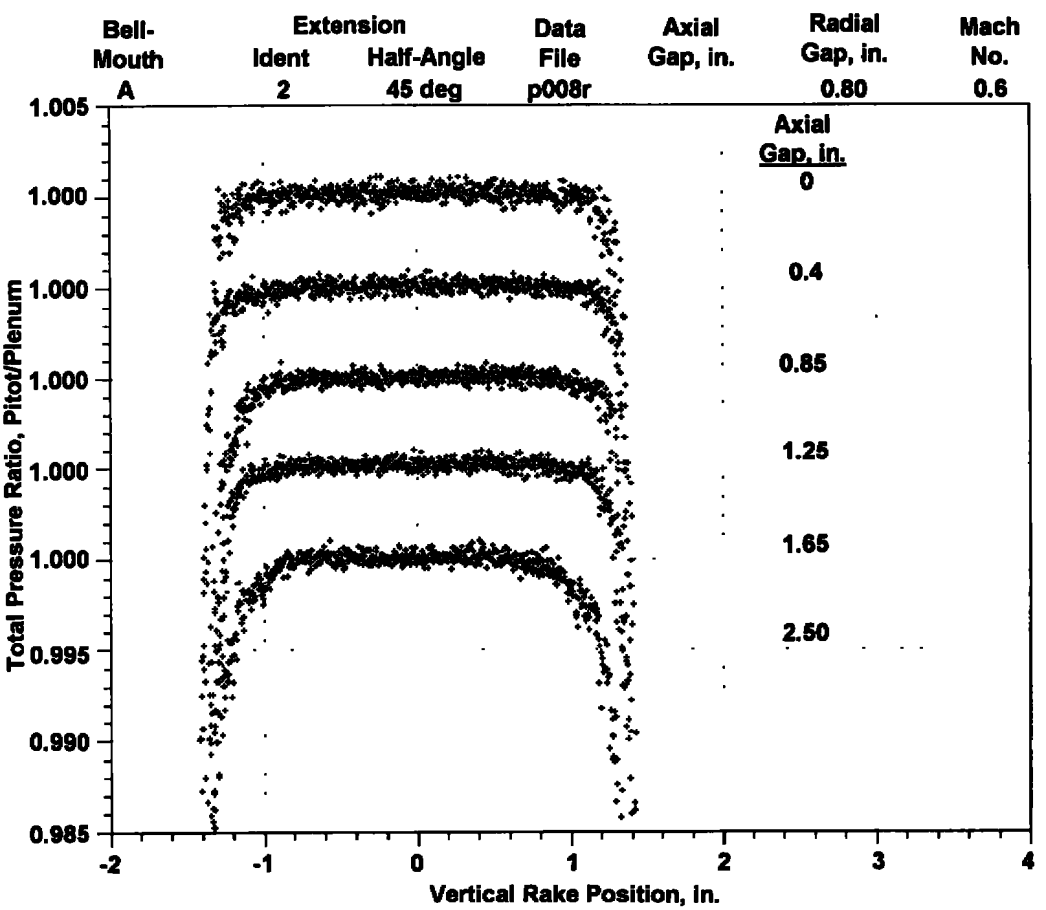

b. Radial gap = 0.85 in.

Figure 33. Continued.

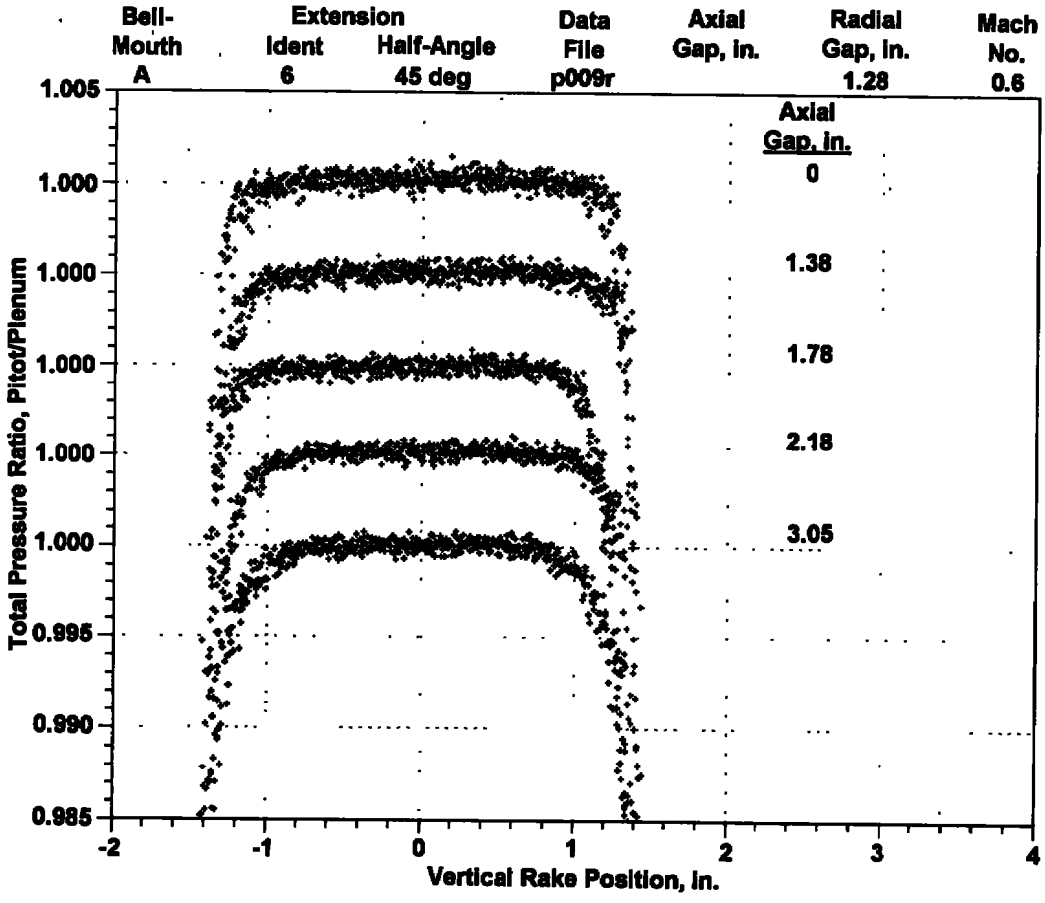

c. Radial gap = 1.30 in.

Figure 33. Concluded.

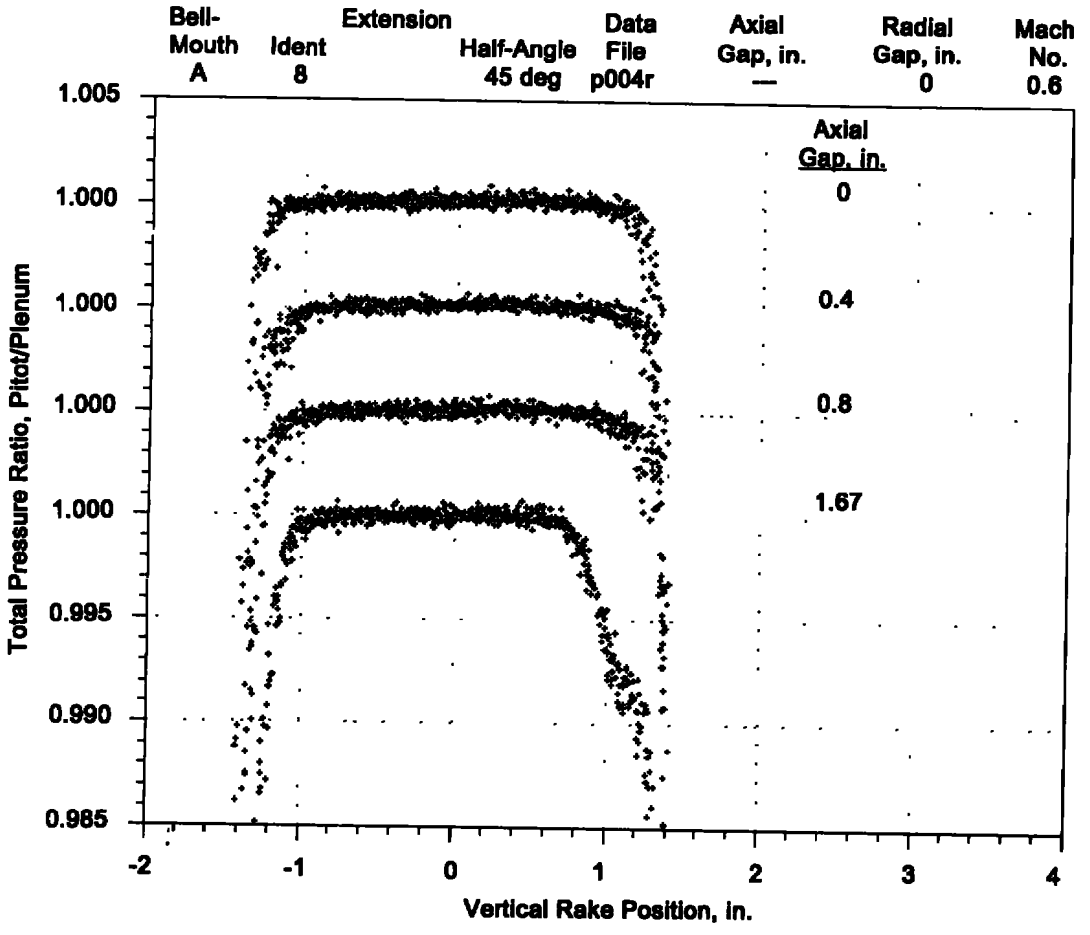

a. M = 0.6, baseline

Figure 34. Comparison of total pressure profiles for two Mach numbers in Bellmouth A.

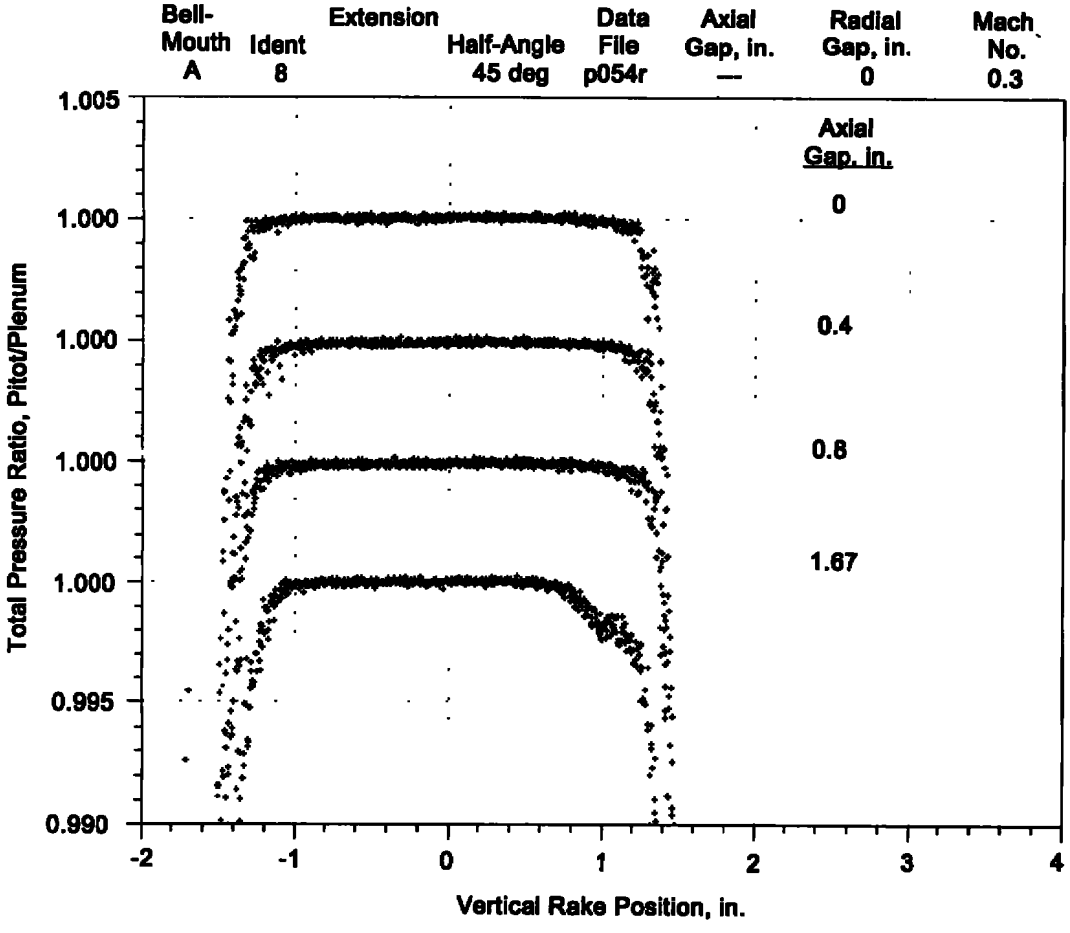

b. M = 0.3

Figure 34. Concluded.

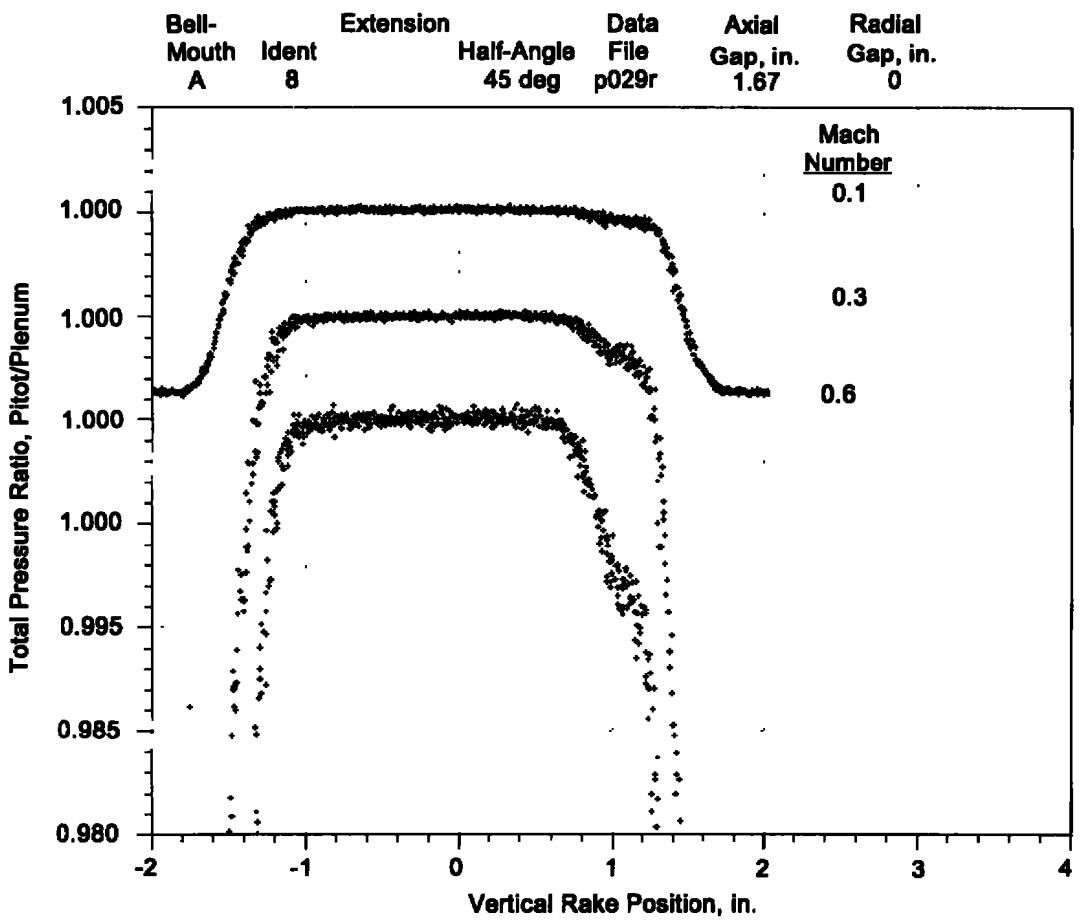

a. Total pressure ratio parameter

Figure 35. Effect of Mach number variation on total pressure profiles in Bellmouth A for large axial gap and zero radial gap.

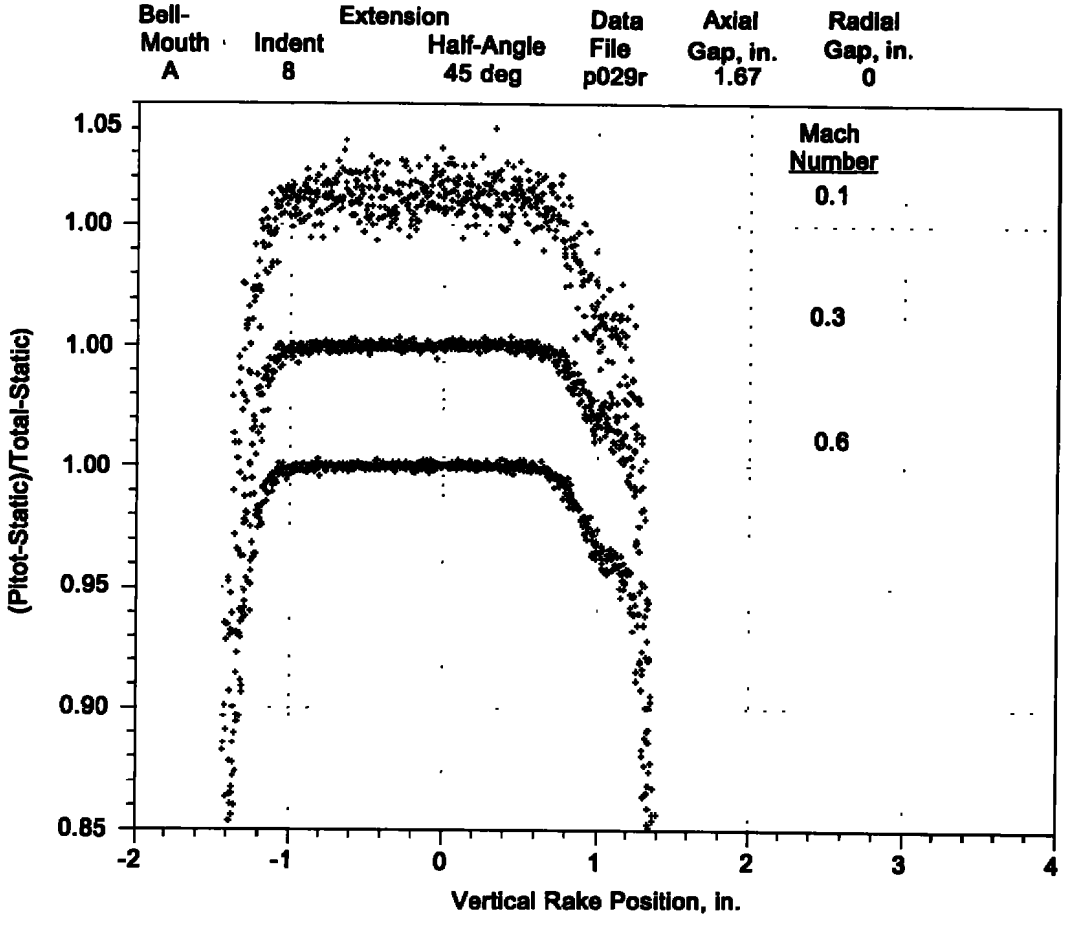

b. Dynamic pressure ratio parameter

Figure 35. Concluded.

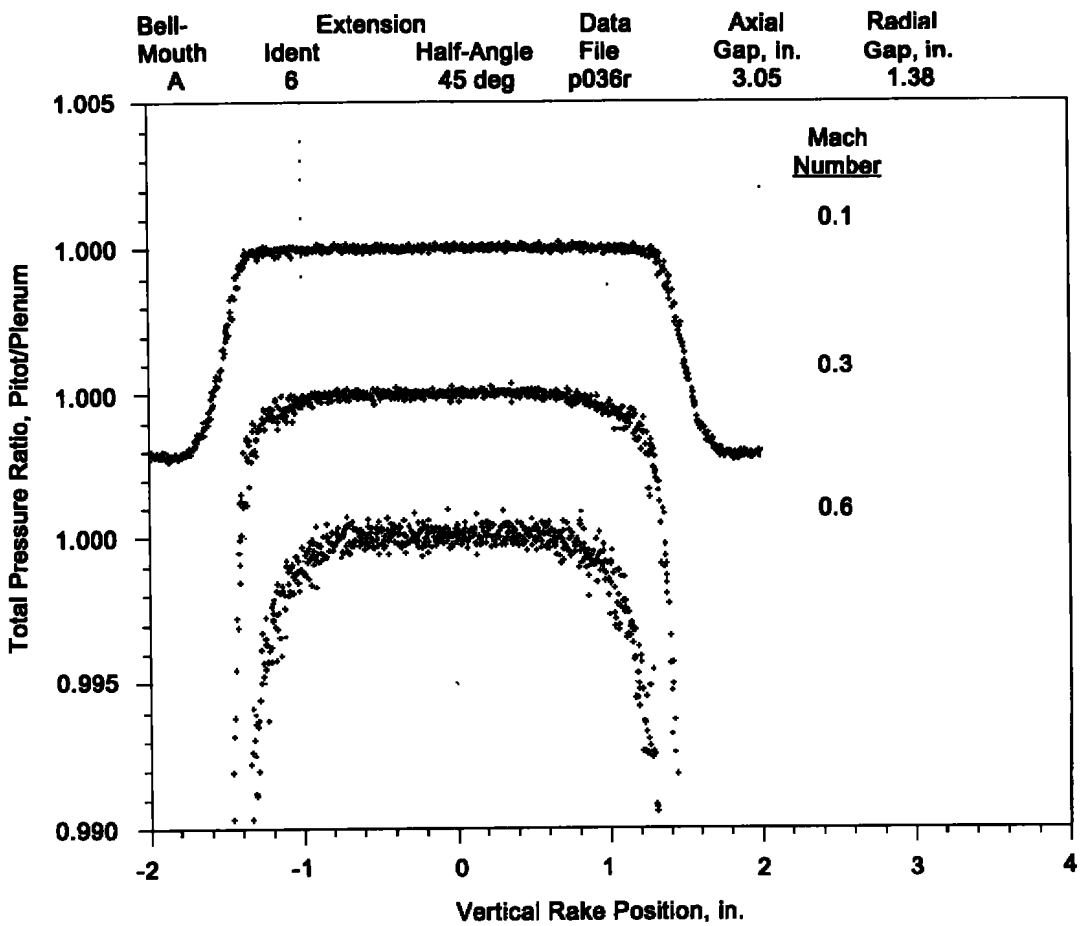

a. Total pressure ratio parameter

Figure 36. Effect of Mach number variation on total pressure profiles in Bellmouth A for large axial and radial gaps.

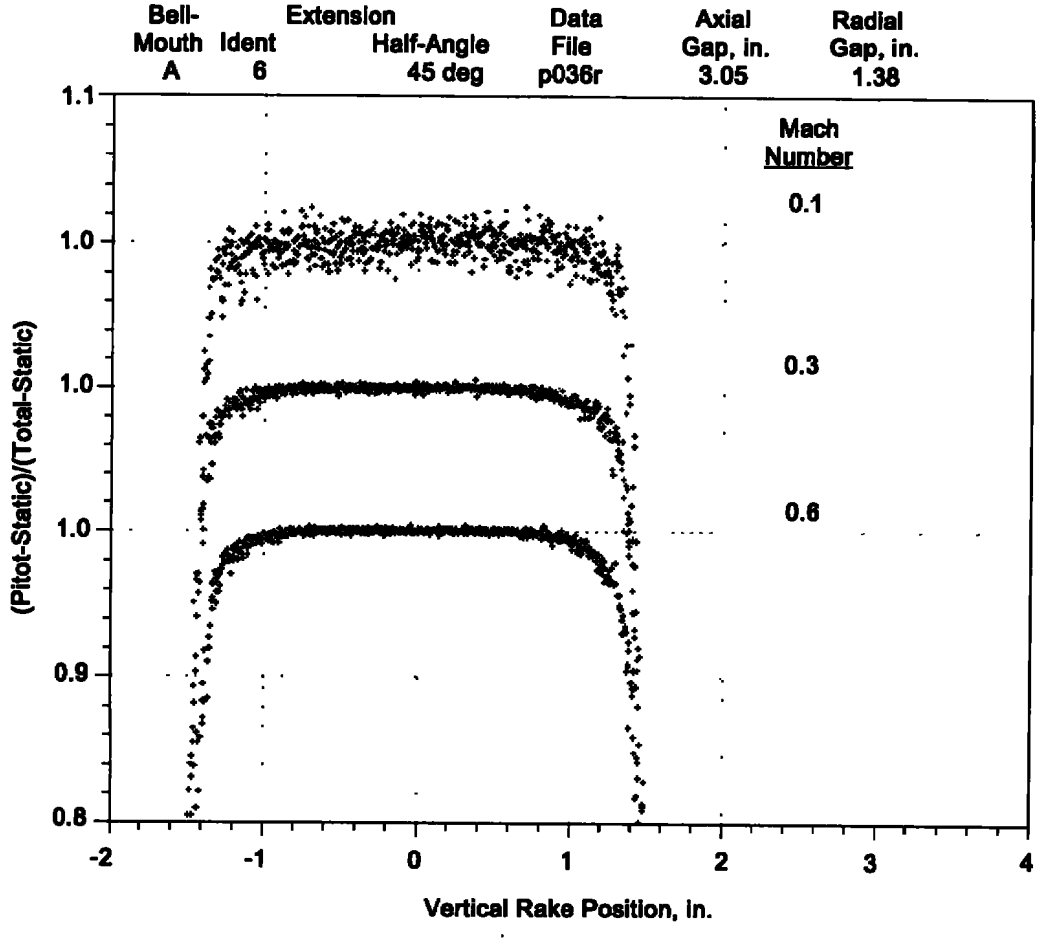

b. Dynamic pressure ratio parameter

Figure 36. Concluded.

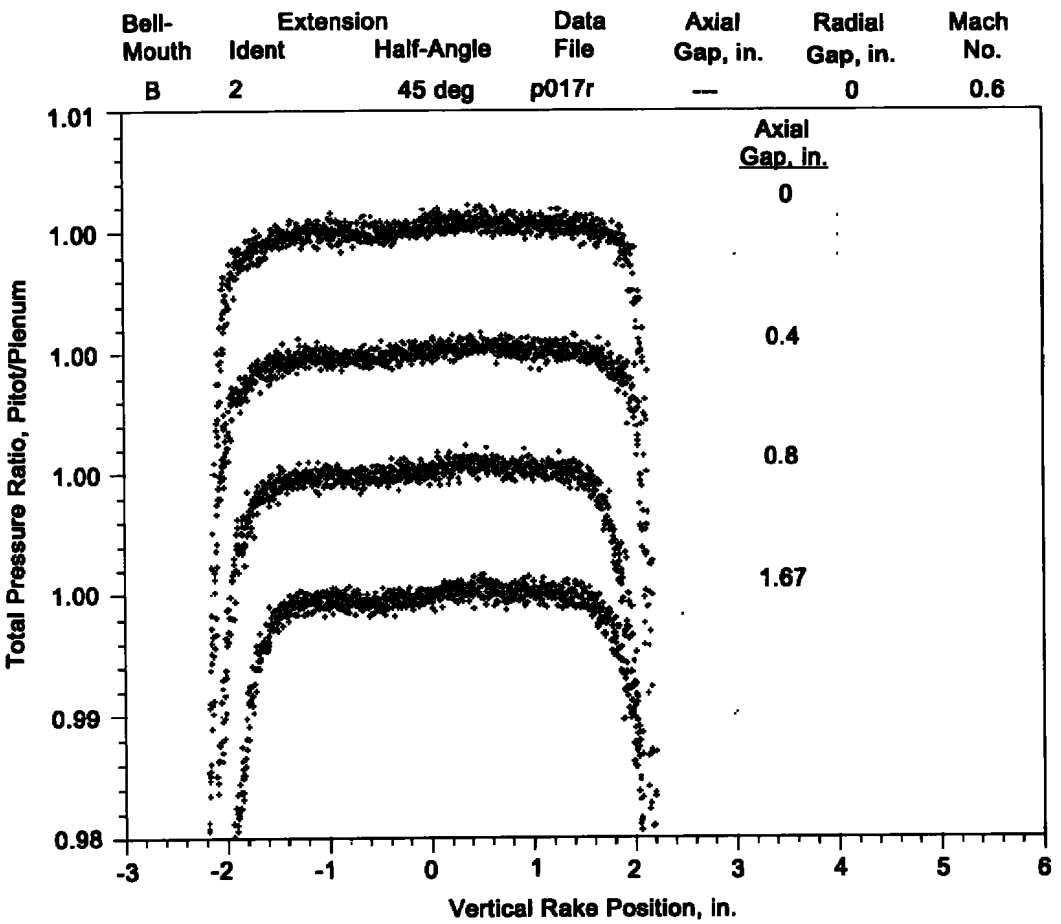

a. Radial gap = 0

Figure 37. Effect of increasing axial gaps on total pressure profiles in Bellmouth B.

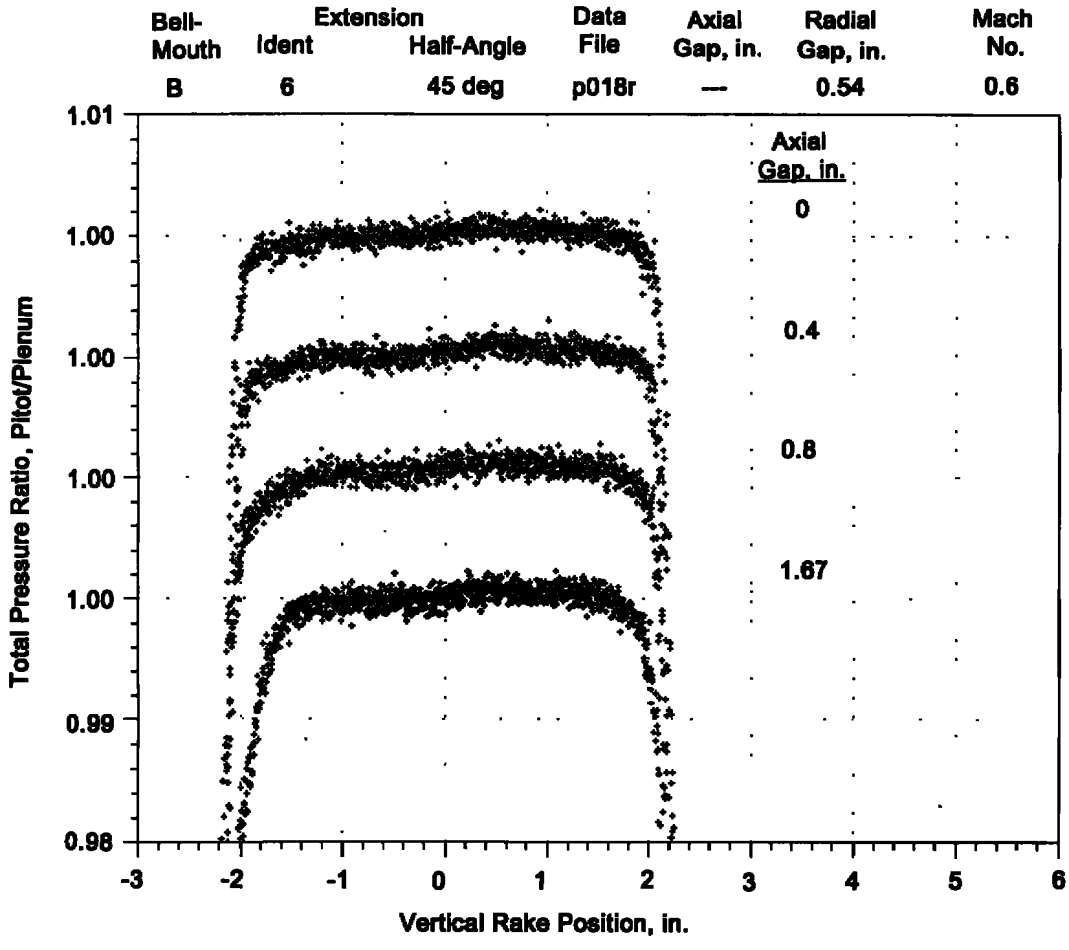

b. Radial gap = 0.54 in.

Figure 37. Continued.

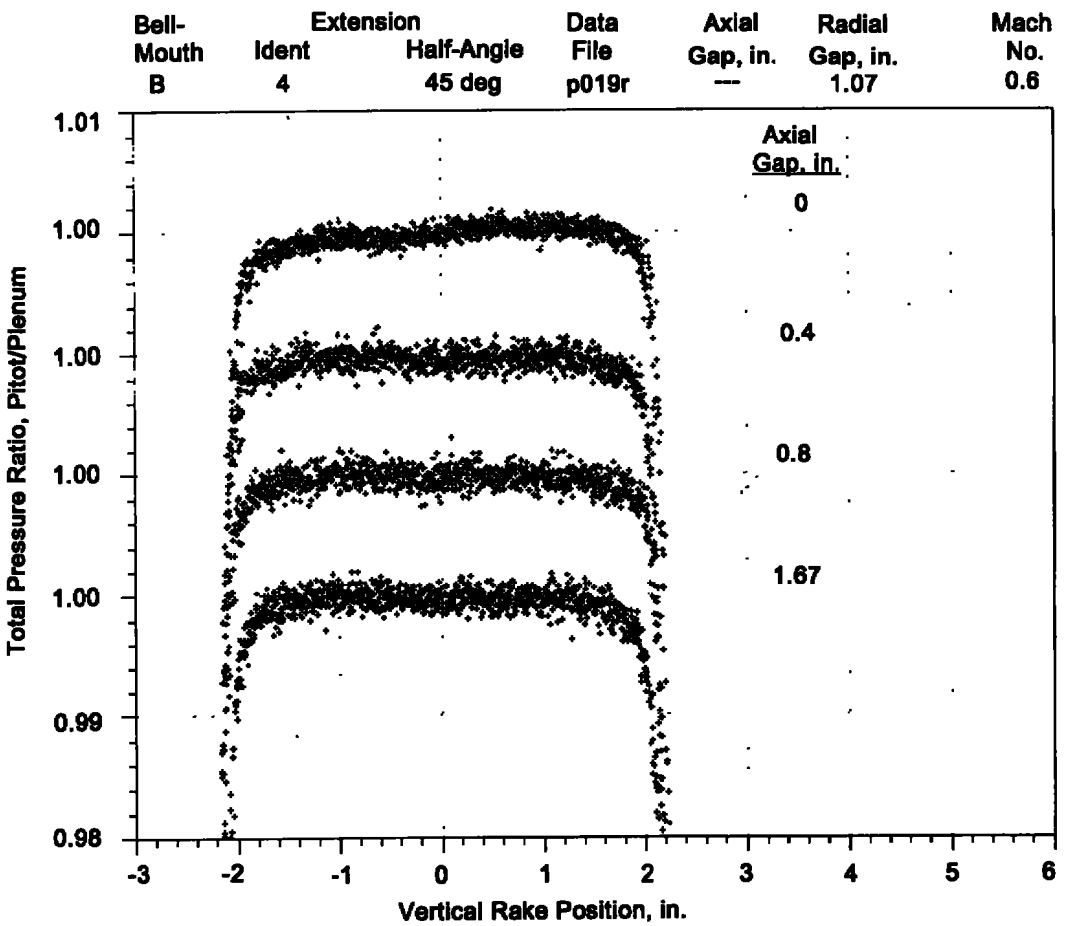

c. Radial gap 1.07 in.

Figure 37. Concluded.

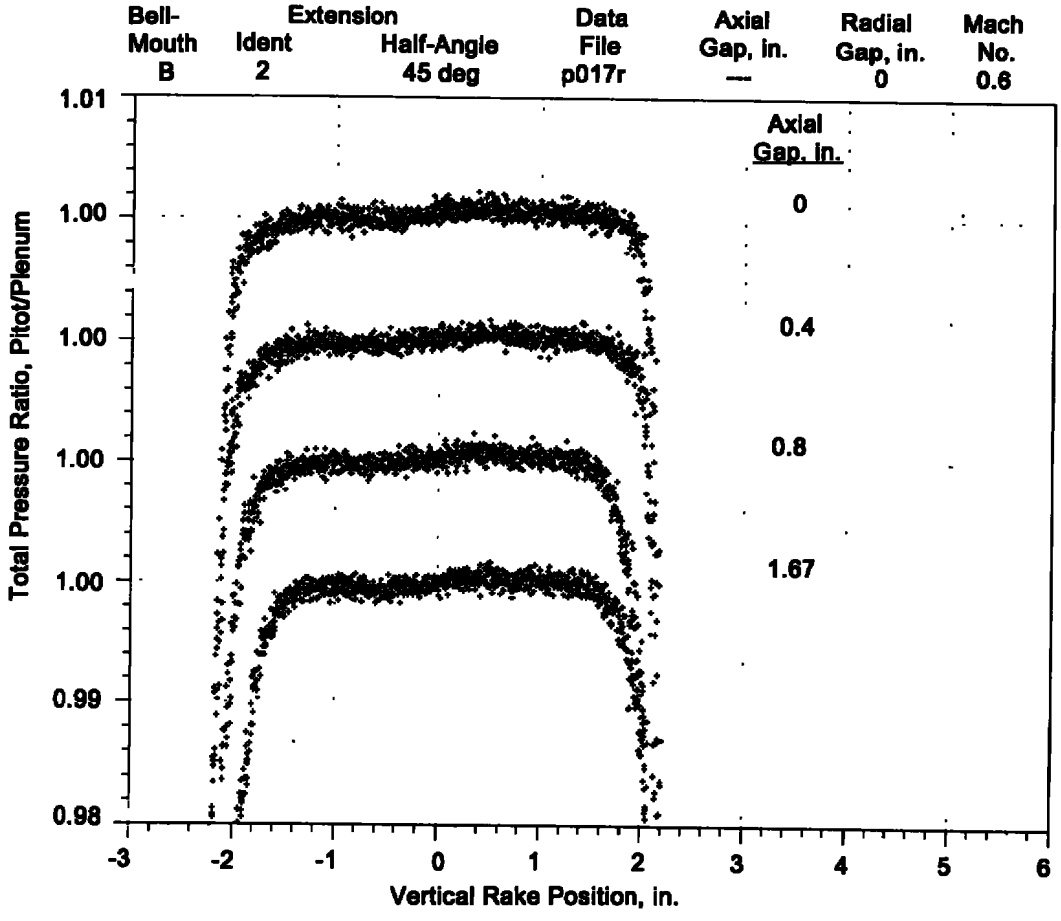

a. Fixed extension roll orientation baseline

Figure 38. Effect of extension roll orientation on total pressure profiles in Bell-mouth B for large axial gap and zero radial gap.

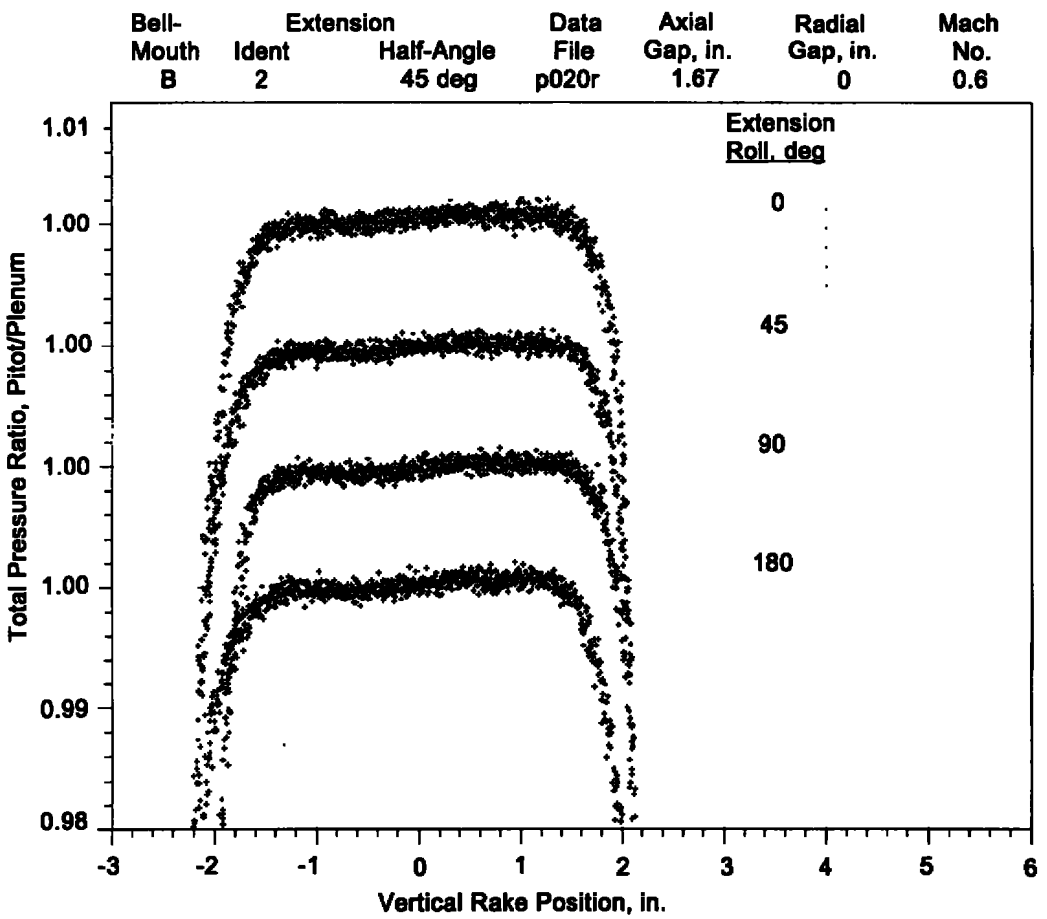

b. Variable extension roll orientation, axial gap = 1.67

Figure 38. Concluded.

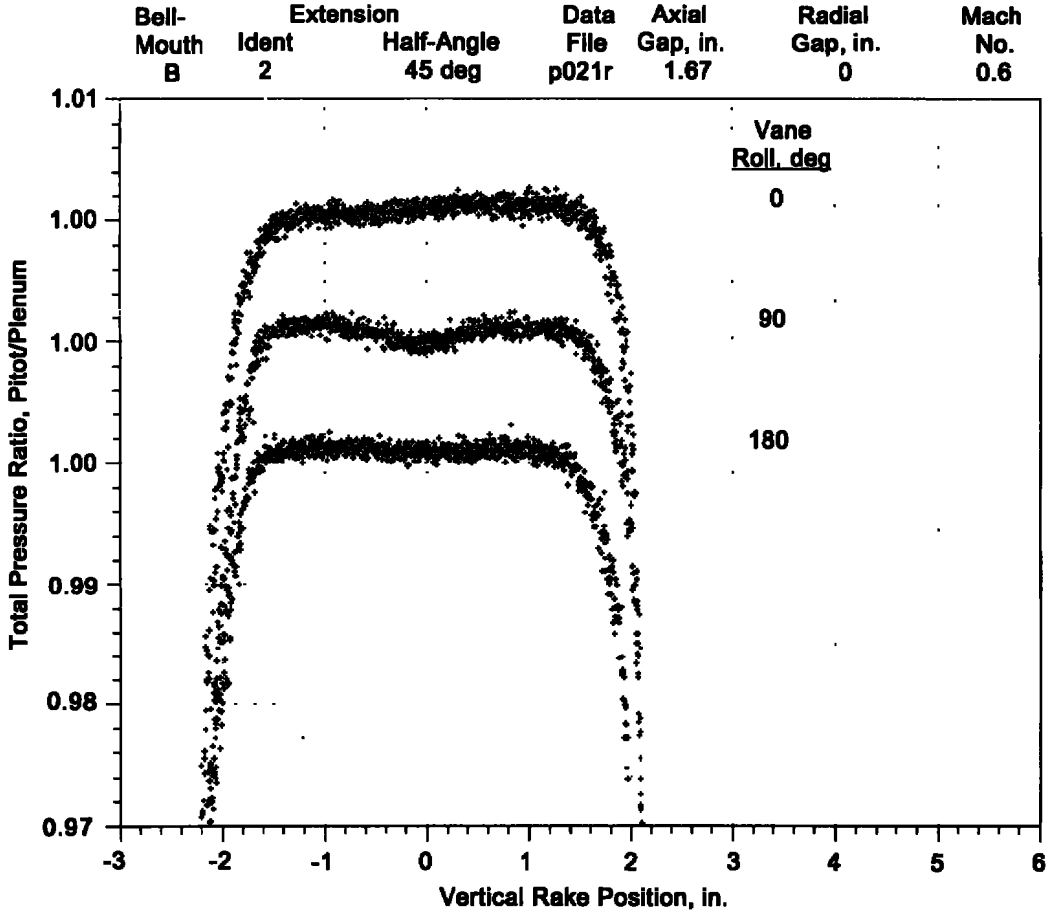

Figure 39. Effect of flow-straightening vane orientation on total pressure profiles in Bellmouth B.

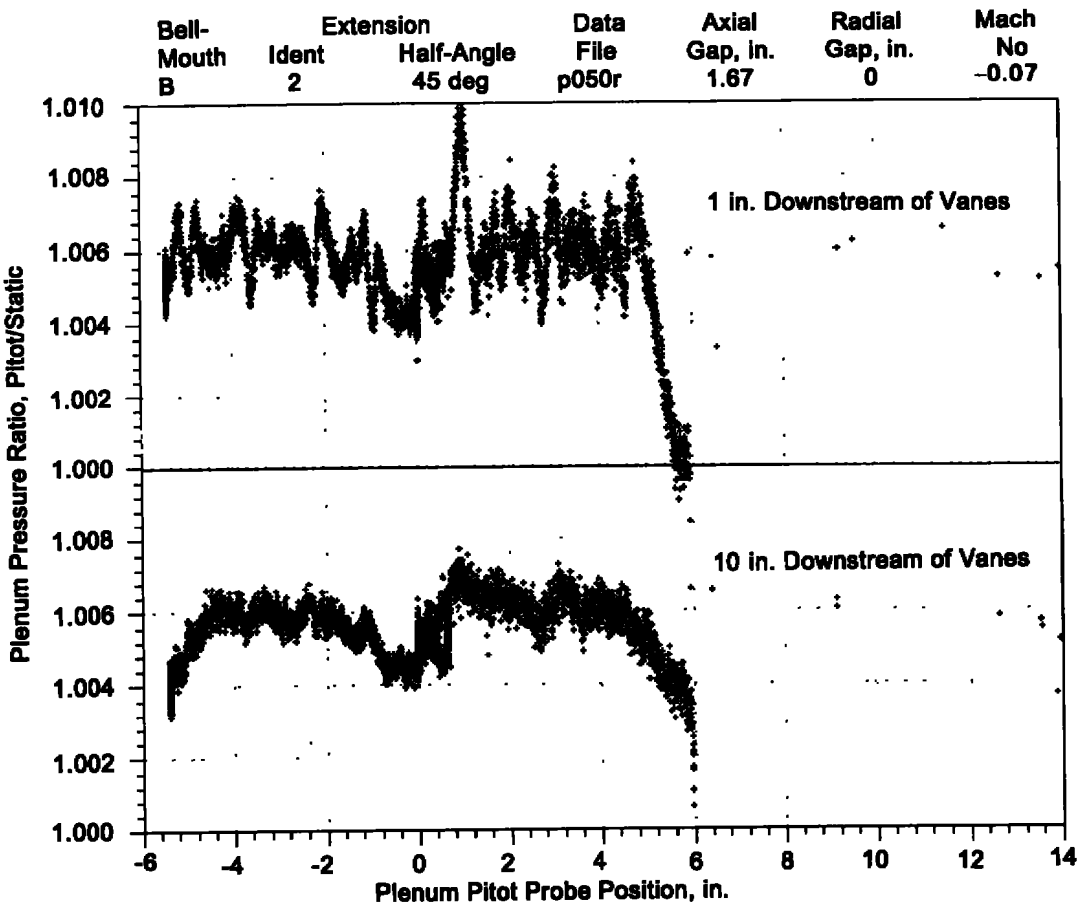

Figure 40. Comparison of plenum total pressure profiles at two locations.

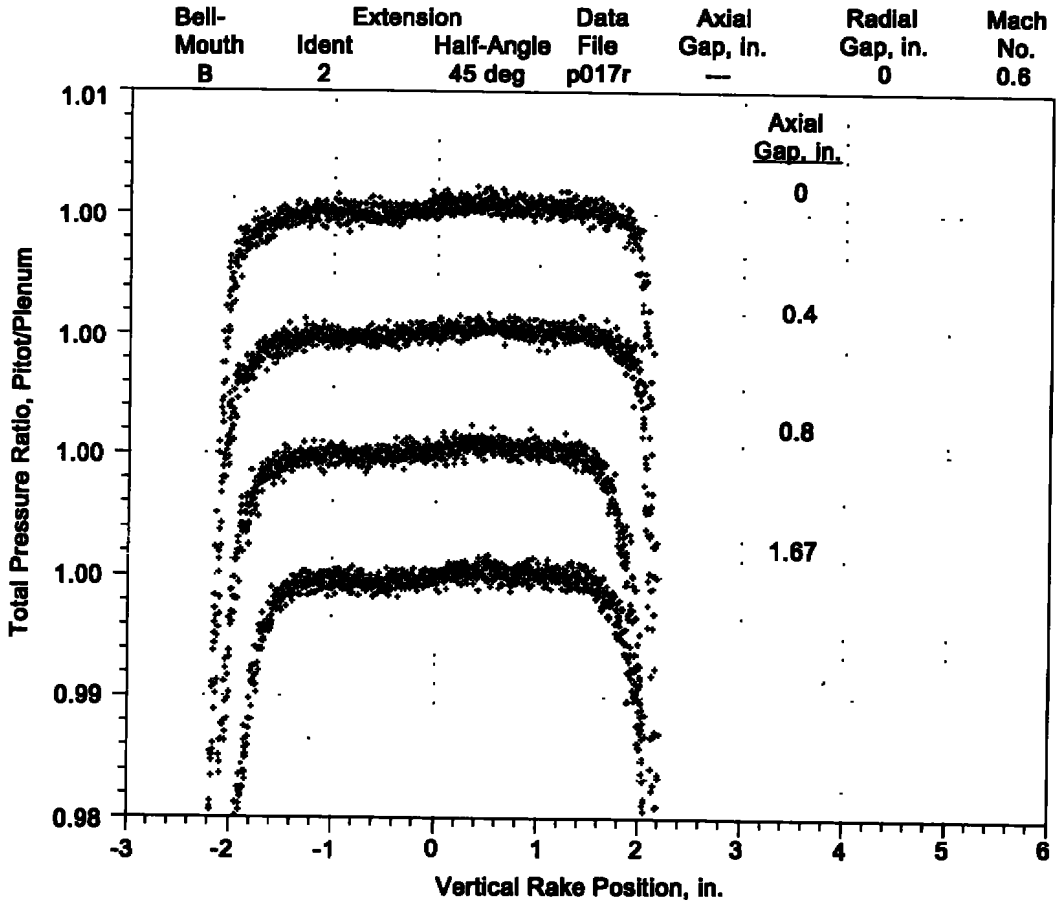

a. M = 0.6, baseline

Figure 41. Comparison of total pressure profiles for two Mach numbers in Bellmouth B.

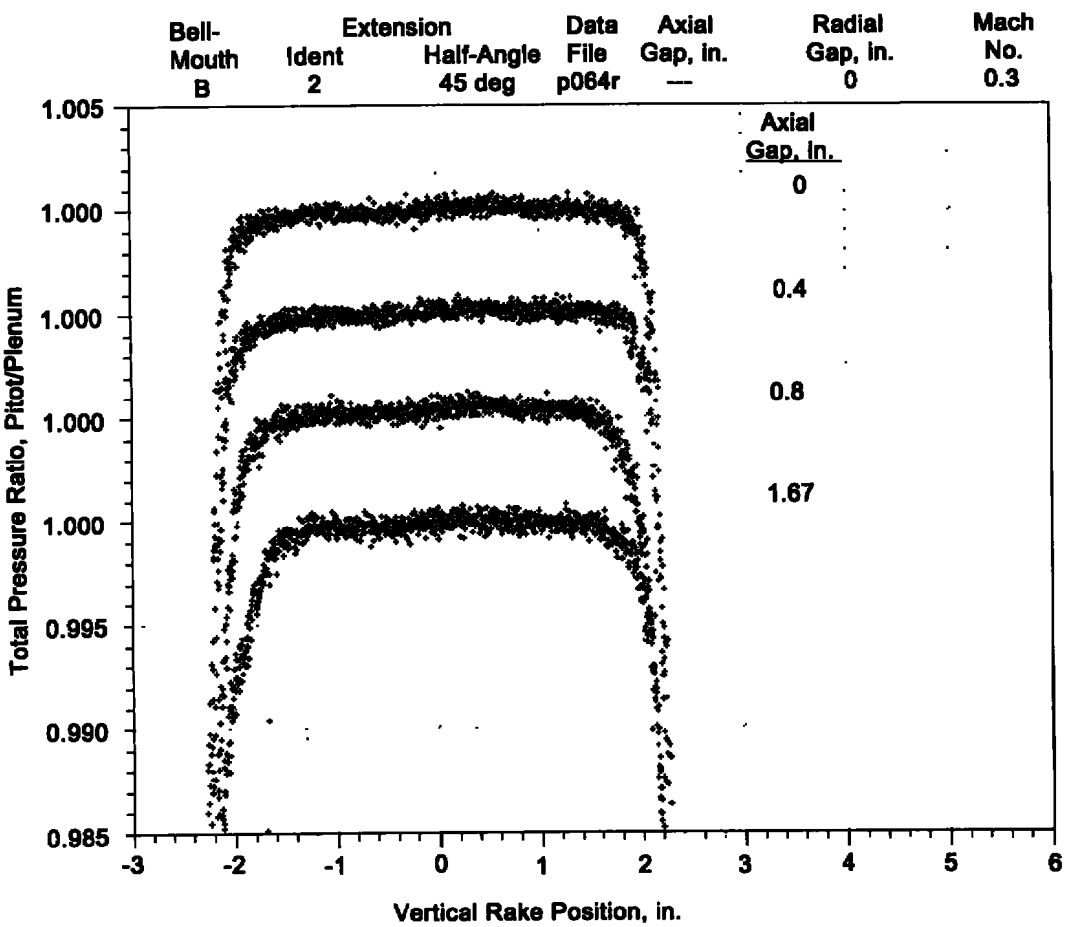

b. M = 0.3

Figure 41. Concluded.

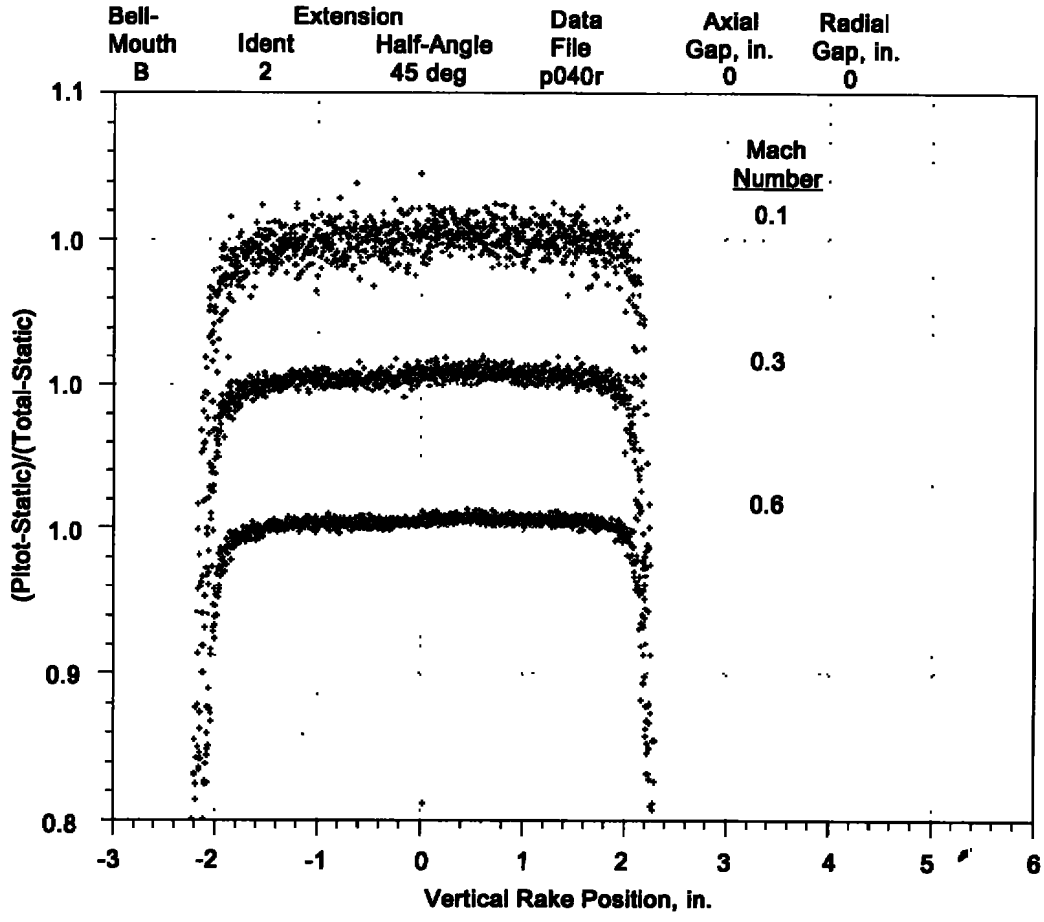

a. Axial gap = 0

Figure 42. Effect of Mach number on total pressure profiles in Bellmouth B for zero radial gap.

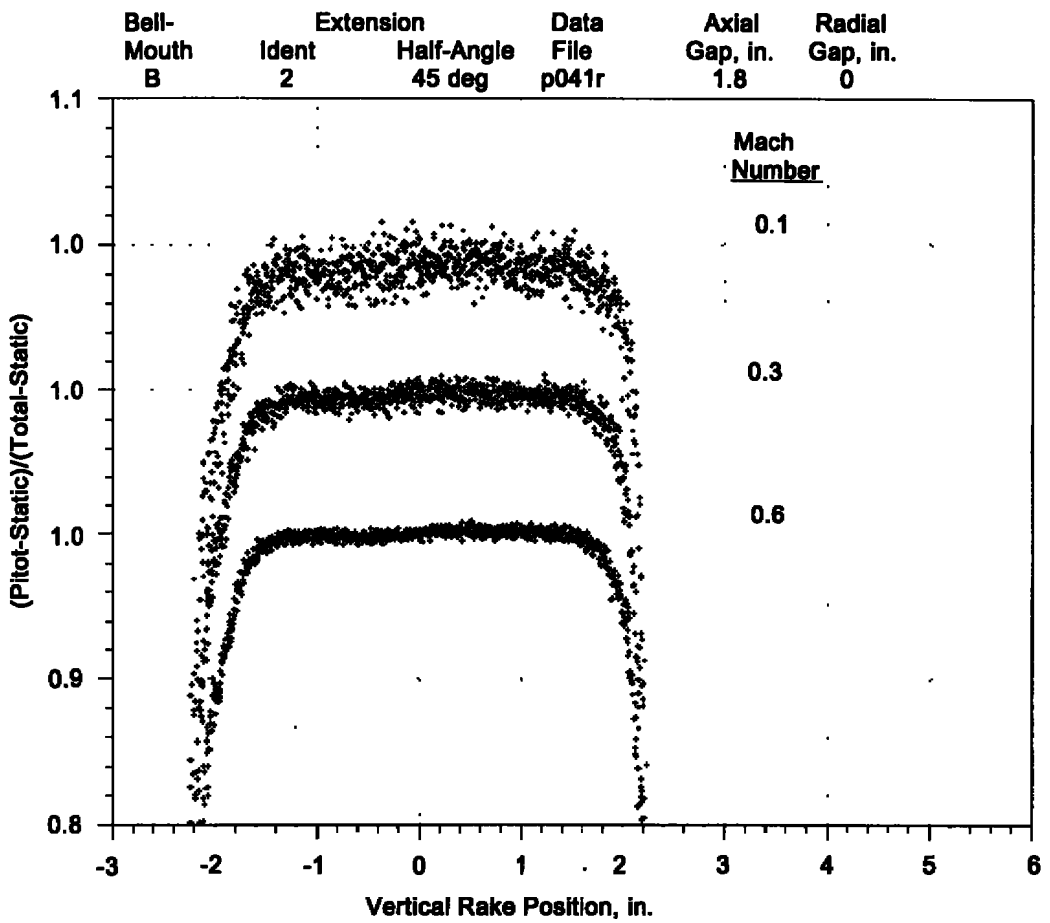

b. Axial gap = 1.67 in.

Figure 42. Concluded.

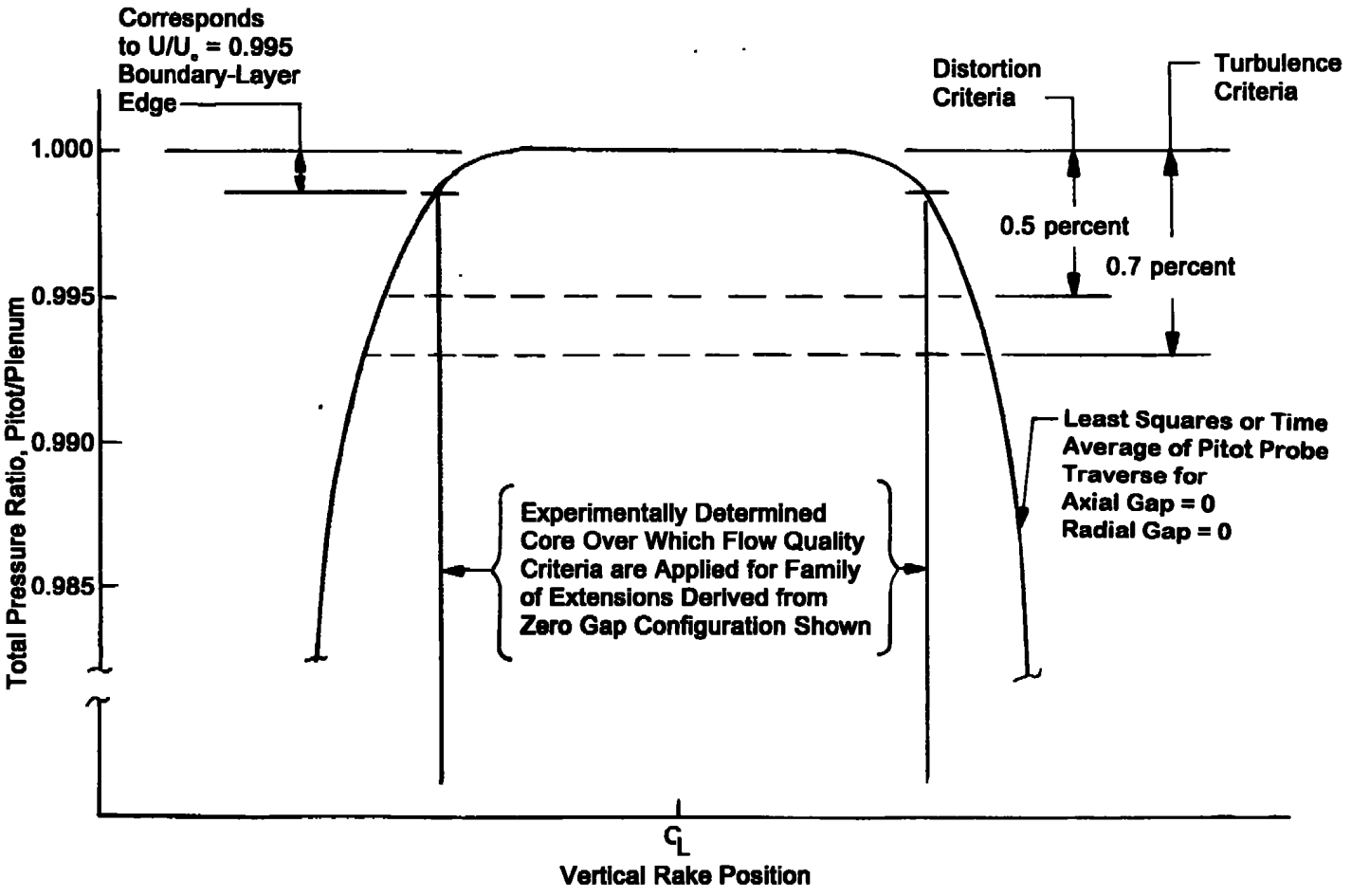

a. "Core" determination

Figure 43. Process for evaluating flow quality parameters.

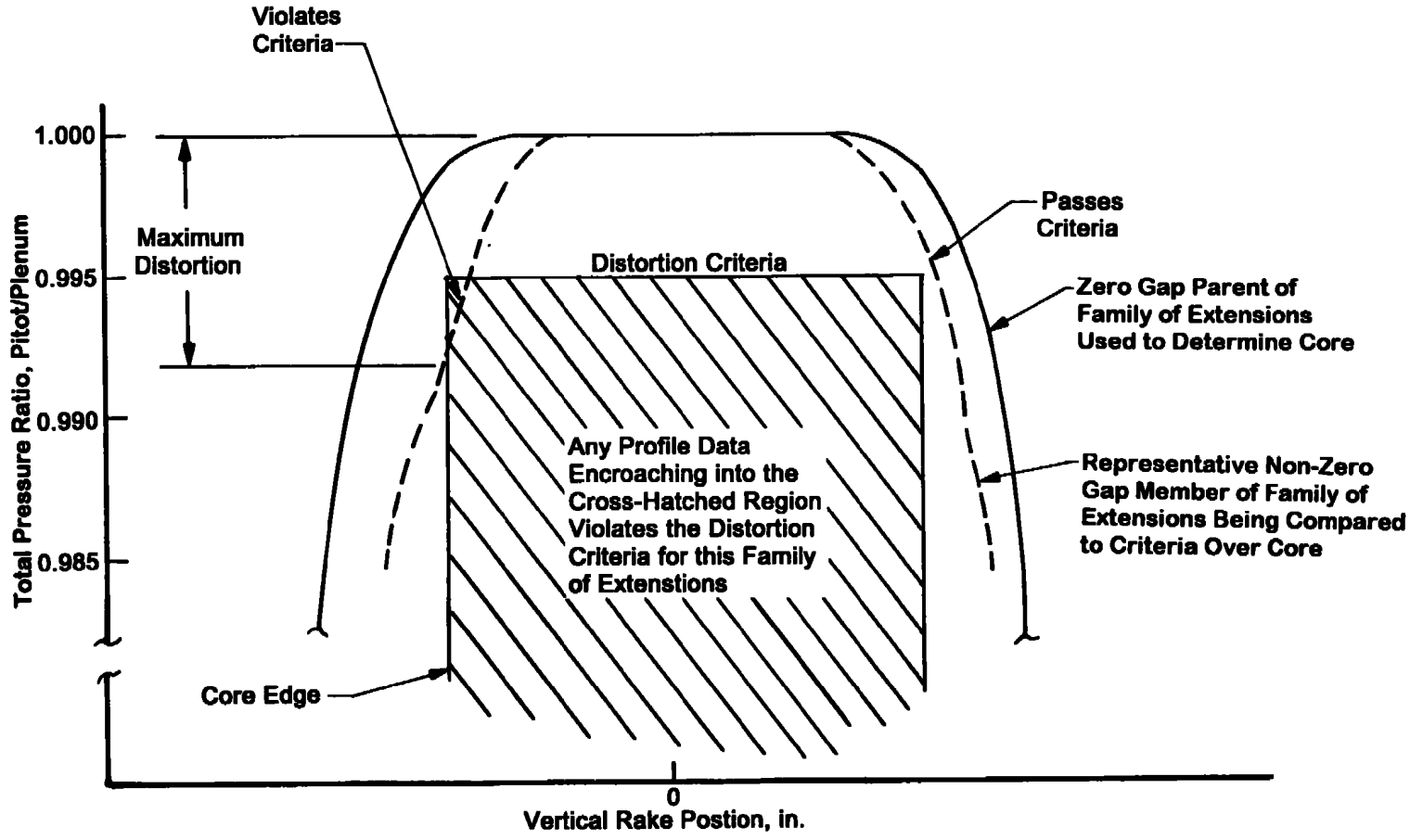

b. Distortion parameter evaluation

Figure 43. Concluded.

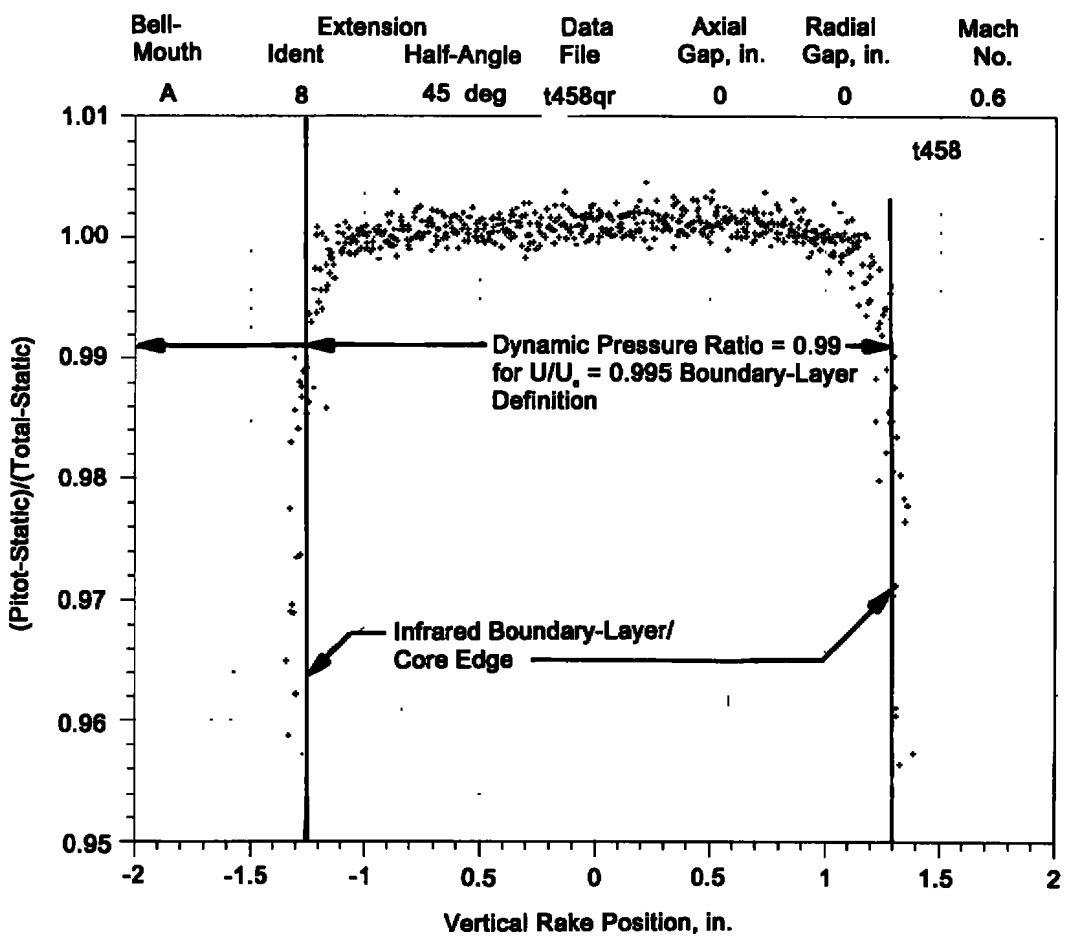

Figure 44. Example of core measurement for zero axial and radial gaps.

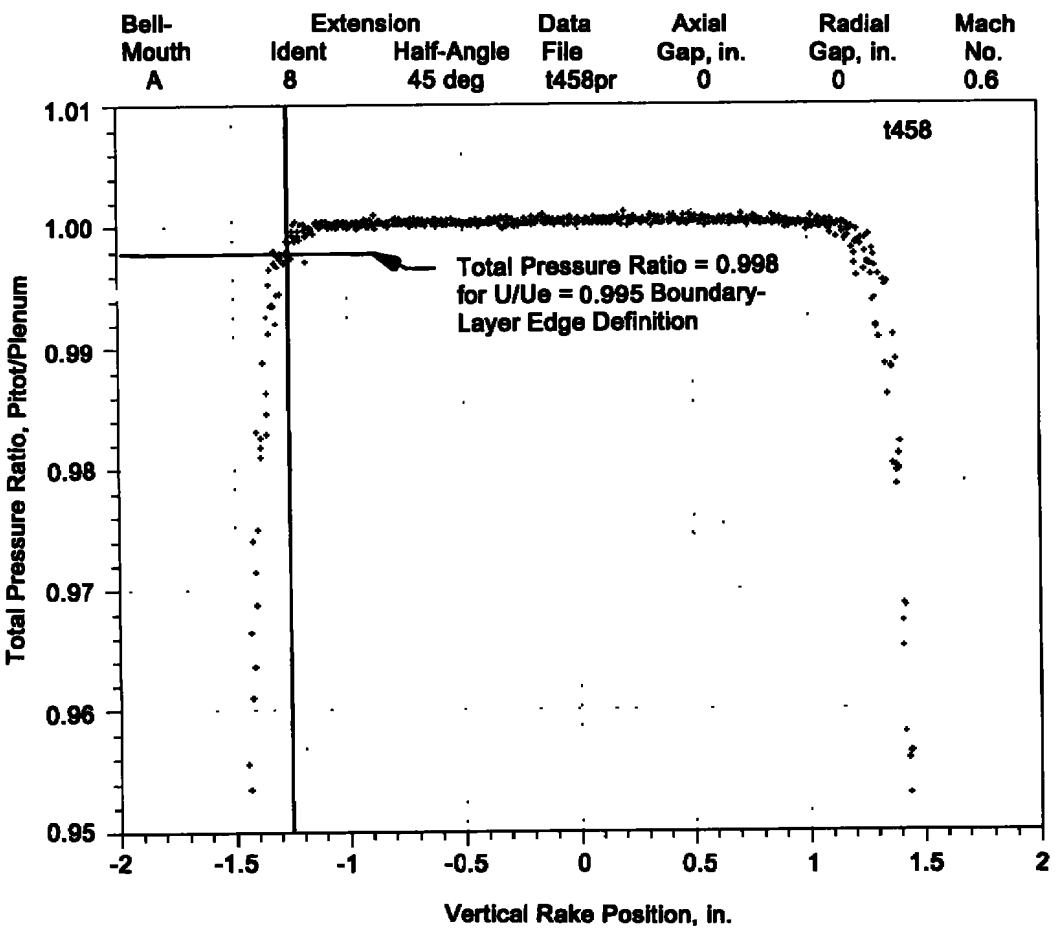

a. Axial gap = 0, baseline core

Figure 45. Example of distortion measurement.

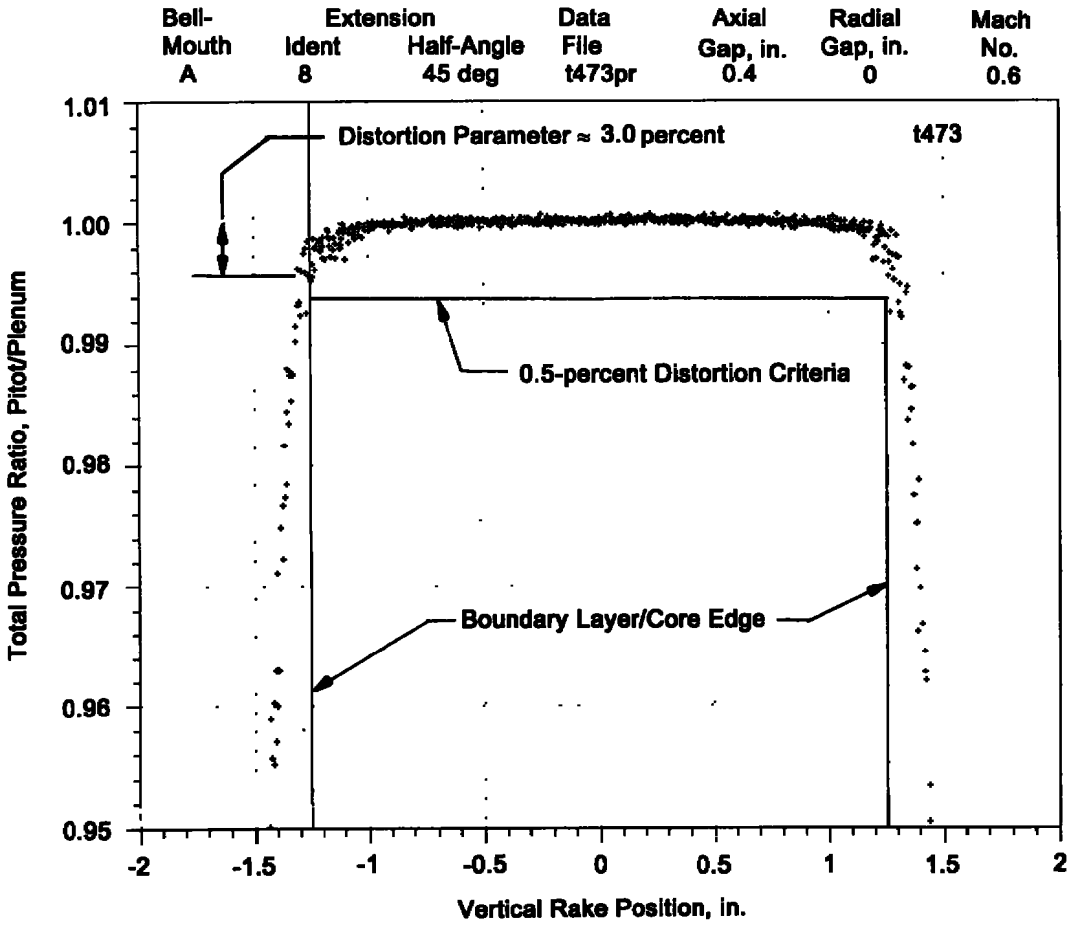

b. Axial gap = 0.4 in.

Figure 45. Continued.

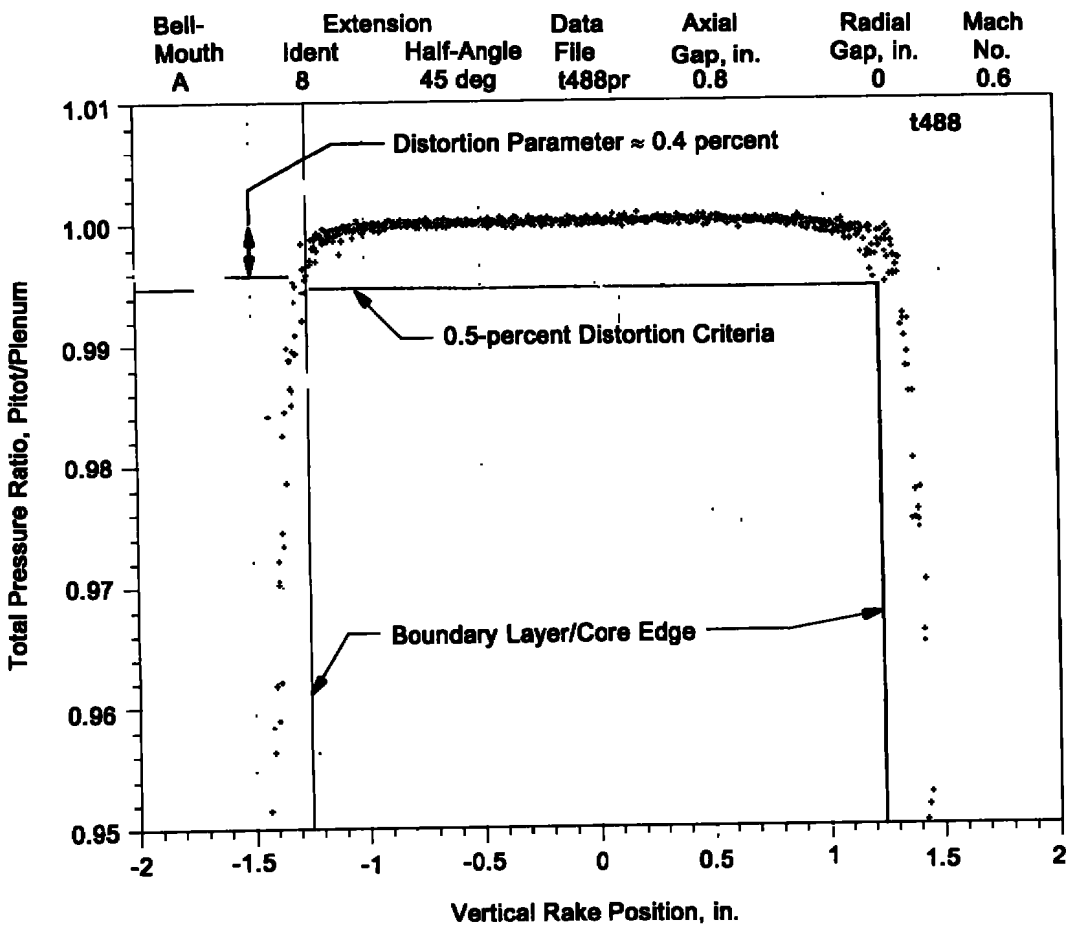

c. Axial gap = 0.8 in.

Figure 45. Continued.

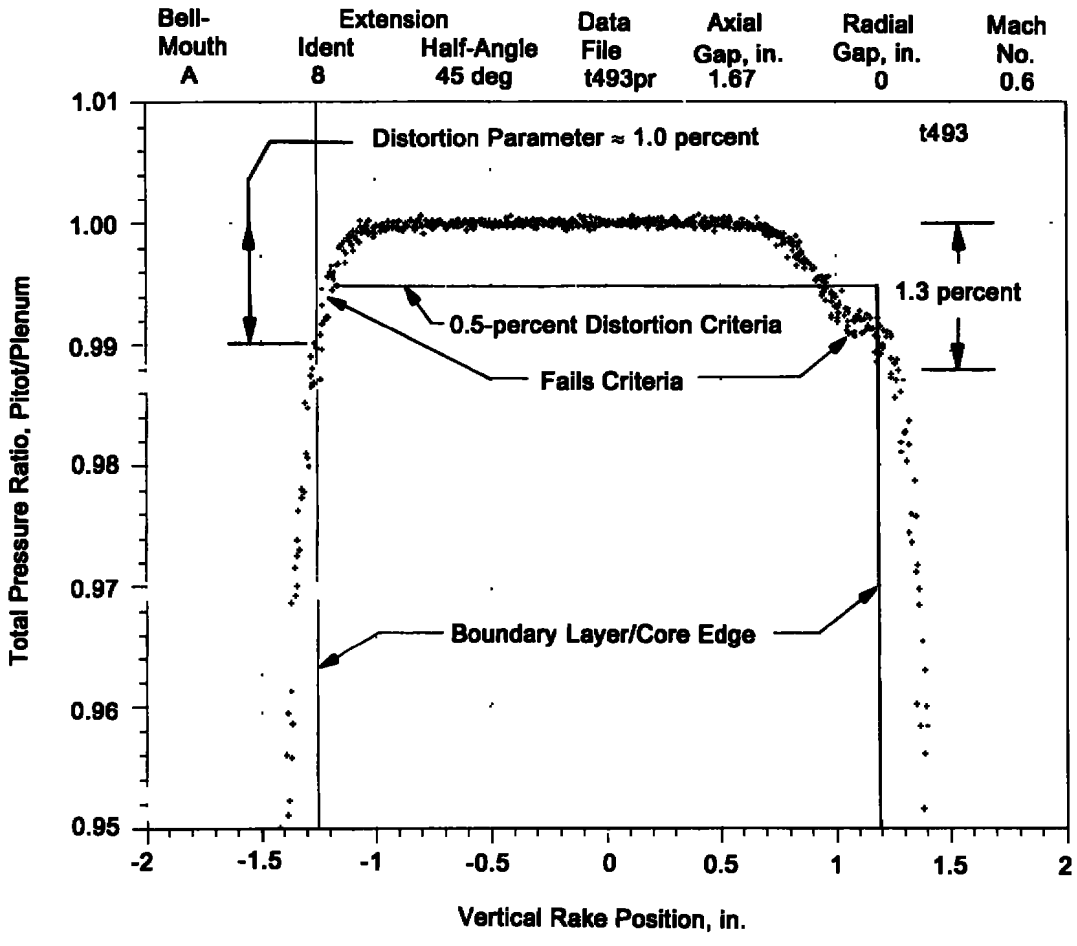

d. Axial gap = 1.67 in.

Figure 45. Concluded.

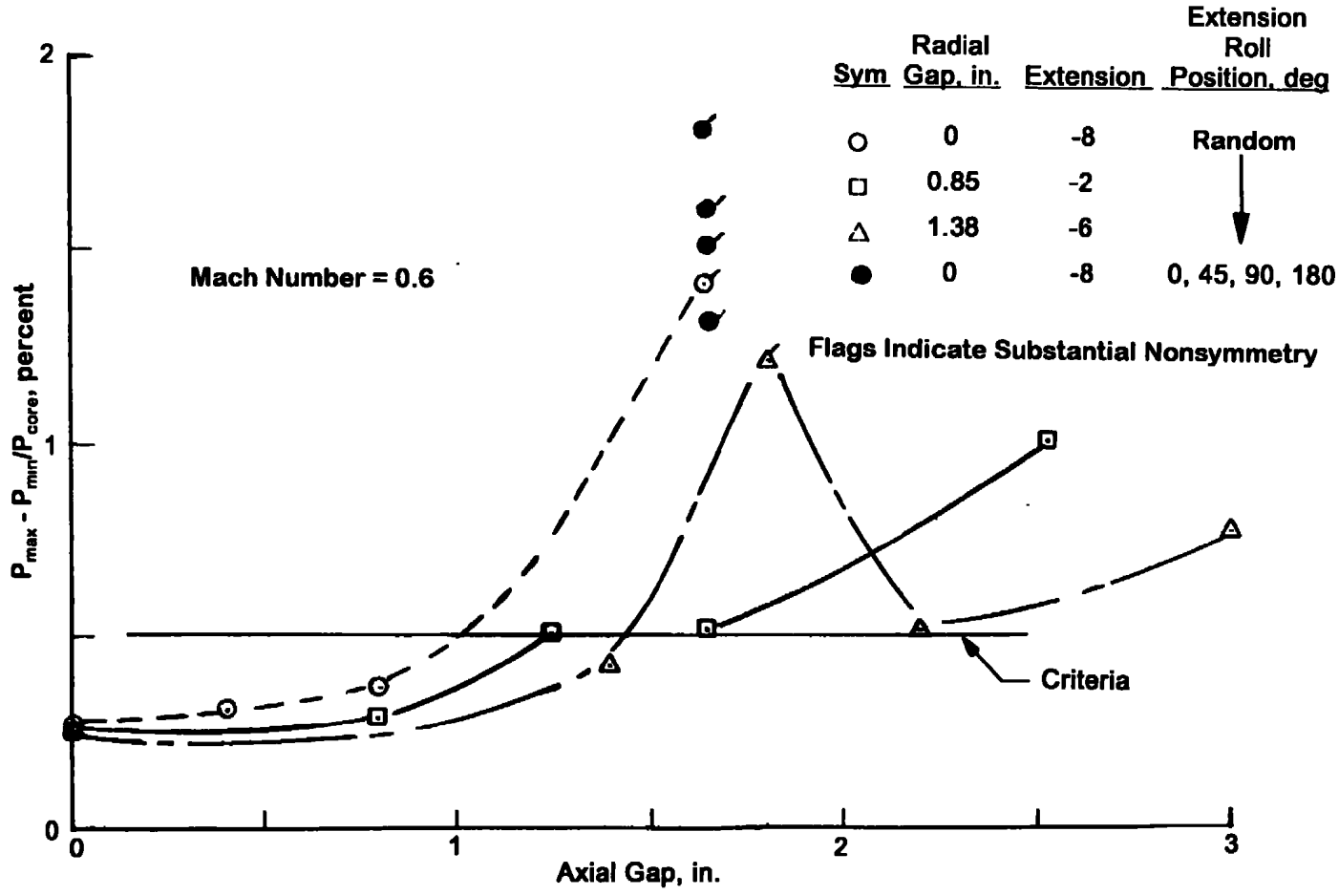

a. Fixed extension half-angle, 45 deg

Figure 46. Comparison of distortion parameters with criteria for Bellmouth A.

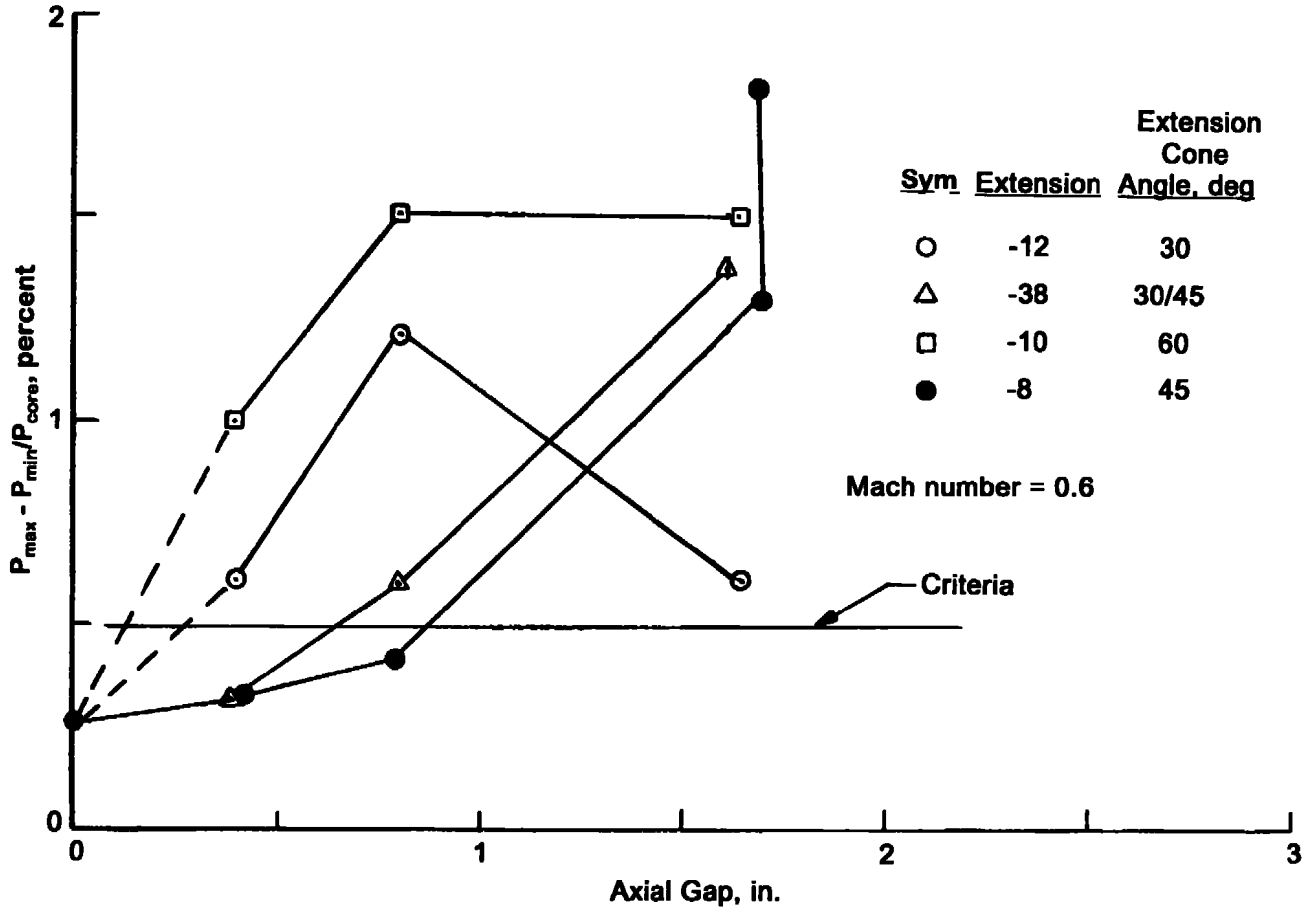

b. Fixed radial gap = 0

Figure 46. Concluded.

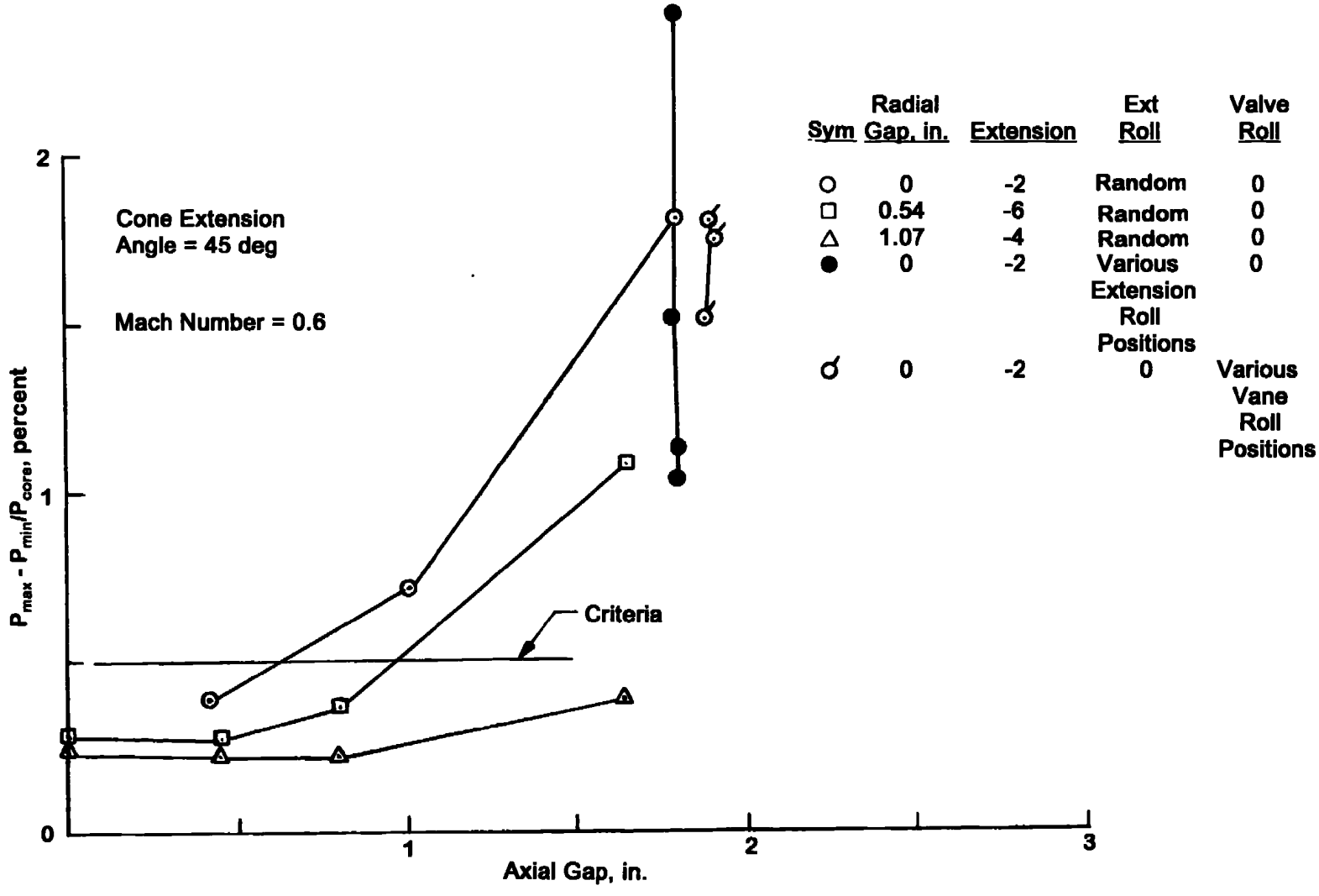

Figure 47. Comparison of distortion parameters with criteria for Bellmouth B.

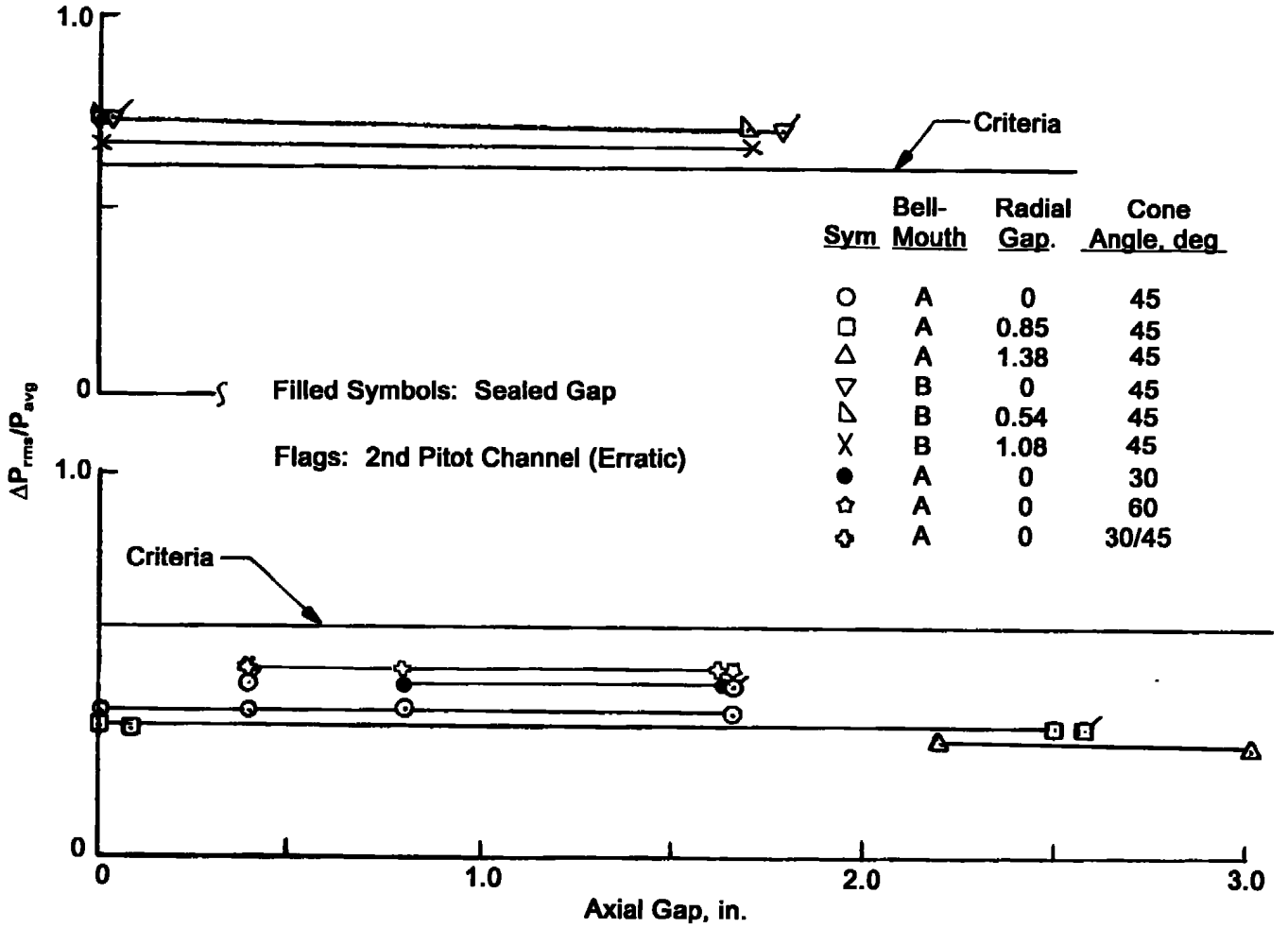

Figure 48. Comparison of single-point turbulence parameter evaluated on bell-mouth axis with criteria for Mach no. = 0.6.

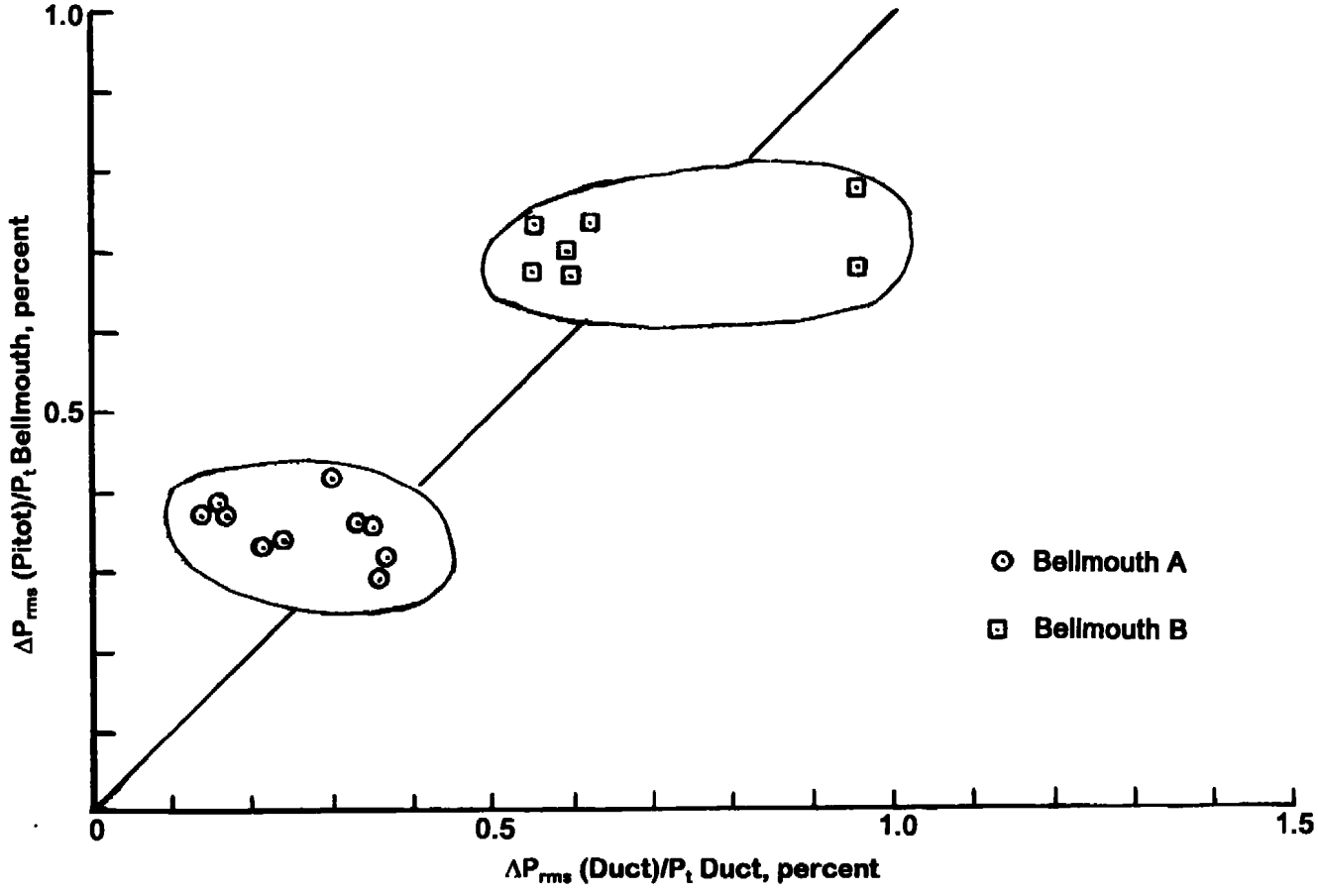

Figure 49. Comparison of turbulence parameters in air supply ducting and on bellmouth axis for Mach No. = 0.6.

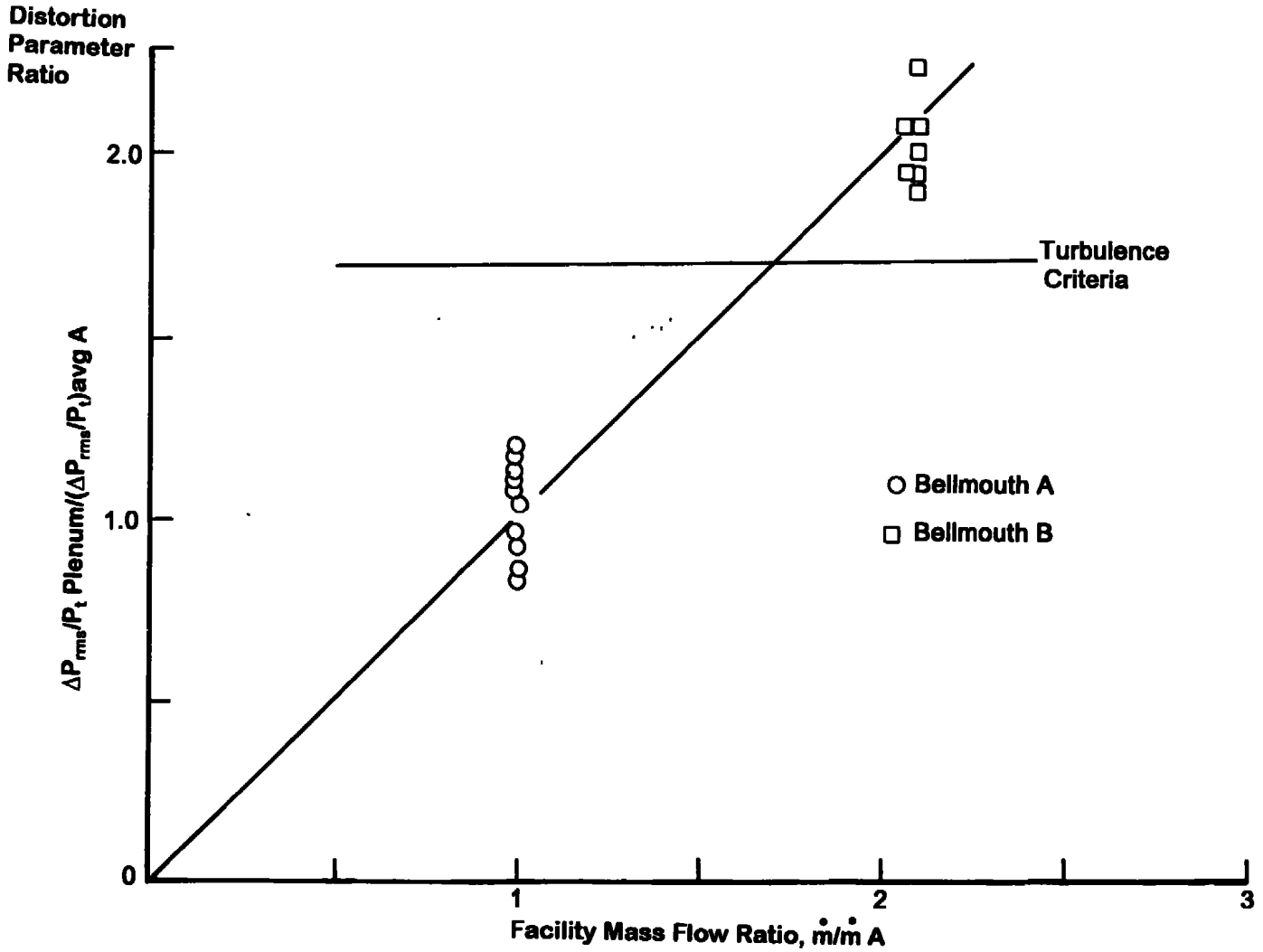

Figure 50. Correlation of bellmouth axis turbulence parameters with facility mass flow rate for Mach no. = 0.6.

Pressure Range, 14 to 18 psia	Elemental Pressure Instrument Errors		Pressure Parameter Errors· Precision Limit (± 2S) Bias Limit (± B) Uncertainty (± (B + 2S))			
Operating Conditions	Bias and Precision Limits		P_P/P_t	$P_P - P_\infty/P_t - P_\infty$		
	± B	± S		M = 0.1	M = 0.3	M = 0.6
Short term drift immediately following calibration (< 1 hour)	± 0 002	± 0 0005	± 0.0002 ± 0 0001 ± 0.0004	± 0.04 ± 0.02 ± 0.08	± 0.004 ±0.002 ± 0 008	+0 002 ±0 0005 ±0 003
Long term drift following calibration under thermally stabilized conditions	± 0 005	± 0.0005	± 0.0005 ± 0.0001 ± 0.0007	± 0 1 ± 0.02 ± 0.14	± 0.01 ± 0 002 ± 0.014	± 0 003 ± 0.0005 ±0.004
Controlled thermal drift during high mass flow operating conditions	± 0.01	± 0.0005	± 0.001 ± 0.0001 ± 0.0012	± 0.2 ± 0.02 ± 0.22	± 0 02 ±0 002 ± 0 044	± 0.006 ± 0 0005 ± 0 007

Note: Uncertainties apply for channel-to-channel comparative analysis.

Figure 51. Measurement uncertainty.

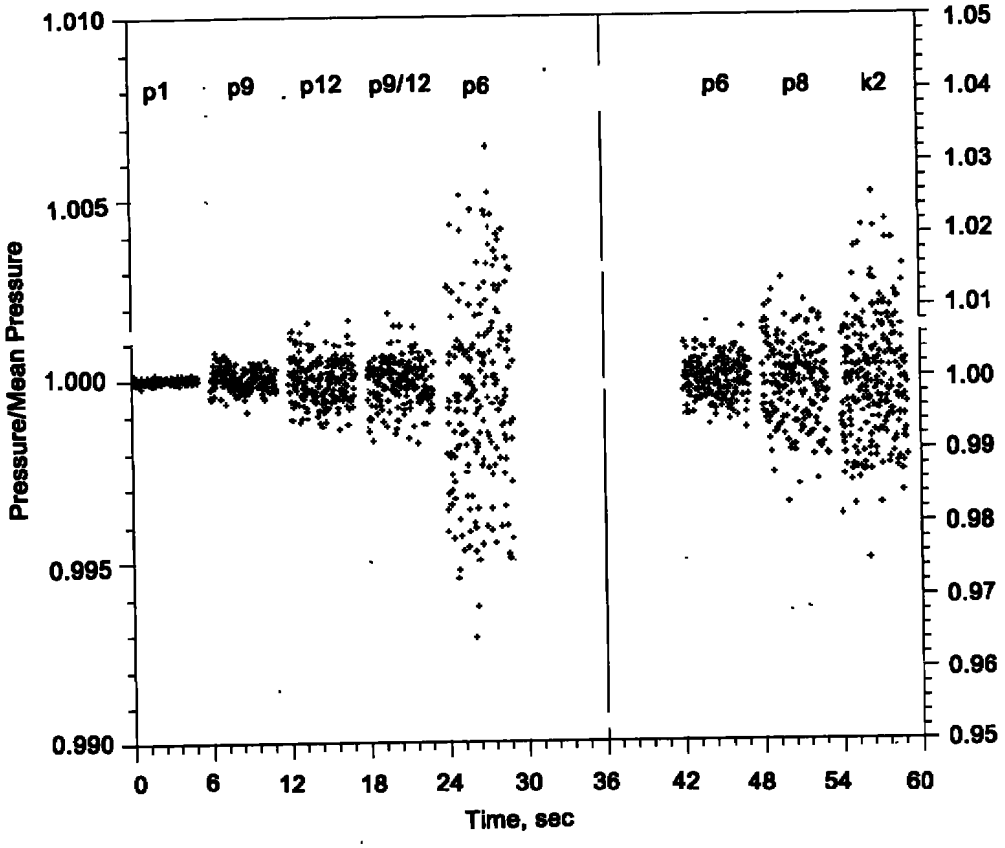

Figure 52. Turbulence effects on pressure measurements.

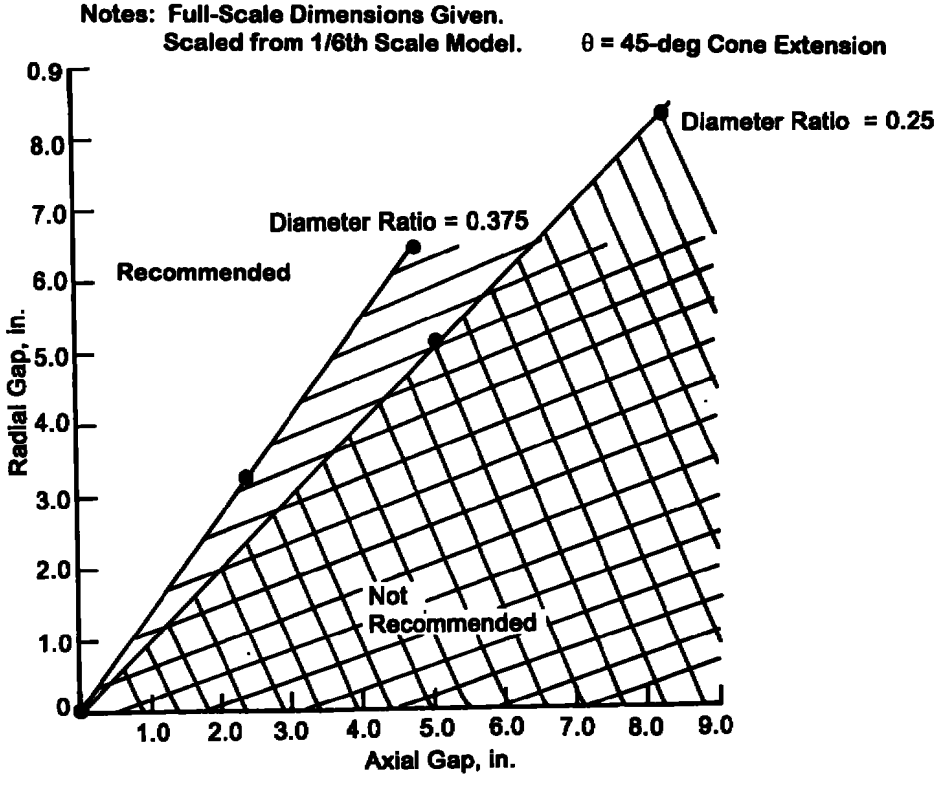

Figure 53. Bellmouth extension design guidelines.

Table 1. Test Summary

Extension Configuration and Test Condition Schedules		Tests Performed									
		Bellmouth A						Bellmouth B			Bellmouth C
Extension Half-Angle	30				✓						
	30/45					✓					
	45	✓	✓	✓					✓		
	60						✓				
	90									✓	✓
Radial Gap	0	✓			✓	✓	✓			✓	✓
	0.85		✓								
	1.38			✓							
	0, 0.54, 1.07								✓		
Axial Gap	0									✓	✓
	0, 0.4, 0.8, 1.67	✓			✓	✓	✓		✓		
	0, 0.85, 1.25, 1.65, 2.52		✓								
	0, 1.28, 1.78, 2.18. 3.05			✓							
Mach No.	0.1, 0.3, 0.6	✓	✓	✓	✓	✓	✓	✓	✓	✓	✓
Bellmouth Rake Survey	Traverse: Down, up	✓	✓	✓	✓	✓	✓	✓	✓	✓	✓
	Fixed: upper, center, lower pro ections of bellmouth wall	✓	✓	✓	✓	✓	✓	✓	✓	✓	✓

Note: 1. A ✓ for a row means all conditions in that row were tested.
2. A ✓ in a vertical column means all conditions in that column were tested.

Table 2. Plenum Mach Number

Bellmouth/Plenum Mach Number	Bellmouth Mach Number		
	0.1	0.3	0.6
A	<0.01	0.02	0.03
B	0.014	0.042	0.073
C	0.023	0.066	0.112
no bellmouth	0.07		

NOMENCLATURE

B Bias
d Full-scale bellmouth exit diameter
D Full-scale plenum diameter
DR Diameter ratio
M Mach number
P Pressure
S Precision
U Velocity

Subscripts

e Edge
P Plenum
rms Root mean square
t Total
∞ Static